ASD-TDR-63-340

RESEARCH ON PHOTOEMISSION

TECHNICAL DOCUMENTARY REPORT NO. ASD-TDR-63-340
March 1963

Electronic Technology Laboratory
Aeronautical Systems Division
Air Force Systems Command
Wright-Patterson Air Force Base, Ohio

Project No. 4156, Task No. 415605

(Prepared under Contract No. AF 33(657)-8041
by: Department of Electrical Engineering
University of Minnesota, Minneapolis 14, Minnesota
Edited by: W. T. Peria)

NOTICES

When Government drawings, specifications, or other data are used for any purpose other than in connection with a definitely related Government procurement operation, the United States Government thereby incurs no responsibility nor any obligation whatsoever; and the fact that the Government may have formulated, furnished, or in any way supplied the said drawings, specifications, or other data, is not to be regarded by implication or otherwise as in any manner licensing the holder or any other person or corporation, or conveying any rights or permission to manufacture, use, or sell any patented invention that may in any way be related thereto.

Qualified requesters may obtain copies of this report from the Armed Services Technical Information Agency, (ASTIA), Arlington Hall Station, Arlington 12, Virginia.

This report has been released to the Office of Technical Services, U. S. Department of Commerce, Washington 25, D. C., for sale to the general public.

Copies of ASD Technical Reports and Technical Notes should not be returned to the Aeronautical Systems Division unless return is required by security considerations, contractual obligations, or notice on a specific document.

ABSTRACT

Techniques in general usage in the laboratory are described. Included are those used to obtain high vacua, to provide clean surfaces to deposit Na on these surfaces and to measure their work functions. A method used to fabricate hemispherical grids is also described.

Various studies of sodium covered surfaces are described. The dependence of work function on the degree of coverage is not reproducible and seems especially to depend on whether the sodium is laid down as atoms or as ions. Electron diffraction studies show that the surface structure of the Ge crystal is changed in the presence of the adsorbed Na and a detailed description of the effect of temperature on the structure is given. Secondary electron emission was also studied as a function of Na coverage and preliminary energy analyses of the secondary electrons are presented.

A study of the surface properties of Ge using field-emission microscopy was initiated as an extension of the above-described studies of Na overlayers on Ge. Field electron emission patterns were observed from two Ge emitter tips with their surfaces in the original contaminated state. Attempts to clean the surfaces by high field desorption have so far been unsuccessful.

A system for the production and investigation of photo-emissive yield dependence on thickness, temperature and composition of Na_3Sb films is described. From the results of an experiment with this system, some speculations are made concerning film formation processes.

A glovebox and argon purification facilities were obtained and were integrated into one system. This system is to be used in the synthesis and the measurement of the conductivity and Hall effect of Na_3Sb in bulk form.

Brief descriptions are given of the apparatus to be used in a study of anomalous photovoltaic effects in evaporated and sputtered Ge films.

PUBLICATION REVIEW

The content of this report represents the scientific findings of an Air Force sponsored program. It does not direct any specific application thereof. The report is approved for publication to achieve an exchange and stimulation of ideas.

FOR THE COMMANDER:

A. H. Dicke
Chief, Thermionics Branch
Electronic Technology Laboratory

TABLE OF CONTENTS

LIST OF ILLUSTRATIONS

LIST OF ILLUSTRATIONS (continued)

LIST OF TABLES

1. INTRODUCTION AND SUMMARY

The general objective of the research described in this report is to augment the understanding of photoemitters and the photoemission process. While little attention has been given to the measurement of photoemission itself, a large portion of the program is concerned with the details of the lowering of surface barriers by alkali adsorption; this process is of obvious importance to photoemission. Another phase of the program is concerned with the semiconducting properties of the photoemitting alkali antimonides, with emphasis on the correlation of properties with composition. Again the relation to the photoemission process is obvious.

More recently a third phase has been added to the program. It has no direct bearing on the understanding of photoemission but is related in the sense that the phenomena under study have potential applications in areas where photoemitters are now used. This phase is concerned with the understanding of the large photovoltaic effects observable in thin films of certain semiconducting materials.

The various experiments carried out under the three phases of the program are outlined below while the progress is described in more detail in later sections of the report. Details of earlier work on the same topics may be found in refs. 1 through 7.

1.1 Experimental Techniques

Although all sections of the report contain descriptions of experimental techniques, those common to more than one experiment are assembled in a single section (Sec. 2.1) for convenience. There will be found descriptions of the vacuum techniques employed, and of the methods used in sputtering, sodium deposition and measurement of the work function. There is also a brief description (Sec. 2.1.5) of the preparation of hemispherical grids for use in the slow electron diffraction study.

1.2 Overlayer Studies

1.2.1 A Study of the Influence of Adsorbed Na on the Work Function of Ge

The lowering of the surface barrier of solids by the adsorption of electropositive species is an extremely important phenomenon in any application of electron emission. In the case

Manuscript released by the author 29 March 1963 for publication as an ASD Technical Documentary Report.

of photoelectric emission, the long-wavelength threshold can be greatly extended by the adsorption of alkali or alkali-earth elements. Associated with this extension is a sharp decrease in work function. It is the purpose of this portion of the program to provide a better understanding of this phenomena for certain selected systems.

The work on this phase of the project dealt with the system Na on Ge. Ge was chosen because of the extensive theoretical and experimental information available in the literature, having to do with its semiconducting properties, and also because the general method for preparing atomically clean surfaces of single Ge crystals is thoroughly developed and is widely accepted. Sodium was chosen as the overlayer material because of the large effect it could be expected to produce, and also because it is more convenient to work with in a vacuum system than the more conventionally used cesium.

The object of the experiment is to start from the atomically clean surface, depositing measured amounts of sodium and measuring the influence this sodium has on the work function.

During the course of the experiment it became necessary to develop techniques for producing a clean surface, depositing Na and measuring work function shifts, and a large portion of the experimental work dealt with refining these techniques. These techniques are described in Sec. 2.1.2 (argon sputtering), Sec. 2.1.3 (Na deposition), and Sec. 2.1.4 (work function measurement).

After the refinement of these techniques was completed, measurements were taken on the 111 face of a Ge crystal. Preliminary measurements indicate that the dependence of work function on overlayer coverage is more complex than the dependence of photoelectric threshold on overlayer coverage. Furthermore, the results indicate that the dependence may be influenced by the method of deposition used, that is, the results for atomic deposition (Fig. 8) may differ from those for ionic deposition (Fig. 9).

1.2.2 Electron Diffraction Studies of the Structure of Na Adsorbed on Ge

Surface overlayer studies on germanium and silicon have been undertaken in this laboratory because of the profound effect of surface barrier reduction on electron emission. Motivation for electron diffraction studies was provided by a desire for understanding the mechanism of surface barrier reduction by an adsorbed surface overlayer. Because knowledge of surface structure will greatly enhance progress towards this goal, slow electron diffraction studies are being made on clean germanium

surfaces with various sodium overlayer coverages. Structure changes as a result of the deposited overlayer are being observed.

Slow electrons are diffracted predominately by the first few atom layers near the surface. Thus the pattern observed is characteristic of the surface structure and the bulk structure only enters as a second order effect. The periodicity of a single crystal does not extend to the vacuum surface in most cases because a "perfect" surface is not usually the lowest energy state. Rearrangement of the surface layers is normally required to achieve strong chemical bonding among surface atoms. Since the surface must be in register with the bulk, many of the symmetry properties of the bulk structure are reflected in the surface structure. However the size of the unit surface mesh is normally larger than that of the bulk because of the rearrangement process. Thus fractional order beams are observed which are characteristic of the surface structure only.

Electron diffraction studies have been made on the (111) face of two intrinsic germanium single crystals. One crystal was cut from an ingot, mechanically polished, and etched in CP-4. The other crystal was grown in the form of a thin ribbon and required no polishing. Because the ribbon crystal had a "natural" optically flat surface which was much smoother than the surface obtained on the ingot crystal, electron diffraction studies are being made almost exclusively on this crystal.

Electron diffraction patterns were observed from both crystals after an argon sputtering treatment followed by a high-temperature annealing. In addition to the strong integer order hexagonal pattern characteristic of the germanium (111) plane, weaker 1/2 order beams were observed indicating a double spaced surface mesh in agreement with other workers (refs. 12, 27). Also detected were 1/8 order beams centered around the (1/2 1/2) beam (Fig. 12).

Deposition of sodium had the effect of first relaxing the double surface spacing at low coverages and then of dimming the pattern increasingly as a monolayer coverage was approached. Sodium coverage was monitored by measuring the work function of the crystal with a low energy electron gun (Sec. 2.1.4). It is believed that the sodium did not contribute significantly to the diffraction pattern (because of its relatively small atomic number) and that the changes observed resulted from substrate structure changes only.

Very remarkable changes in the diffraction pattern were observed while heating the crystal after deposition of sodium. Heating the crystal slightly (approximately 100°C) by radiation from a 200 watt lamp at low overlayer coverages produced a very strong Ge (111) 4-Na pattern (see Sec. 2.2.2 for definition of

notation) while low temperature heating at full coverage produced a Ge (111) 1-Na structure. Those basic structures were the only two stable structures observed during evaporation and deposition of sodium. Conversion of the Ge (111) 4-Na structure to the Ge (111) 1-Na structure and vice versa required heating in all cases. The temperature required for the conversion process depended on the history of the crystal as well as the overlayer coverage, suggesting that the sodium may have diffused into the crystal rather than evaporating during heating. This conjecture is supported by secondary electron emission results as explained in Sec. 2.2.3.

As mentioned above, the electron diffraction patterns obtained from sodium covered germanium surfaces are probably characteristic only of the germanium structure. The presence of sodium is manifested in the diffraction pattern only through the resulting changes in the germanium structure. Thus a unique surface model may be impossible with the present data. However no final conclusions are being made since further study and analysis are needed.

1.2.3 Secondary Electron Emission from Na-Covered Ge

Secondary electron emission may be separated into three processes: (1) the production of internal secondary electrons by excitation from the primary electron beam, (2) migration of the secondary electrons through the crystalline lattice to the vacuum-solid interface, and (3) the escape of the internal secondary electrons into the vacuum. The first two processes are determined by the bulk properties of the crystal and are relatively independent of sample treatment. The third process, however, is strongly dependent on the exact nature of the surface and is therefore influenced by environment and crystal treatment. Thus it is important to know the surface structure in a reliable study of secondary emission.

The surface properties which have important effects on the escape of internal secondary electrons are the electron affinity, internal electric field, and surface structure or order. The most important effect is the electron affinity which determines a lower bound on the internal electron energy required for escape into the vacuum. Surface structure strongly affects the energy loss mechanism of internal electrons as they approach the surface as well as their reflection coefficient from the vacuum-solid boundary. A third effect which is important for semiconductors and insulators is the internal electric field which is a function of bulk impurity concentration, surface order, and foreign atom overlayers. The internal electric field plays an important role whenever it extends over a distance comparable to the mean escape depth of secondary electrons.

The tube (Fig. 10) designed for electron diffraction studies of sodium overlayers on germanium is ideal for studying the effect of the surface condition on secondary electron emission. Cleaning the crystal by argon bombardment and subsequent observation of the electron diffraction pattern provides a high degree of confidence that a clean, well ordered surface has been obtained. Having obtained a clean surface, it is possible to observe the effect of electron affinity by deposition of a sodium overlayer. The electron affinity is inferred from work function measurements. Because the work function is affected by the internal field as well as the electron affinity, it is necessary to make some conjectures concerning the effect of sodium overlayers on the internal field.

The electron diffraction chamber is conveniently used for measuring secondary electron yields and energy distribution of the secondary electrons. The spherical grid geometry allows energy distribution curves of secondary electrons to be obtained quite accurately by employing the retarding field method. The derivative of the retarding field curves is obtained electronically (Fig. 20) and displayed directly on an X-Y recorder.

A series of secondary emission yield curves for various overlayer coverages were taken (Fig. 14) on the ingot germanium crystal. The maximum yield increased from a value of 1.29 after cleaning to 5.86 at optimum overlayer coverage. The primary electron energy at maximum yield increased from about 600 eV to about 2 k eV. The low energy end of the secondary emission yield curves is expanded and shown in Fig. 15. Structure in these curves is resolved at primary energies of about 9 eV and 23 eV and appears to be related to the reflection of low energy electrons. These observations are in agreement with experiments by Shullman and Ganichev (ref. 33).

Several curves of secondary electron emission vs. work function are demonstrated in semi-logarithmic plots shown in Figs. 16, 17. There appears to be an exponential dependence of secondary electron yield on work function over the major part of the interval explored. However, breaks in the curves are observed at a work function value near 4 eV which may have a relation to the observed break in the work function vs. overlayer coverage curves on germanium (Fig. 18). Possible interpretation of the break is given in terms of internal field changes resulting from sodium overlayer coverage.

The secondary yield is calculated by using the total number of electrons emitted from the solid. One should distinguish between three obvious categories: (a) elastically reflected primaries, (b) inelastically reflected primaries, and (c) "true" secondaries. Energy distribution curves of the secondary electrons resolve the three types of emitted electrons. The low

energy or "slow" peak corresponds to the true secondaries. The peak centered about the primary energy corresponds to the elastically scattered electrons while the peaks having energy near the primary energy correspond to primary electrons which suffer inelastic collisions. The energy difference between the elastic peak and the inelastic peaks correspond to characteristic energy losses resulting from quantum excitations in the crystal.

Energy distribution curves for clean germanium are illustrated in Fig. 21. A characteristic energy loss of about 17 eV is observed which is interpreted as an electron plasma excitation. A broadening of the slow peak was observed with decreasing primary energy. This is consistent with the fact that electron affinity reduction is most effective in enhancing the yield at high primary energies (compare Figs. 16, 17). Casual observation of the elastic and inelastic primary peaks indicated no obvious change with Na coverage. Improved equipment obtained recently should result in greater accuracy of those measurements enabling the effect of electron affinity on the energy distribution to be resolved.

1.2.4 Field-Emission Microscopy

As a complement to the other studies of the Na:Ge system, a study using the technique of field-emission microscopy was initiated this period. This technique allows the simultaneous study of several crystal faces, the cleanliness of which can be observed at any time. The high fields inherent in the device may be employed to clean the surface by field desorption of the contaminating films. As is well known, the field-emission microscope is particularly suited for the study of adsorption phenomena. In particular, work function changes and the characteristic energies associated with adsorption and surface diffusion may be determined, and the anisotropy in coverage observed for the Na:Ge system. Thus the technique will be a very valuable addition to those already available in the laboratory.

Observations of a clean tungsten emitter have been made in a simple microscope. An improved microscope has been constructed for observation of Ge emitters and for the proposed adsorption studies. A Ge emitter structure (Fig. 24) was designed which forms its own heating loop and which can be accommodated in a commercial electron microscope for determination of the emitter geometry. The geometry of the emitter tip must be known if quantitative evaluation of the field emission data is to be made. Several emitters employing this design have been fabricated. A simplified emitter structure has been employed temporarily until the techniques pertinent to tip formation and cleaning have been developed.

A basic requirement of the proposed studies is the attainment of an atomically clean emitter surface after the high vacuum conditions have been attained. Attempts to clean Ge emitters using field desorption have, so far, been unsuccessful. An improved field desorption technique will be used in the future.

1.3 Studies of the Compound Na_3Sb

1.3.1 Studies of Na_3Sb Films

The alkali antimonide family of semiconducting films is of considerable interest because of their outstanding photoemissive properties. Of the family, Cs_3Sb has been the most widely studied, no doubt due to its high quantum efficiency in the visible spectrum. Probably because of its relatively low efficiency and high threshold energy, Na_3Sb has received very little attention. Na_3Sb was chosen for the initial investigation of this phase of the research in an effort to gain an insight into the mechanism responsible for the high quantum efficiency associated with the whole group of alkali antimonides as well as to obtain specific information concerning the semiconducting properties of this relatively unstudied compound. Furthermore, it will be advantageous to compare semiconducting properties of the films with those of the bulk Na_3Sb being studied in another phase of the project.

It is the intention of this investigation to correlate the photoemissive yield with semiconducting properties and deposition parameters by performing conductivity, photoconductivity, Hall effect, lifetime, photoelectric and energy distribution measurements on the films during and subsequent to film deposition and formation.

A beam evaporation method for film deposition appeared to be better suited to this type of investigation than the more conventional vapor reaction methods. A large part of this interval was devoted to the development of the evaporation method and suitable means of rate control. An attempt was made to obtain a measurable rate control by means of a double evaporation technique, whereby bulk Na and Sb were evaporated onto metal heater blocks and subsequently re-evaporated at known and controllable temperatures. However, due to several difficulties, this attempt was discontinued.

A new vacuum evaporation system (Fig. 26) was developed in which the materials are evaporated from metal containers, the temperatures of which are known and easily controlled. Bulk Sb is placed in one evaporator prior to evacuation and Na is vacuum distilled into the other evaporator. The evaporation rate is determined by measuring the frequency shift of a vibrating quartz

crystal (Fig. 25) exposed to the evaporation; the frequency shift is proportional to the mass of the deposited material. It is advantageous to calibrate this device by measuring the thickness of several evaporated films with multiple beam interference techniques. While performing such a calibration it is worthwhile to determine some preliminary photoemissive yield dependence on film thickness, composition and temperature.

For these purposes the evaporation unit was connected to a trolley system containing 12 movable substrates with evaporated Au electrodes. The final thickness of the films deposited on these substrates can be measured with the interference techniques mentioned. Also included are provisions for measuring substrate temperature and photoemissive yield during film deposition and heating.

To date, only one Na_3Sb film has been formed in this system. Na was deposited in varying amounts on a previously deposited Sb layer while the photoemissive yield of the sample was measured at several stages of the Na deposition; heating of the sample was also monitored with photoemission measurements. Accompanying these depositions and heatings were subsequent spectral yield measurements. The final peak yield was 2×10^{-2} electrons/incident quantum.

The results of this one experiment led to qualitative speculations concerning the film formation process. It appears that near stoichiometry was obtained in the photosensitive surface region, with much less Na present than that necessary for complete stoichiometry. Although heating did produce some yield changes, activation appeared to go nearly to completion at room temperature. It was also possible to make some speculations concerning the effects on photoemissive yield produced by Na in excess of stoichiometric proportions.

1.3.2 Studies of Bulk Na_3Sb

The most efficient photoemitters currently available are the group of alkali antimonides. Although thin films of these compounds have been extensively studied and are known to be semiconductors, they have never been prepared in bulk form for the purpose of carrying out standard semiconductor evaluation experiments. It is the purpose of this phase of the project to prepare one of the alkali antimonides (viz., Na_3Sb) in a compact, polycrystalline form and to measure the resistivity and Hall effect versus temperature for selected specimens. Such information should provide an improved understanding of the defect levels and the electron scattering processes and should be regarded as only a first step in a program which later might include such measurements as magnetoresistance, photoconductivity or other types which the preliminary work may prove to be desirable.

A glovebox system in which the preparation and measurements will be carried out was constructed. The subassemblies of an argon purification train were purchased. These subassemblies and the glovebox system were connected to form a system in which Na_3Sb can be made and tested (Fig. 30).

1.4 Anomalous Photovoltaic Effects in Semiconductor Films

1.4.1 Evaporated Ge Films

During this period, a study of the anomalous photovoltaic effect in evaporated semiconducting films was initiated. Anomalous photovoltages two orders of magnitude greater than the band gap have been reported in CdTe, Ge, and Si films (refs. 62, 63). The purpose of this phase of the research effort is to attempt to discover the mechanism responsible for these anomalous photovoltages and to determine the conditions necessary for the production of this mechanism.

A vacuum system, in which the films may be evaporated and measurements made, has been constructed. Special attention has been given to the angle of deposition, substrate temperature, and the pressure of residual gases.

1.4.2 Sputtered Ge Films

During this period, the construction of a tube for studying photovoltaic effects of sputtered Ge films was initiated. The results can be compared with those from evaporated films to investigate the controlling parameters of the anomalous photovoltaic effects.

2. SUMMARY OF TECHNICAL PROGRESS

2.1 Experimental Techniques

2.1.1 Vacuum Techniques

Experimental studies of surface properties require an ultrahigh vacuum environment, free of contaminating oil or mercury vapors. The possibility of such contamination is always present in diffusion pump systems, no matter how well they are trapped. Ion pumps (refs. 8, 9), or titanium sputter pumps as they are called in this laboratory, are used exclusively on this project for all high vacuum work, including the critical surface studies. Since no grease valves or other possible sources of oil or mercury vapors are used in our vacuum systems, the possibility of this type of contamination is excluded.

Shown in Fig. 1 are the sputter pumps constructed in this laboratory. These differ only in minor respects from the 911-1402 Vac Ion pump available commercially from Varian Associates. The

latter is an all-metal pump whereas the pumps used here employ a Pyrex envelope. The glass envelopes are better adapted to our experimental tubes, permit visual inspection of the pump operation and condition, and are readily constructed with available facilities. The dimensions of the pump where chosen so as to be accommodated by the pole faces of a Varian 911-0001 permanent magnet. The pump is operated with the anode at 3-5 kV dc with respect to the cathode and in a magnetic field of approximately 1200 gauss perpendicular to the plane of the cathode. In most cases, magnetic and electrostatic shielding of the pump is required to prevent the high fields present from interfering with electrical measurements. Also, at least one bend is introduced in the tabulation connecting the pump to the system in order to intercept stray sputtered Ti atoms.

The starting procedure for the sputter pumps is as follows: The system is first pumped down to a pressure of about 0.5-1 Torr with a mechanical forepump (cryogenic forepumps are sometimes used instead of the mechanical forepumps). A titanium flash bulb, consisting of a tungsten filament wrapped with titanium wire, is used to reduce the pressure to the range where the sputter pump can be started. After outgassing the filament of the flashbulb, the forepump is sealed off from the system. The filament is then heated to incandescence, and the titanium is evaporated onto the walls of the bulb. The freshly evaporated titanium getters strongly, reducing the pressure to about 10^{-3} Torr in five minutes or so. A voltage is then applied to the pump until a discharge is initiated. This usually occurs at about 600 volts. The voltage is increased slowly; usually the pump current is kept below 20 mA. However, as much as 50 watts of power can be expended for short periods during the starting procedure if the pump envelope is cooled with a fan. After reaching 1000 volts, it is usually possible to increase the voltage rapidly to the full operating voltage with no appreciable increase in pump current. The flashbulb is sealed off from the system once the pump is clearly operating well.

Typically, a pressure of 1×10^{-7} Torr is reached in an hour or so. Pressures of the order of 10^{-10} Torr or lower are obtained regularly after a bakeout at 350°C for about 12 hours. The pump and magnet are baked with the system. The pump current is limited to 2 or 3 mA during bakeout (and later outgassing operations) by limiting the rate of temperature rise. After completion of the bakeout, further outgassing of filaments and other metal parts is accomplished by conventional methods employed in all high vacuum work. Radio frequency heating is used for the most part, but electron bombardment, thermal radiation and, of course, resistive heating are also used. When required, the adjacent glass is cooled by a fan.

A method developed in this laboratory which is particularly convenient for heating small parts consists of focusing the radiation from an incandescent source onto the part being heated. Usually a 500 watt projection lamp with an aluminized spherical reflector is employed for this purpose and the temperatures attained are remarkably high (e.g., 1100°C for a 1/2" diameter x .01" thick tungsten disk). This method has been found to be particularly useful for heating the Ge crystal samples being studied under this contract as well as for other nonconductors. Sensitive measurements can be made during heating because the light source is relatively noiseless.

All of the pressure measurements below 10^{-5} Torr are made using calibration curves of pressure versus sputter-pump current. This data has been obtained in this laboratory using a Bayard-Alpert type ion gauge as a standard. The calibration obtained differs very little from that quoted by Varian for the 911-1402 Vac Ion pump when one accounts for the difference in size of the two pumps. Pressure measurements in the approximate range of 10^{-5} to 1 Torr, when required, are made with a high-pressure triode ionization gauge designed after Schulz and Phelps (ref. 10). These are used, for example, to measure the argon pressure in the sputtering experiments.

Except as noted, the gas-admission systems employ Granville-Phillips Type C ultrahigh vacuum valves. These are greaseless, bakeable, all-metal valves which can be used as controlled leaks.

In an attempt to provide a more versatile and contamination-free vacuum environment in which to perform photoemission studies, an all-metal, bell jar type ultrahigh vacuum system has been designed and constructed. This all stainless steel system is bakeable and utilizes cryogenic forepumps and a titanium sputter pump. All seals are made by means of shear-seal type flanges and metal gaskets. Provision has also been made to automatically maintain the pressure of the vacuum system at any desired pressure in the range from 10^{-3} to 10^{-9} Torr. Control is accomplished by means of a servo-controlled Granville-Phillips variable leak valve. This feature was incorporated because this particular system is to be used in gas adsorption studies.

There are a number of advantages to be gained in the use of this type of system as compared with the conventional method of using glass envelopes. At present, each experiment requires the construction of a specialized glass envelope configuration which is generally unusable for other experiments. Many times small modifications evolved in the course of an experiment require the construction of a new glass envelope. In contrast with this situation, the base plate of this vacuum system includes a number of electrical feed-throughs and a rotary motion feed-through so that many different types of experiments can be carried

out in the relatively large space provided in the bell jar. Speed in assembling and modifying electrode structures, accurate and reproducible alignment of electron guns, etc., are also some of the advantages of the new system. In addition, the problems involving shielding from electrical noise are simplified in that a grounded all-metal system will provide excellent shielding.

On the basis of early experience there seems to be some disadvantages associated with an all-metal bell jar system. Visibility of the internal apparatus is limited to areas directly opposite the viewing ports. Also, the metal bell jar precludes the use of rf heating to outgas internal metallic structures. However, for many applications, including the photovoltaic studies for which the system is currently being used, it appears that these disadvantages will present no great problem.

2.1.2 Argon Sputtering

Since a clean surface is of prime importance in the study of surfaces, it was essential that a method be developed by which an atomically clean surface could be obtained. The method used for all the work on Ge and Si was argon ion bombardment. The technique used was a slight modification of that developed by Farnsworth and his associates (refs. 11, 12). The initial version of the discharge tube used to create an argon plasma has been previously described (ref. 6, p. 7). During this period both the discharge tube and the method of purifying the argon have been modified.

The argon used is spectroscopically pure argon supplied by the Air Reduction Company in one liter Pyrex flasks. The argon is purified by allowing it to remain in contact with freshly flashed Ti and Mo films in the inlet line. These films serve to "getter" impurities from the argon. The argon is further purified in a cataphoresis tube of the type described by Riesz and Dicke (ref. 13). The cataphoresis tube consists of a section of 12 mm O.D. Pyrex tubing, approximately 40 cm long. The anode is a flat 5/8" Ti disk. The cathode is a hollow Ti cylinder, 3/8" D x 3/4" long. The argon pressure in the cataphoresis tube is in the range 1 to 20 Torr. The tube voltage in operation is 200-225 volts and the discharge current is 50-60 mA. A ballast resistor is used to limit the discharge current. The discharge is maintained for at least 24 hours before the argon is admitted to the main body of the tube. The argon is admitted from the anode end of the cataphoresis tube. Riesz and Dicke claim that the impurity concentration at the anode end is 10^{-4} times that at the cathode end of the cataphoresis tube.

The modified version of the discharge tube used to create the argon plasma which is needed for sputtering is shown schematically in Fig. 2. The cathode consists of 4..001" x .040"

W ribbon filaments in parallel. A Ta heat shield surrounds the filaments to prevent excessive heating of the tube envelope. The anode is a Ti ring, 1 1/2" in diameter, spaced 1" from the cathode. This anode has a 3/4" diameter hole in the center of it. Also included is a W disk, 1 1/4" in diameter, spaced 1" from the anode. This disk is held at cathode potential during operation. A magnetic field of the order of 180 gauss is applied along the axis of the discharge tube. The field is produced by two coils which surround the discharge tube. The field serves to confine the plasma to the central portion of the discharge tube and allows the discharge to be maintained at lower argon pressures than were previously possible. This is desirable since it allows the sputter pump to be started with less difficulty than experienced previously. Secondly, since less argon is pumped each time, the useful life of the pump is extended.

The filament current used is 23 amps. A potential of 30 volts is maintained between anode and cathode. The discharge current is approximately 1/2 amp for an argon pressure in the range 5×10^{-4} to 10^{-3} Torr.

Two types of auxiliary anodes have been used. Both are approximately 3/4" in diameter x 1/2" long. A W mesh is welded to the open end of the auxiliary anode, in such a fashion that it is also in contact with the tube envelope. This anode and mesh arrangement prevents the plasma from entering the main body of the tube and sputtering metal parts (e.g., the W trolley rods) which are at crystal potential. The first type of auxiliary anode (illustrated in Fig. 2) has a closed end plate, and a slot in the side through which the crystal is inserted during sputtering. The second type has a square hole in the end plate and the crystal is moved directly behind this during sputtering. The auxiliary anode is held at main anode potential during sputtering, and the bombarding energy is determined by the potential maintained between the anode and the crystal. With this arrangement, and the conditions mentioned previously, a bombarding current of 50-100 $\mu A/cm^2$ can be drawn to the target.

It should be noted that although this arrangement has been used only in the experiments on Ge and Si, it can be used to clean metal surfaces also, should the need arise. Furthermore, by applying an rf voltage to the crystal, insulators can also be sputtered.

2.1.3 Development of a Method for Na Deposition

The initial version of the ion gun used to deposit Na has been previously described (ref. 4, p. 2). The sodium ions were in this case obtained by thermal ionization on a tungsten filament, of atoms evaporating from a sodium reservoir. Certain difficulties

with this gun manifested themselves in the study on Si (ref. 6, p. 21). First it was found that Na atoms could reach the target when the gun was in operation. This meant that the integrated ion current was not an accurate measure of the amount of Na deposited, since the neutral Na atoms gave no contribution to the current to the crystal. Secondly, it was found that the Na deposited on the anodes of the gun made them sensitive to light from the hot W filaments used in the gun. The resulting photocurrent was collected by the crystal and this masked the ion current. Finally, some ions were deposited on the tube envelope between the last anode of the ion gun and the target, and this charge affected the uniformity of the ion beam. These difficulties suggested that two changes be made in the gun design which would considerably improve its performance. The Na atoms which reached the target presumably came from Na which had been deposited on the glass walls in the vicinity of the filaments. When the filaments were heated, the glass was also heated by radiation, and this Na would be evaporated onto the crystal. To alleviate this difficulty, a collimator was placed between the Na reservoir and the filaments. The collimator consisted of two Pyrex disks, sealed to the walls of the tube. Each disk had a small circular hole in it, so that a Na beam was directed onto the filaments. The geometry was such that the Na atoms which did not strike the filaments would be deposited on a cool portion of the glass walls where re-evaporation would be unlikely. Furthermore, if this Na were re-evaporated, it could not reach the target.

The second modification which was made consisted of the addition of a cylindrical grid which extended from the ion gun to the target. This grid served two purposes. First, it collected the photoelectrons emitted from the sensitive surfaces of the ion gun. Secondly, by placing a small potential on it, any effects due to glass charging were eliminated. Since the ions passed down the axis of this cylindrical grid, it could also be used to improve the focus of the gun.

This modified version of the ion gun was mounted in the tube structure described in Sec. 2.2.1 of this report. The performance of the ion gun was checked using the same Ge crystal that was used in the experiment described in that section. The filaments of the ion gun and the Na reservoir were heated, but the crystal was biased so that no Na ions could reach it. The crystal was allowed to remain in front of the ion gun for 20 minutes after which time the work function was again measured. No change from the value corresponding to the cleaned surface was obtained. The present method of measuring the work function detects a work function shift of less than .05 eV. For the cleaned surface, this corresponds to roughly 1 or 2% of a monolayer. Since one monolayer can be deposited quite easily

in 20 minutes with the ion gun, it was concluded that less than 2% of the Na striking the crystal will be atoms, under normal operating conditions.

The ion gun anode and target were then biased for normal operation and Na was deposited. During this deposition there was no evidence of glass charging, or of a photoemission current to the crystal. In order to check for the latter possibility, light from an external source was shone on the anodes of the ion gun. No charge in the current to the crystal was observed. During this deposition one further undesirable feature of the ion gun was revealed. Using the present method of obtaining Na in the tube (i.e., the reaction of Na_2CrO_4 and Si in a nickel container) sufficient Na could not be produced to obtain a complete curve of work function vs. coverage over the range 0-2 monolayers. This method of Na production is described in further detail elsewhere (ref. 1, p. 12). This problem meant that either a larger supply of Na must be introduced to the tube, or a new ion source must be found. The latter alternative was pursued.

It is well known that certain of the aluminosilicates emit a positive ion current when heated (refs. 14, 15). In particular, the work of Blewett shows that the compound "β-Eucryptite" is an efficient Li ion emitter, when heated to temperatures of the order of 1000°C. The chemical formula for "β-Eucryptite" is $LiAlSiO_4$. This suggests that a type A zeolite, which has the chemical formula $NaAlSiO_4$, might be an efficient Na ion emitter. To test this postulate, a small amount of type 4A zeolite was melted in a quartz crucible. A .010" Pt-10% Rh filament was dipped into the melted zeolite and removed rapidly. A small amount of the zeolite remained on the filament. The filament was then heated in vacuum and a current of positive ions was drawn to a collector which was biased negatively. Currents up to 500 μA could be drawn at a collector voltage of -1000 V, when the zeolite was heated to 1000°C. No evidence of Na depletion was seen over a period of 1 hour, although the current would decrease slightly over longer periods of time.

A similar zeolite emitter was constructed and mounted in a modified ion gun. This structure is shown in Fig. 3. A flat Ta shield was placed at the end of the cylindrical grid structure. This shield has a 1 cm x 1 cm square hole in the center of it, and the crystal could be moved behind it during deposition; so ions would only be deposited on the cleaned portion of the crystal. This shield was maintained at crystal potential; it also served to improve the uniformity of the ion beam striking the crystal. The anodes of the gun are 3/4" in diameter and 3/4" long. The cylindrical grid is 1 1/4" in diameter and is 3" long. A Ni grid is placed between the ion emitter and

the first anode, and serves to control the ion current reaching the target. The entire structure is mounted on sapphire rods. The uniformity of the deposition was checked by a method described in Sec. 2.2.1. The following are typical of the potentials applied during deposition: control grid = - 5 V; first anode = - 400 V; second anode = - 60 V; cylindrical grid = - 12 V; Ta shield and target = - 22 1/2 V. (The potentials are with respect to the filament.) When the emitter is heated to approximately 800°C, a target current of the order of 0.1 μA is obtained. This current is strongly influenced by emitter temperature and control grid bias.

This type of ion source has one further advantage over the previous source, that is, it may be used as an ion source of other alkali metals. Studies have been made of the efficiency and extent of Na replacement (in the zeolite structure) by other alkali ions (refs. 16 and 17). These results show that a large fraction of the Na ions may be replaced by other ions, in an exchange reaction. Presumably these ions could also be emitted in a similar manner. In particular, it is now feasible to consider overlayer experiments using, for example, Cs. These experiments were previously extremely difficult to perform because of the high vapor pressure of Cs, and because of difficulties in obtaining a pure source of the alkali metals in a vacuum tube. To date, no work has been done on the fabrication of such ion sources.

An alternative method of Na deposition was also developed. This consisted of a thermal evaporator composed of a Na reservoir and a glass collimator similar to that used in the first modification of the ion gun. Since efficient use is made of the Na in the thermal evaporator, the Na may be produced by the $Na_2CrO_4 + Si$ reaction. The absolute amount of Na deposited in this manner cannot be measured, but relative amounts can be measured by holding the evaporator at a constant temperature, and measuring the length of time that the crystal is exposed to the Na beam.

2.1.4 Measurement of Work Function

Two methods have been developed to measure the work function shift of the crystal. The first method involves the use of the shift in I-V characteristics of a diode, using the crystal as the anode. In order to obtain a monoenergetic electron beam at normal incidence, a low energy electron gun was needed. The gun design chosen was a modified version (ref. 18) of the Farnsworth gun (ref. 19). This gun uses an electrostatic deflection system to prevent tungsten and other impurities (which may be evaporated from the filament) from passing directly through the gun to the target. The gun is shown schematically

in Fig. 4a. All parts are Advance alloy except for the filament and filament leads. The filament is of tungsten, .001" x .040" x 3/8" long, and the filament leads are .040" Ta. In Fig. 4a, F is the filament and H the heat shield. Electrons are accelerated to G, deflected by G_2 to A, and then focused by B. A shield S prevents electrons from escaping between A and B. The opening in G_1 and A is 3/16" in diameter and has W grids over it, with 20 .001" W wires over each opening. A and B are cylinders, 3/4" in diameter. They are constructed so that the middle diaphragm in B is 3/4" from the diaphragm in A, and 3/4" from the last diaphragm in B. The holes in the diaphragms in B are 1/16" in diameter. The entire gun is mounted on .060" sapphire rod insulators for mechanical stability.

In normal operation, G_1, A, and B are given the same small positive potential (e.g., 8 volts) with respect to the center tap of the filament power supply. G_2 is given a suitable negative potential to deflect the electrons through the hole in A. This potential is typically in the range - 10 to - 15 volts, and is dependent on the value of the other potentials. S is given a larger negative potential (e.g., - 150 volts). Typical filament currents are 5 A, rms, and the target current for the above conditions is of the order of .5 μA.

The V-I curves are obtained using the circuit shown in Fig. 4b. A General Radio Company meter, model 1230 A, is used as the dc amplifier. The output of the amplifier is applied to the Y axis of an X-Y recorder and the target voltage is applied to the X axis. Typical curves obtained with this arrangement are shown in Fig. 5. Curves B and C illustrate the method used to measure the work function shift, $\Delta\phi$. The curves are typical of those obtained for a clean surface, or for a surface with a low value of coverage. A curve typical of a "dirty" surface, i.e., before ion bombardment, is illustrated by A. These curves show a large increase (about 20% or more of the saturated value) in the target current, at target voltages just above the cutoff point. Thus the shape of these curves can be used to give some indication of the surface condition. Presumably this large increase is caused by a rapidly changing electron reflection coefficient at low electron energies. Curves of the type illustrated by D are often obtained at large values of overlayer coverage. These curves also show an increase in target current at target voltages just above the cutoff point, but the increase is usually 5% or less of the saturated current value. This can probably also be attributed to a change in reflection coefficient (due to the presence of Na) at low energies.

The curves of Fig. 5 illustrate that the beam of electrons is not monoenergetic, but contain an energy spread of approximately 0.8 eV (90% of the current is cut off in a range of

target voltage of 0.8 V). It was postulated that such a large energy spread could have arisen because a unipotential cathode was not used. This postulate was checked by heating the filament with half wave rectified ac. A special circuit was used so that the target current was measured only in that portion of the cycle during which no filament current was flowing, i.e., when all emitting areas of the cathode were at the same potential. No detectable sharpening of the curves was observed. Evidently the major contributing factors to the energy spread are non-normal incidence and a reflection coefficient which is strongly dependent on electron energy, near zero electron energy. The absolute accuracy of this gun is not good due to the uncertainty in the work function of the cathode and the energy spread in the beam. However, the relative accuracy is much better. Work function shifts of .03 eV can be measured.

In order to measure work function shifts more accurately, a method was developed which would measure the contact potential difference (CPD) between a reference material and the Ge crystal. The technique used is a modification of the Kelvin (or vibrating plate) method (ref. 20) for measuring CPD. When two surfaces with different work functions are brought near each other, a field exists between them, and surface charges will be present. As the spacing between these surfaces is varied, the field will vary, and hence the surface charge will vary. This varying surface charge will cause current to flow in an external circuit connecting the two plates. If a voltage is now applied between these plates, the field between them will change. If the field due to the applied voltage just cancels the original field, no surface charge will be present, and no current will flow in the external circuits. Thus the applied voltage can be varied until a null is achieved, and the value of voltage necessary to achieve the null is the CPD of the two materials. If the work function of the reference plate is known, the work function of the unknown can be obtained.

The device which has been developed in this laboratory is shown schematically in Fig. 6a. The reference plate is a 1/4" x 1/4" gold sheet. It is mounted on a .040" Ti wire. The spacing is varied by coupling magnetically to a Kovar strip which is welded to the Ti wire. The spacing can be varied periodically with time by placing an ac signal on the drive coil. The frequency of this signal is one-half the frequency of vibration. In the present arrangement, the natural frequency of the gold reference is 35 cps. A 17.5 cps signal, supplied by a Hewlett-Packard 200 CD oscillator and a 35 watt audio amplifier is used to drive the coil. The spacing between the Au and the crystal is 1 mm. The work function of the Au is determined by the photoelectric (Fowler) method (ref. 21). Light is passed through the quartz window and the emitted photoelectrons are collected

by the "trolley" rods. After the work function of the Au reference has been determined, the crystal can be moved into position in front of the Au and the CPD can be measured. The circuit used is shown in Fig. 6b. The bias voltage is applied using a 3 volt battery and a General Radio Company Model 1454 A Precision Voltage Divider. The output signal is applied to the grid of an electrometer tube (CK 5889), and the output of this preamplifier is fed to a tuned amplifier. This amplifier is an Electronics, Missile and Communications, Inc. Model RJB, tuned to 35 cps.

In preliminary tests with the vibrating capacitor, it was found that the work function shift could be measured to .003 eV, that is, a change of the bias voltage by $\pm$ .003 volts from the null value would produce a detectable change in the output of the tuned amplifier. It was also found that glass charging in the vicinity of gold reference was a problem. If the glass became charged a field would exist between the glass and the gold reference plate. Any motion of the reference plate would produce a change in this field, and a current would flow in the external circuit. Since this current would change the apparent current due to the CPD of the gold and the Ge, the null voltage would also be changed, and an erroneous CPD would be measured. It was found that whenever the crystal would be moved along the "trolley" rods, the glass would become charged. This was manifested by an apparently unstable CPD, that is, one that changed with time. After the crystal had been allowed to remain in front of the Au reference for approximately 30-40 minutes, no change in the CPD could be detected. Apparently after this time all the charge on the glass had decayed away and the true CPD was being measured. This effect can probably be alleviated, or at least substantially reduced, by forming a conductive coating on the inside walls of the tube, in the region about the vibrating capacitor. This would prevent any possibility of glass charging.

2.1.5 Preparation of Hemispherical Grids

A method for constructing high-transmission hemispherical grids for use in an electron diffraction chamber has been developed. The grids have the following advantages: (1) the transmission is nearly uniform over the entire hemisphere, (2) the grids are bakeable to high temperatures and (3) they are constructed completely of nonmagnetic materials.

Chromium was chosen as the plating metal because its hardness results in a very rigid screen. However, it was found that chromium could not be plated directly to the tungsten mesh because the minimum plating current required for the process caused a large variation in potential over the screen, resulting

in nonuniform coverage. This problem was circumvented by first plating a layer of copper, which requires much less plating current, with sufficient thickness to carry the required current for the chromium plating process.

The method of construction is illustrated in Fig. 7(a). A knitted tungsten mesh type 0005 R 120 W 2-1/8 obtained from the Metal Textile Corp., Roselle, New Jersey, was stretched over a spherical Pyrex flask and held in place with a .015" Advance wire stretched around the sphere circumference. The wire became attached to the mesh during plating and gave necessary support to the grid upon removal from the flask. The flask was lowered into the plating solution such that the wire ring was submerged (Fig. 7(a)). Very uniform plating was obtained when the Advance wire ring was used as an electrical connection to the tungsten mesh and a cylinder was used as an anode. After removal of the screen from the sphere, a .010" Advance strip was welded around the inner diameter of the hemisphere (Fig. 7(b)) such that the mesh was "sandwiched" between the wire and the strip. This gave permanent support to the screen as well as providing a convenient means for mounting the grid.

A general copper plating bath (ref. 22) was used for the initial plating and a hard chromium plate (ref. 23) for the final plating. Copper plating current densities of 70 mA per in^2 were used for the duration of 20 minutes. Chromium plating required a current density of 2 amps per in^2 for 75 minutes. A copper anode was used for the copper plating and a lead anode for the chromium plating. Extreme cleanliness in the chromium plating procedure is needed to produce good results.

2.2 Overlayer Studies

2.2.1 A Study of the Influence of Adsorbed Na on the Work Function of Ge

This experiment consists of cleaning the surface of the crystal (a four-step process), depositing known amounts of Na on the crystal, and measuring the work function of the crystal. In the present tube, Na can be deposited by two methods, both of which are described in Sec. 2.1.3. Changes in work function can be measured by two methods, described in Sec. 2.1.4. The experimental procedure is described in more detail in the following sections.

Crystal Cleaning Procedure for Work Function Studies

The general method used for producing a clean Ge surface has been previously outlined (ref. 6, p. 4). The cleaning procedure consists of four parts:

1. chemical etching

2. outgassing

3. argon ion bombardment

4. annealing.

The crystal is etched previous to insertion into the experimental tube. The etch used is a standard CP-4 etch consisting of 25 parts fuming nitric acid, 15 parts glacial acetic acid, 15 parts hydrofluoric acid (49%), and 1 part bromine. The etching solution is kept at 0°C and the etching time is 1 minute. Following the etch, the crystal is rinsed by replacing the solution with deionized water. The crystal is rinsed twice in deionized water, and once in ethyl alcohol. After the rinse, the crystal is placed in the tube, and the tube is sealed as rapidly as possible. The crystal is exposed to a prepurified nitrogen atmosphere from the time it is removed from the alcohol until the tube is evacuated.

After the tube has been evacuated and "processed" (processing consists of baking at approximately 335°C and outgassing all metal parts; see Sec. 2.1.1), the crystal is ion-bombarded (sputtered). The technique used for argon sputtering is discussed in detail in Sec. 2.1.2. This first ion-bombardment seems to remove any impurities from the surface which may have been deposited during the final glassblowing on the tube. In particular, it prevents the possibility of the diffusion of boron into the crystal during the long outgassing treatment. This effect has been observed by Allen et al., (ref. 24) in a series of experiments on Si.

After the first ion-bombardment, the crystal is heated to approximately 700 - 750°C for 115 hours. The heating is accomplished by focusing the light from a 200 watt projection lamp onto the crystal. A 3" hemispherical mirror is used to focus the light. After the long outgassing period, the crystal is again ion-bombarded. This is followed by an anneal treatment at approximately 600 - 700°C for 15 - 20 minutes. The crystal is given two more ion-bombardment-anneal treatments.

After each ion-bombardment and annealing, the work function was measured using the low energy electron gun described in Sec. 2.1.4. It was found that after the first three ion-bombardment-anneal treatments, the work function had changed, but then remained constant after the fourth. This was taken to indicate that a clean surface had been obtained. It was also observed that after each annealing the work function was .10 - .13 eV higher than the value immediately following the

previous ion-bombardment treatment. This was observed even when the crystal surface was clean, and may be due to a reordering of the surface atoms during annealing.

The performance of the ion gun used to deposit Na was then checked, as described in Sec. 2.1.3 of this report. After these tests were completed, the crystal was again ion bombarded and annealed, and the work function was remeasured. The value previously obtained for the clean surface was again measured, using the low energy electron gun.

Overlayer Studies Using the Thermal Evaporator

After the recleaning described above, the thermal evaporator was heated with an oven. The temperature of the glass wall of the Na reservoir could be monitored with a Pt, Pt-10% Rh thermocouple. After the wall had reached an equilibrium temperature of 83°C, the crystal was placed in front of it for a 2 minute period. The work function was then measured. This cycle (deposit Na for 2 minutes, and then measure the work function) was repeated until the work function remained constant, indicating a coverage of several monolayers. This cycle was also used for all subsequent measurements, unless otherwise noted.

In the first attempt at these measurements, the temperature fluctuated during the run. This fluctuation introduced scatter in the data, since the overlayer coverage was not linearly related to the exposure time. This temperature fluctuation was due to slight changes in the oven voltage (and hence oven temperature) and also to air currents over the oven. In subsequent measurements, the oven voltage was held constant with a constant-voltage transformer and an insulating shield was placed around the oven and evaporator arm to reduce the stray air currents. With these precautions, the evaporator temperature could usually be held constant to $\pm$ 1°C or less.

The Na was removed from the crystal by heating. It was observed that if the crystal was heated to a given temperature for about 10 minutes, further heating at the same temperature would not remove any more Na, since the work function would remain constant. This was also observed when Na was evaporated from a Si crystal in a previous experiment (ref. 6, p. 20). However, in the experiment on Si, a work function maximum was observed in the evaporation process; no such maximum was observed in the present measurements.

After the work function had been returned to the value for the clean surface, the surface was again ion-bombarded and the crystal was re-annealed. The evaporator was then heated to

a temperature of 79.9°C. During this run, the evaporator temperature remained constant to within ± 1°C. Measurements were again taken after every two minutes of exposure time.

The results are shown in Fig. 8a. The curve differed considerably from the one relating photoelectric threshold to overlayer thickness obtained previously (ref. 5, Fig. 5a) and also from those relating work function to overlayer thickness for Ge:Ba, Ge:BaO, InSb:BaO, and Ta:BaO (ref. 5, Figs. 5b and 6). Instead of having one sharp break separating two linear portions, the present data displays several breaks. This typical behavior was reproducible in a sense. Several curves were obtained, starting each time from a surface that had been ion-bombarded and annealed. The general shape was always obtained, and the breaks in the curve occurred at the same energy each time.

The value of the work function for the cleaned surface (4.45 eV) seems low, but was determined assuming a value of 4.54 eV for the work function of W. If the work function of the filament were higher, say 4.80 eV, then the work function of the cleaned surface would be 4.70 eV, in better agreement with the values obtained by other investigators (ref. 25). A second argument to strengthen this suggestion is that the work function of the target for large values of exposure time should be just that of Na, approximately 2.3 eV (ref. 26). This is the value one obtains from the present data if the work function of the filament is assumed to be 4.8 eV.

In order to check whether the same behavior could be obtained without ion bombardment of the surface, the Na was removed by a gentle heating, which was followed by a heat treatment at approximately 700°C for 15 minutes. The standard 2 minute deposition-measurement cycle was again used and the results shown in Fig. 8b were obtained. The evaporator temperature was 83.0°C during this run and remained constant within ± 0.15°C. The same general shape was again obtained, with breaks occurring at the same values of work function as in previous runs.

In order to determine whether the nearly flat portion of the curve (Fig. 8) which occurs at a work function of about 2.9 eV might be due to a "rearrangement" of Na on the surface, the crystal was again gently heated to remove the Na, and then ion bombarded and annealed. Na was again deposited and measurements made after every two minutes of exposure to the evaporator. When the flat portion of the curve was reached, however, Na was deposited for two minutes, and then the crystal was removed from its position in front of the evaporator. The crystal was allowed to stand for 10 minutes before a measurement was made. This procedure was repeated until the steeper portion of the curve was reached, after which the standard deposition-measurement cycle was again used. The results are shown in

Fig. 8c. During this run, the evaporator temperature was 86.4°C and remained constant within ± 0.1°C. Therefore a shorter exposure time was needed to reach full coverage than for the run shown in Fig. 8a. However, the same general behavior was again exhibited. The results were also reproducible (in the same sense as those of Fig. 8a) and Fig. 8c represents a typical curve for this type of deposition-measurement cycle. The flat portion in question was again present, and so it seems unlikely that a "rearrangement" of Na, requiring some time, is responsible for it.

One can obtain a relative measure of the evaporation rates for the different temperatures by using the vapor pressure-temperature curve for Na. This was done, and the relative slopes of the curves of Fig. 8 were compared with the relative evaporation rates. Only a very poor correlation could be obtained. No suitable explanation has been found for this poor correlation, nor has one been found for the general behavior exhibited in these curves.

An attempt was made to obtain photoemission data from the crystal in the same tube, but the attempt was unsuccessful. It was hoped that photoemission data might help to explain the complex behavior of the curves of Fig. 8. Apparently some Na had deposited on the metal parts in the vicinity of the crystal (e.g., the crystal carrier, the W trolley rods, etc.) and made them photoelectrically sensitive. When light was shone on the crystal, some stray light reached these sensitive surfaces, and the resulting photocurrent from them masked any photocurrent from the crystal itself.

Overlayer Studies Using the Ion Gun

The results obtained with the thermal evaporator stressed the importance of being able to determine the work function more accurately than .030 eV, the accuracy attainable with the low energy electron gun. This need led to the development of the vibrating capacitor described in Sec. 2.1.4.

After the measurements using the thermal evaporator were completed, the tube was opened and the vibrating capacitor installed. The modified version of the ion gun, using an aluminosilicate Na ion source was also installed. This is the version described in Sec. 2.1.3. Following these modifications, the tube was again evacuated and processed. The same Ge crystal was used. The crystal was cleaned using the same techniques as before and preliminary tests of the ion gun were made. In order to check for the possibility of negative or neutral impurities in the positive ion beam, all potentials on the gun were maintained at their usual values, but the target was biased

+ 22-1/2 V with respect to the filament. The filament was heated to operating temperature and the crystal was allowed to remain in front of the gun for one hour. At normal deposition rates, full coverage could easily be obtained in this period of time. The vibrating capacitor was used to check for any change in work function. It was found that the work function had increased by about .05 eV during this time. This change was judged small enough to be ignored.

The uniformity of the ion deposition was also checked. A small amount of Na (less than 0.1 monolayer) was deposited on the crystal using the ion gun. The work function of the crystal was measured, using the electron gun, at several places on the portion of the crystal which received Na. It was found that the work function variation over this area was less than .03 eV. Since the work function is particularly sensitive to small differences in overlayer coverage at this low overlayer coverage, the uniformity was quite good.

The surface was then recleaned by sputtering and the dependence of work function on overlayer thickness was measured (using the ion gun as a Na source) using the low energy electron gun to measure work function shifts. This dependence was measured several times, each time starting from a clean surface. A typical curve is shown in Fig. 9. It is seen that the dependence measured for ionic deposition differs from that for atomic deposition in several respects. First, only two breaks occur in the curve. The first one is most pronounced and occurs at a coverage of 0.17 monolayers, when the work function has been reduced by 0.8 eV. The second break is just detectable and occurs at a coverage of 0.50 monolayers, corresponding to a work function decrease of 1.28 eV. Secondly, this curve is always concave upwards, while those of Fig. 8 have a portion which is concave downward. Finally, the curve of Fig. 9 exhibits no flat portion as do the curves of Fig. 8. (For the purposes of this discussion one monolayer is arbitrarily defined as that coverage for which there is one Na atom on the surface for each surface Ge atom. θ is the fractional overlayer coverage, i.e., $\theta = 1$ corresponds to 1 monolayer.)

It should be noted that the Na was always removed from the surface by sputtering during this set of measurements. This precaution was taken as a result of the measurements described in Sec. 2.2.2 which tend to indicate that the Na diffuses into the bulk if the crystal is heated with Na on the surface. However, since this crystal had been heated with Na on the surface during the measurements using the thermal evaporator, it is possible that some doping of the bulk with Na occurred.

Since these measurements are by no means completed, one can only speculate as to the reasons for the differences in the curves of Figs. 8 and 9. It is possible that these curves depend strongly on the annealing treatment given the crystal after each sputtering. Steps have been taken to reproduce this annealing as accurately as possible, although this is difficult, since temperature measurement poses several experimental difficulties. It would be of interest to measure the work function vs. overlayer coverage on a surface which has been sputtered but not annealed, using both types of deposition, since the sputtering parameters can be reproduced much more easily. Secondly, it is possible that the impinging Na ions disrupt the surface when they strike. This could be checked by varying the target potential from run-to-run to determine whether the energy of the impinging ions is of any importance. Thirdly, it is possible that some change in the crystal occurred when the tube was opened, resulting in a different dependence on coverage. This can also be checked quite easily by using the thermal evaporator and rechecking the curves of Fig. 8.

It is also possible that there are other alkali ions in the Na beam, resulting in a different curve. This suggestion seems less feasible than the previous ones, and would be more difficult to check. It could presumably be done using a mass spectrometer, however. Finally, it might be possible that there is some intrinsic difference between the adsorption mechanisms for ions and for atoms.

These results show that a number of measurements must be made before the lowering of the surface barrier can be understood. Other Ge crystals should be studied in order to rule out the possibility that the complex dependence of work function on coverage is a result of Na doping of the crystal. This could have occurred during the first set of measurements when Na was removed by heating.

2.2.2 Electron Diffraction Studies of the Structure of Na Adsorbed on Ge

Electron Diffraction Tube

A tube for studying the sodium overlayer structure on a germanium surface cleaned by argon ion bombardment has been constructed and is shown schematically in Fig. 10. The tube includes provision for cleaning the crystal by argon-bombardment, measuring the work function employing a low energy electron gun, and depositing sodium by evaporation; the details of these procedures are described in Sec. 2.1. Work function measurements indicate the amount of sodium deposited which is correlated with the electron diffraction data. The electron diffraction

chamber is also used for measuring yields and energy distribution of the secondary electrons, the latter being possible because of the spherical geometry.

The electron diffraction chamber is similar to one previously constructed in this laboratory (ref. 6). The chamber consists of two concentric hemispherical chromium plated tungsten grids (see Sec. 2.1.5) plus a hemispherical fluorescent screen formed on the spherical glass envelope. The inner grid is enclosed on the bottom by Advance sheet metal to create a field free region surrounding the crystal. Two openings remain to allow the trolley rods and crystals to pass through the chamber. The second grid, held near filament potential, prevents inelastically scattered electrons from reaching the fluorescent screen. It was extended cylindrically downward from the diameter of the hemisphere with Advance sheet metal to assure maximum suppression of inelastically scattered electrons. The fluorescent screen was formed by depositing powdered zinc sulfide on the spherical glass envelope which had been previously coated with a transparent stannous oxide conducting film for electrical contact. A post acceleration of 2 kV is used to excite the screen. Another transparent fluorescent screen was mounted below the inner chamber (Fig. 10) for checking operation of the electron gun by allowing the beam to pass through the screen at the bottom of the inner chamber and be post accelerated to excite the screen.

The electron gun used for diffraction measurements is identical to those used for secondary electron emission measurements in this laboratory. The gun produces a beam current of 0.1 μamp at 10 eV energy and increases to 1.0 μamp at 100 eV energy. The beam may be focused to a diameter less than 1 mm.

Two germanium crystals, each having the (111) face exposed, are being used in the present experiment. One was cut from a 50 ohm-cm n-type germanium single crystal ingot, mechanically polished and treated with CP-4 etch. The other was a thin 21 ohm-cm single crystal ribbon obtained from the Westinghouse Research Center through the courtesy of S. O'Hara. The ribbon crystal has a much smoother surface than the ingot crystal, requires no surface treatment, and is thus more suitable for surface studies. The crystals are mounted on movable tungsten trolley rods, the movement of which is accomplished by magnetic coupling from outside the tube. Movable trolley rods are necessary to allow the crystal to be moved through the diffraction chamber. The crystals are heated by radiation from a 200 watt lamp outside the tube.

Two sputter pumps, separated by a Granville-Phillips valve, are mounted beneath the station in a magnetically shielded oven which allows the pumps to be baked independently of the tube.

The pump which is directly connected to the tube is used only for maintaining high vacuum while the pump separated from the tube by the valve is used during tube processing and for evacuation of argon. The valve is used to regulate the flow into the pump during the removal of argon from the tube and for isolating the contaminated pump from the system when the crystals are clean. The tube is processed in the standard manner used in this laboratory (Sec. 2.1.1) using a bakeout temperature of 300°C. An ultimate tube pressure of less than 10^{-10} Torr is achieved as measured by the sputter pump. The actual pressure in the tube is somewhat greater due to pumping impedance.

Slow Electron Diffraction Experiments

Discussion of electron diffraction experiments is often confusing because of the wide range of nomenclature used in the literature. Recently a memorandum by Elizabeth A. Wood and J. J. Lander of Bell Laboratories was circulated among those working on surface structures in an effort to unify the terminology. The following discussion employs their suggested notation.

In general, the periodicity of a single crystal does not extend to the vacuum because of the rearrangement in the surface region normally required to achieve a minimum energy configuration. The region near the surface having different structure from the bulk is defined as the selvedge. The structure beneath the selvedge having three dimensional periodicity is called the substrate. The selvedge in the present case consists of the deposited overlayer and the displaced substrate atoms and has two dimensional periodicity on a clean, well ordered surface.

The structure of the selvedge is designated "surface structure" to distinguish it from the substrate structure. Since the surface structure has two dimensional periodicity, it is convenient to define a two dimensional surface unit mesh parallel to the surface plane. Because the surface structure must be in register with the substrate structure, it will exhibit many of the symmetry properties of the substrate. In particular, the period of the surface structure is normally a multiple or submultiple of the substrate structure. Because many surface structures may be considered, it is expedient to define a "stationary" unit mesh to which they may be referred. For studies on the Ge (111) surface, this is taken as the hexagonal structure of the (111) plane. Thus a 60° rhombus substrate unit mesh is defined and illustrated in Fig. 11(a). The corresponding two dimensional, conventionally defined, reciprocal lattice is again a hexagonal structure which is rotated 30° with respect to the real lattice (see Fig. 11(b)).

The description of the surface in relation to the substrate unit mesh is given in the following quotation from the Bell Telephone Laboratories memorandum.

"1. The name of the substrate (e.g., α - SiO_2, Ge, NaCl).

2. The substrate plane parallel to the surface in terms of its conventionally defined indices (e.g., Ge (111), NaCl (100)).

3. The ratio of the repeat distance, a_s, of the surface structure net to the repeat distance, a, of the substrate primitive mesh; also b_s/b if necessary, e.g., Ge (111), 30°; Ni (011) 2 x 3 (read "2 by 3"). Note that 2 $\sqrt{3}$ means $2\sqrt{3} \times 2\sqrt{3}$. 30° signifies that the surface unit mesh is rotated 30° with respect to the substrate unit mesh.

4. (Separated from the above by a short dash.) The identification of foreign atoms, if any, responsible for the surface structure.

e.g., Si (100) 4
Si (100) 12-P
Ni (011) 1 x 3 - O."

Interpretation of the surface structure from the electron diffraction pattern is visualized most easily through the two dimensional reciprocal lattice. For example, consider the interpretation of the Ge (111)-2 structure with the aid of the reciprocal lattice shown in Fig. 11(b). The double surface unit mesh which has the same orientation as the substrate unit mesh merely doubles the number of points in the reciprocal lattice as shown. The reciprocal lattice points are labeled with conventionally defined Miller indices which are related to the substrate unit mesh. Thus multiple surface periodicity requires the use of fractional indices. For example, 1/2 order beams in the reciprocal lattice direction (1 1) are labeled (1/2 1/2). It is convenient to use multiple Miller indices to identify multiple order beams. For example, the second order beam in the (1 1) azimuth is designated by the Miller indices (2 2).

The projection of the observed diffraction pattern on a plane normal to the direction of the incident beam is directly related to the reciprocal lattice. By definition, the length of the reciprocal lattice vector is the reciprocal of the distance between the corresponding grating lines (e.g., if $r^* = h\,a^* + k\,b^*$, then $r^* = 1/d_{(hk)}$ where $d_{(hk)}$ signifies the distance between surface grating lines having Miller indices (hk). According to Bragg's diffraction law (for normal incidence)

$$\sin \theta = \lambda / d_{(hk)} = \lambda \; r^*_{(hk)}$$

where θ is the angle between incident and scattered beams and λ is the wavelength of the incident beam. Thus a diffracted beam having Miller indices (hk) will be observed whenever $1/\lambda > r^*_{(hk)}$ and this beam will make an angle with the normal given by Bragg's law. If a circle of radius $1/\lambda$ is drawn in the reciprocal lattice (see Fig. 11(b)), it is easily seen that the pattern contained within this circle is identical to the pattern observed on the spherical fluorescent screen when projected on a plane normal to the incident beam.

In the above discussion, it was assumed that the electrons were scattered from a two dimensional crystal. This is a reasonable first approximation because of the low penetration depth of slow electrons. The atom layers below the surface have the effect of producing maxima and minima in the intensity of the diffracted beams according to whether they interfere constructively or destructively. The modulation of the intensity observed in the diffracted beams becomes increasingly important with increasing energy, as more layers contribute to the scattering process. Observations of the energy at which these extrema occur gives information concerning the position of the atoms in the layers below the surface.

Electron diffraction patterns were observed from both the ingot crystal and the ribbon crystal after the argon bombardment cleaning and high-temperature annealing. The pattern from the ribbon crystal was considerably stronger than from the ingot crystal because of its smoother surface. However the surface plane of the germanium ribbon appeared to be about 2° - 3° from the (111) plane according to the observed pattern. Although one must be aware of this fact when interpreting the data, it is not believed to effect the gross properties of the pattern.

A Ge (111) 1 structure was observed from the ingot crystal after an argon cleaning treatment and an annealing at about 700°C for 100 hours. A brief annealing treatment at approximately 800°C produced a Ge (111) 2 structure. However, the 1/2 order beams were very weak and could not be strengthened through various surface cleaning and annealing treatments. Apparently the CP-4 etch produces a surface which is too rough to be suitable for electron diffraction measurements. Because of this difficulty, the ingot crystal was abandoned in favor of the ribbon crystal for electron diffraction observations.

A light argon cleaning treatment using 200 eV ions at 30 μamps/cm^2 for 30 minutes plus a brief annealing at approximately 500°C was sufficient to produce a strong diffraction

pattern from the ribbon crystal. In addition to the strong integer order beams, 1/8 order beams were observed along some azimuths. Figure 12 illustrates the pattern observed on the clean crystal. Only a few of the 1/8 order beams were detected indicating that the structure had a periodicity 8 times that of the substrate in only a few azimuths. Perhaps further analysis will reveal a logical configuration which produces the observed pattern.

The double spacing surface structure is in agreement with others (refs. 12,27) for the (111) face of cleaned germanium. However Lander (ref. 27) observed that the 1/2 order beams were doublets which required a 12 x 12 surface unit mesh. The interpretation of the 8 order structure in the present case, follows that suggested by Lander (ref. 27) for his observations. It is conjectured that the Ge (111) 2 structure produces strains which are relaxed by a displacement giving a much larger surface unit mesh (8 x 8 in this case).

The mode of operation for the electron diffraction chamber was somewhat different from that suggested by Lander (ref. 28). Lander found that operating the inner grid 100 volts above crystal potential "sharpened" the pattern at low energies. This mode of operation decreases the "time of flight" of the diffracted electrons which decreases distortion from stray fields and spreading of the beam due to electron-electron interaction. Attempts to operate the present tube using this suggested potential configuration may have sharpened the pattern at intermediate energies (30 - 100 eV), but loss of resolution occurred at extremely low energies. In particular, the 1/8 order structure was not resolved leaving a "smear" around the (1/2 1/2) beam locations. It is believed that the shielding provided by the 180° hemispherical grids plus the advance sheet which completely enclosed the crystal was sufficient to allow the inner grid to be operated at crystal potential without appreciable distortion from external fields. The loss of resolution when attempting to operate the inner grid above crystal potential is not understood.

The data taken on the electron diffraction patterns consisted of recording the energy at which the diffracted beams exhibited maxima and minima in intensity along with comments on the relative intensity and width of the extrema. The words narrow, medium, and broad are used in the following to indicate extrema widths in the neighborhood of 2°, 5° and 10° respectively. The data taken on the clean germanium ribbon is tabulated in Table I. Errors in the recorded energies are due primarily to non-normal incidence of the incident electron beam on the (111) plane of the sample.

Table I

Electron Diffraction Observations of the Ge(111)-2 Structure on the Clean Surface

Beam	V_{max}	V_{min}	Intensity	Width
(0 1/2)	12.3		medium	broad
(0 1)	21			
(0 1)		30		narrow
(0 1)	42		bright	medium
(0 3/2)	54		dim	medium
(0 2)	62		bright	medium
(0 2)		91		narrow
(0 2)	106		medium	narrow
(0 2)	182		medium	narrow
(0 5/2)	76		dim	medium
(0 3)	134		medium	medium
(0 3)		177		medium
(0 3)	190		dim	medium
(0 4)	210		medium	medium
(11)	41.5		medium	narrow
(11)	56		dim	narrow
(11)	97		bright	narrow
(22)	172		medium	narrow
(21)	90		medium	medium
(21)		99		medium
(21)	110		medium	narrow
(21)	187		dim	narrow

It should be emphasized that although the pattern exhibited apparent six-fold symmetry, it was three-fold in the strictest sense because the axis of the crystal perpendicular to the (111) plane possesses three-fold rotational symmetry. This causes diffracted beams differing in azimuth by 60° in the "six-fold" pattern to pass through extrema at slightly different energies. Further analysis of the data is needed to determine whether it is sufficient to allow construction of a surface model with any degree of confidence. It may be that a more accurate method of recording data, such as measuring the intensity of the diffracted beam with the spot photometer as a function of incident electron beam energy, is needed.

Deposition of sodium was monitored by measuring the resulting work function change employing a low energy electron gun (Sec. 2.1.4). This method measures changes in work function with a sensitivity of .03 eV, but does not establish an absolute scale. As a reference point, the work function value of 4.79

obtained on the (111) surface of clean germanium by Dillon and Farnsworth (ref. 25) was used. The recorded work function is obtained by subtracting the measured work function shift from this value.

Initial deposition of sodium resulted in loss of intensity of the fractional order beams. This effect was first observed at a measured work function of 4.57 eV. At a work function of 4.39 eV the 1/2 order beams were just visible and they disappeared completely after sodium deposition had decreased the work function to 4.02 eV. During this period of deposition the integer order structure became sharper, indicating greater surface order. The electron diffraction data taken at this point is tabulated in Table II.

As mentioned above, it is believed that the sodium affects the pattern predominantly through the changes it produces on the germanium structure since it does not make an appreciable direct contribution to the scattering process. The strong Ge (111) 1-Na structure obtained after a small amount of sodium has been deposited indicates that the sodium overlayer relaxes the surface strains and results in increased surface order. Using data obtained on work function vs. overlayer coverage (Sec. 2.2.1), the density of sodium atoms required to relax the Ge (111) 2 structure may be determined. It is hoped that further study will produce a model which predicts this result.

Only very slight changes in the diffraction pattern were observed upon further deposition of sodium which reduced the work function to 3.02 eV. This should be compared with the minimum work function of about 2.3 eV obtainable with full sodium coverage. The slight decrease in intensity observed during this stage of evaporation was probably caused by interference from the deposited overlayer. This would be expected if the overlayer were not well ordered.

At this point, the crystal was gently heated by irradiation. The exact temperature was not known but was judged to be between 100°C and 200°C. A very dramatic effect was observed. The work function increased to 3.92 eV and a very strong Ge (111) 4-Na structure was produced. Observations are recorded in Table III. The 1/4 and 1/2 order beams were clearly visible and exhibited six-fold symmetry indicating predominate scattering from the top germanium layer. The 1/4 order beams were visible at energies down to 1.9 eV (corrected for contact potential difference). The pattern was distorted at these low energies due to stray electric and magnetic fields but was readily identifiable.

Further deposition of sodium on the Ge (111) 4-Na structure corresponding to a work function decrease to 2.92 eV left the pattern unchanged except for a noticeable loss in intensity. A

Table II

Electron Diffraction Observations on the Ge (111) 1-Na Structure Taken After Initial Deposition of Sodium on the Clean Surface

Beam	V_{max}	V_{min}	Intensity	Width
(01)	11.3		medium	medium
(01)	24.5		bright	narrow
(01)		29		narrow
(01)	35		medium	narrow
(01)		42		narrow
(01)	52		bright	narrow
(02)	70		medium	broad
(02)	114		bright	medium
(02)	175		dim	narrow
(03)	138		medium	broad
(03)	186		medium	medium
(03)	228		medium	medium
(04)	220		medium	medium
(11)	50		medium	medium
(11)	100		bright	narrow
(11)	132		dim	narrow
(22)	170		medium	medium
(22)	197		medium	narrow
(22)	239		bright	narrow
(21)	92		medium	broad
(21)	123		bright	medium
(21)	193		medium	narrow
(21)	244		bright	narrow
(12)	112		medium	medium
(12)	138		medium	medium
(12)	178		medium	medium
(12)	223		dim	narrow
(42)	283		dim	medium
(24)	277		dim	medium
(13)	169		bright	narrow
(31)	179		bright	narrow

Table III

Electron Diffraction Observations on the Ge (111) 4-Na Structure

Beam	V_{max}	V_{min}	Intensity	Width
(0 1/2)	6.3		bright	narrow
(0 1/2)	13.3		dim	medium
(1/2 0)	5		dim	broad
(1/2 0)	13.5		bright	medium
(0 1)	11.6		bright	broad
(0 1)		17		medium
(0 1)	22		bright	medium
(0 1)	34		bright	broad
(0 1)		28.8		medium
(10)	10		bright	broad
(10)		13.2		medium
(10)	16		bright	broad
(10)		19.5		medium
(0 5/4)	26		dim	medium
(0 5/4)	34		medium	medium
(0 5/4)		42		narrow
(0 5/4)	49		bright	narrow
(5/4 0)	31		medium	medium
(5/4 0)	42		medium	narrow
(5/4 0)	64		dim	medium
(0 3/2)	45		medium	medium
(0 3/2)	67		medium	medium
(0 3/2)	95		dim	medium
(3/2 0)	41		dim	medium
(3/2 0)	77		dim	medium
(3/2 0)	104		dim	medium
(02)	59		bright	broad
(02)	88		medium	medium
(02)	126		dim	medium
(11)	80		medium	medium
(11)		73		medium
(11)	109		dim	medium
(21)	33		medium	medium
(21)	44		dim	medium
(21)	62		dim	medium

very low temperature (less than 100°C) heating treatment at this coverage increased the work function to 3.37 eV and removed the fractional order beams almost beyond detection. Subsequent sodium deposition removed the Ge (111) 4-Na structure entirely, leaving only integer order beams. Deposition of sodium was continued to full coverage with no change in the Ge (111) 1-Na structure except for loss of intensity.

The crystal was then given a sequence of heating treatments at increasing temperatures and the resulting patterns observed. The Ge (111) 1-Na pattern increased considerably in intensity through initial heating treatments during which the work function increased to 3.5 eV. The data tabulated in Table IV was taken at this stage. Comparison of Table IV with Table II shows that the two Ge (111) 1-Na structures are not the same.

Further heating treatments gradually brought back the Ge (111) 4-Na structure. It was first detected at a work function of 3.92 eV and became very strong at a coverage corresponding to a work function of 4.37 eV. This pattern appeared to be identical to that recorded in Table III. The pattern gradually returned to that of the clean crystal as the heating treatments were continued.

Interpretation of the above observations is complicated by the fact that the results depended on the history of the crystal. The work function obtained after sodium deposition and subsequent heating was not a unique function of the temperature to which the specimen was heated, but depended on the amount of sodium deposited. One would not expect this to happen if the sodium were leaving the surface by evaporation. Apparently the sodium diffuses into the crystal during the thermal treatments. This made the effect of subsequent heating treatments less pronounced, presumably due to the sodium concentration gradient at the surface. For example, the temperature required to produce the Ge (111) 4-Na structure after full sodium coverage was much higher than that needed after partial coverage.

The Ge (111) 4-Na structure is conjectured to be a rearrangement of the sodium or germanium atoms formed by heating, when the proper concentration of sodium at the surface exists. The structure is not stable at high temperatures; the sodium can diffuse into the bulk. The following observations are in agreement with the above postulate. After the crystal surface was cleaned by high-temperature heating, sodium was deposited until the work function dropped to 4.27 eV. This value of work function is within the range over which the Ge (111) 4-Na structure persisted in the course of the previous run. Now if the work function is a unique function of the overlayer coverage and if the formation of the Ge (111) 4-Na structure does not

Table IV

Electron Diffraction Observations on
Ge (111) 1-Na Structure Obtained After Full Sodium
Coverage and Subsequent Low Temperature Heating

Beam	V_{max}	V_{min}	Intensity	Width
(01)	13		bright	broad
(01)		16		broad
(01)	29		bright	medium
(01)		34		narrow
(01)	42		bright	medium
(01)	64		bright	medium
(01)	103		dim	medium
(01)	136		medium	medium
(10)	12		dim	broad
(10)		14		medium
(10)	16.5		dim	medium
(10)		20		narrow
(10)	32		medium	medium
(10)		42		medium
(10)	67		bright	medium
(10)	95		medium	medium
(02)	57		medium	broad
(02)		65		narrow
(02)	76		dim	medium
(02)	103		bright	bright
(02)	153		dim	medium
(02)	177		medium	medium
(02)	225		dim	medium
(20)	48		bright	broad
(20)		55		narrow
(20)	63		bright	medium
(20)	75		bright	medium
(20)	105		bright	broad
(20)	171		dim	narrow
(03)	126		medium	broad
(03)	167		dim	narrow
(03)	187		dim	narrow
(03)	340		dim	narrow
(30)	112		medium	broad
(30)	134		bright	medium
(30)	174		dim	medium
(30)	230		dim	medium

Table IV (continued)

Beam	V_{max}	V_{min}	Intensity	Width
(04)	210		dim	medium
(04)	245		dim	medium
(40)	220		dim	medium
(40)	260		dim	narrow
($\bar{1}$2)	42			medium
($\bar{1}$2)	50			medium
($\bar{1}$2)	57			medium
($\bar{1}$2)	75			medium
($\bar{1}$2)	82			narrow
($\bar{1}$2)	100			medium
($\bar{1}$2)	115			medium
(11)	37		bright	bright
(11)	53		medium	bright
(11)	74		bright	medium
(11)	122		dim	medium
(11)	240		medium	medium
(22)	151		dim	medium
(22)	168		medium	narrow
(22)	197		medium	narrow
(12)	90		dim	medium
(12)	110		bright	medium
(12)	132		dim	medium
(12)	188		medium	medium
(12)	220		dim	medium
(21)	88		bright	medium
(21)	111		medium	medium
(21)	145		medium	medium
(21)	199		dim	medium
(21)	226		dim	medium
(24)	268		medium	dim
(42)	280		medium	dim
(31)	171		medium	medium
(31)	206		medium	medium
(31)	231		dim	narrow
(31)	257		dim	narrow
(4$\bar{1}$)	165		medium	medium
(4$\bar{1}$)	192		dim	medium
(4$\bar{1}$)	220		bright	medium

require a surface concentration gradient of sodium, then there should have been enough sodium on the surface to form the structure. However, the same heating treatment previously required to form the structure after large coverages resulted in the return of the work function to a value nearly coincident with that of the clean state and no evidence for the formation of the Ge (111) 4-Na structure was observed. No surface concentration gradient existed at the surface prior to this experiment because of the high-temperature heating treatment given the crystal before sodium deposition. Thus, according to the postulate made above, the sodium easily diffused into the bulk leaving a surface concentration below that needed to form the Ge (111) 4-Na structure.

From the above results, it appears that sodium diffuses into the crystal upon heating and that the most of the structures observed were dependent on a sodium concentration gradient at the surface. Care should be exercised to prevent the diffusion from occurring. Attempts will be made in future experiments to heat the sodium covered crystal at temperatures low enough to prevent inward diffusion of sodium, but high enough to allow rearrangement of surface atoms.

2.2.3 Secondary Electron Emission from Na-Covered Ge

Secondary electron emission studies were carried out on both the ingot germanium crystal and the ribbon germanium crystal. Initial efforts were made on the ribbon crystal because of its smoother surface. However, it was discovered that the ribbon crystal had become contaminated with sodium during the electron diffraction studies and so later measurements were concentrated on the ingot germanium sample.

The secondary emission yield measurements were made employing the bridge technique standard for this laboratory (ref. 29). The conductivity of the germanium sample was sufficiently high to allow steady state measurements to be made. The primary electron beam current was normally less than 10^{-6} amperes and precaution was taken to assure that the yield was independent of the primary current. The two spherical grids and fluorescent screen served as secondary electron collectors for these measurements. It was necessary to post-accelerate the secondary electrons to an energy of 300 eV in order to prevent charging of the fluorescent screen.

In the discussion of results on electron diffraction (Sec. 2.2.2), it was suggested that the sodium overlayer diffused into the crystal upon low temperature heating. This conjecture is consistent with observations on secondary electron emission, the results of which are illustrated in Fig. 13.

Curve 1 was taken on the ribbon crystal after tube processing, but before crystal cleaning. Curve 2 was taken after the electron diffraction studies described in Sec. 2.2.2 had been carried out. The crystal had, at this stage, been "contaminated" with sodium by several sodium depositions and subsequent heating treatments. The dramatic change in yield curve suggests a remarkable change in the characteristics of the sample.

According to Johnson and McKay (ref. 30), the yield of germanium is independent of donor and acceptor concentrations up to 10^{19} per cm^3. It was estimated that about 10^{15} Na atoms per cm^2 had been deposited on the crystal at this stage. A doping concentration of greater than 10^{19} per cm^3 would require that the sodium be concentrated within 10,000 Å from the surface. An argon sputtering treatment which removed an estimated 1000 Å produced no apparent change in the yield curve indicating that either the sample had concentrations of sodium greater than 10^{19} per cm^3 even after this treatment or that Johnson and McKay (ref. 30) did not observe the effect of doping because of surface contamination. The latter suggestion is believed reasonable because the samples used were cleaned only by heating which does not produce an atomically clean surface. Further investigations on the effect of more severe argon sputtering treatments and prolonged high temperature heating may clarify this point.

The effect of sodium overlayers on the secondary emission yield was observed on the ingot sample which had not been contaminated with sodium. A sequence of 15 experimental runs consisting of sodium deposition, work function measurement, and secondary yield measurements were made covering the range from a clean surface to maximum work function reduction. The results of these experiments are illustrated in Fig. 14 where several yield curves are plotted at various overlayer coverages. Intermediate curves are not plotted. Curve 1 corresponds to the clean surface, Curve 6 was taken after the fifth sodium deposition, etc. The work function, total sodium deposition time, and maximum yield corresponding to each yield curve are tabulated in Table V. The maximum yield increased by a factor greater than 4 while the primary energy at which the maximum yield occurred increased from approximately 600 eV on the clean crystal to about 2 keV after optimum coverage of sodium. After the minimum work function had been achieved, further deposition of sodium resulted in a decreased yield illustrated by Curve 15, Fig. 14.

The magnitude of the yield enhancement is approximately the same as observed by Borziak and Sarbei (ref. 31) for evaporated germanium films with BaO overlayers. However, they observed that the maximum yield occurred at a BaO coverage corresponding to a work function value of 3.0 eV even though a

Table V

Results Obtained During Yield vs. Sodium Coverage Experiments

Curve	Work Function	Deposition (Time (min.)	Max. Yield
1	4.79	0	1.29
2	4.68	7.5	1.36
3	4.48	22	1.49
4	4.21	37	1.72
5	4.03	50	1.88
6	3.76	90	2.17
7	3.62	120	2.69
8	3.38	165	3.29
9	3.01	225	3.91
10	2.88	285	4.62
11	2.71	375	5.05
12	2.45	465	5.42
13	2.33	555	5.63
14	2.31	645	5.86
15	2.31	635	5.61

minimum work function of 1.9 eV could be achieved at optimum coverage. This is compared to a maximum yield occurring at about 2.3 eV for sodium-covered germanium. This discrepancy may be due to one or more of several possible factors. First, Borziak and Sarbei used evaporated germanium whereas a single crystal was used in the present experiment. Secondly, these workers had no direct means of measuring the work function but inferred it from earlier photoemission studies. A third possibility which is not believed likely is that the overlayer has a direct effect as well as an indirect effect (electron affinity reduction) on the yield which would cause the yield to be sensitive to the type of overlayer.

The low energy ends of the yield curves are expanded in Fig. 15. Structure in these curves is seen at primary energies of about 9 eV and 23 eV which is obviously related to the reflection coefficient (the curve of which is shown in the same figure) and is not characteristic of the "true" secondary yield. Reflection measurements were made by holding the two spherical grids 3 volts above electron gun filament potential so that only those electrons losing less than 3 eV energy upon interaction with the crystal are measured. The structure observed in the reflection coefficient is similar to observations by Shul'man and Ganichev (ref. 33).

The change of secondary emission yield by work function reduction is clearly demonstrated by the curves in Figs. 16, 17 which are semi-logarithmic plots of yield vs. work function for several values of primary energy. The yield appears to be an exponential function of the work function over most of the range measured. However, a break is observed in the curves at a work function value near 4 eV. Observation of Fig. 18, which is a plot of work function vs. coverage (evaporation time) strongly suggests that the first break in this curve is related to the break in the yield vs. work function curves. The origin of the break in these semi-logarithmic plots may be related to changes in the internal field caused by deposition of sodium. The following suggests a possible explanation for the break in terms of band bending at the surface during the initial stages of evaporation.

Studies of work function (ref. 25), surface recombination velocity (ref. 11), and field effect (ref. 32) all indicate that a clean germanium surface is p-type and that it may even be degenerate (ref. 32). This means that the valence band is nearly coincident with the Fermi-level at the surface as illustrated in Fig. 19(a). The valence band is essentially "pinned" at the Fermi level over a wide range of doping concentrations because of acceptor type surface states (ref. 25).

Experiments on silicon in this laboratory (ref. 6) and elsewhere (ref. 34) suggest that the initial effect of alkali metal overlayer deposition is to "bend" the energy bands down at the surface until the bottom of the conduction band is coincident with the Fermi level at the surface (Fig. 19(b)). As illustrated in Fig. 19(a), the work function, ϕ, is the sum of the electron affinity, χ, and the distance in energy between the bottom of the conduction band and the Fermi level at the surface, σ^-. Now it is possible that initial deposition of sodium results in a very rapid change in σ^- while χ does not change appreciably. Thus the work function is reduced by about .5 eV more than is the electron affinity during this period of evaporation. It is this effect which is the basis of the proposed model.

The internal field is not effective in enhancing the yield providing that the distance over which the field extends is long compared with the mean escape depth of secondary electrons. This is believed to be the case in germanium where the mean escape depth corresponding to 500 eV primary electrons is suggested to be about 50 Å (ref. 30) while the internal field depth for near intrinsic material is about 1000 Å (ref. 35 and ref. 6, p. 37). The amount of sodium required to produce the first break in the work function vs. overlayer coverage curve is about 0.1 monolayer according to experiments done in this laboratory (Sec. 2.2.1). Thus it is only the dipole layer associated with

this initial layer that is effective in reducing the electron affinity, and consequently in enhancing the yield, whereas both the dipole layer and the changing internal field contribute to work function reduction. Once the amount of sodium required to bend the conduction band down to the Fermi level at the surface has been deposited, further deposition results in decreasing the work function and electron affinity by the same amount. Since it is the electron affinity reduction that effects the yield, it is only the range of coverage above the break that should be considered in fitting a theory to a curve of yield vs. electron affinity. If the yield depends exponentially on the electron affinity, it is interesting to extend the straight line fit on the semi-log plots (Figs. 16,17) to work function values higher than the break as shown. According to the above discussion, the energy difference between the extended dashed line and the solid line is a direct measure of σ. In particular, this difference corresponding to no sodium coverage should indicate the value of σ for clean germanium. These observed values (Figs. 16 and 17) appear to be reasonable, i.e., they are approximately equal to the energy gap. A similar argument can be made for extending the straight line fit between the first and second break of Fig. 18. The result of this extension indicates a value of .42 eV for σ on clean germanium.

Energy distributions of the secondary electrons were also measured in the electron diffraction chamber using the retarding field method. The circuit used for these measurements is shown schematically in Fig. 20. The retarding voltage was applied to the two spherical grids while the fluorescent screen was used to collect the secondary electrons having sufficient energy to penetrate the grids. A 300 volt bias was used to post-accelerate transmitted electrons to the screen in order to prevent charging of the screen. The particular grounding scheme was chosen to minimize capacitive current to the collector when the ac method described below was employed.

A small ac signal of about .5 volts was generated by a model 200 CD Hewlett Packard oscillator. The resulting ac collector current was detected by a Type 1231-B General Radio Amplifier which was tuned to the oscillator frequency. The low energy end of the energy spectrum was scanned with the switch S (Fig. 20) in position 2 while the high energy end was scanned with the switch in position 1. The variable dc voltage was produced by a motor driven helipot source. Energy distribution curves were traced by feeding the variable retarding dc voltage and the output of the amplifier into a Model HR92 Houston Instrument X-Y recorder.

Results of the energy distribution measurements on the cleaned ribbon crystal are shown in Fig. 21 where the energy scale is broken to allow the high energy peaks and the slow peak

to be shown on the same graph. The vertical scale is arbitrary and different for the two energy regions. A characteristic energy loss of about 17 eV is observed which is interpreted as a plasma excitation. This is near the value of 15.8 eV determined from the classical plasma frequency formula

$$\omega^2_p = \frac{4\pi Ne^2}{m}$$

where N is taken as the number of valence electrons per cc. This value is also in close agreement with other experiments on transmitted electrons (ref. 36) and back-scattered electrons (ref. 33). A suggestion of another characteristic energy loss of about 10 eV is seen in Curve 3. This may be related to a characteristic loss of 9 eV reported by Shul'man and Ganichev (ref. 33).

The width of the slow peak in the energy distribution curves (Fig. 21) is seen to decrease with increasing primary electron energy. This suggests that electron affinity reduction should have a greater effect in enhancing the yield at high primary energies. This is indeed the case as shown in Figs. 16 and 17.

The secondary electron energy distribution has not been observed as a function of sodium overlayer coverage to date because of lack of time and a desire for better instrumentation. The General Radio Amplifier has recently been replaced by a Model RJB Electronics, Missiles, and Communications Lock-In Amplifier. This instrument is phase-sensitive so that it discriminates against capacitive currents and allows a higher signal frequency to be used. A lower noise level and overall greater sensitivity are then obtained. It is hoped that energy distribution curves in the primary energy range less than 100 eV may now be observed.

2.2.4 Field-Emission Microscopy

A study of the surface properties of Ge using the field-emission microscope (ref. 37) (henceforth designated FEM) was initiated this period in order to complement the photoemission and work function studies. The system Na:Ge is of particular interest because of the concurrent studies of the effect of Na overlayers on the photoelectric threshold and work function of Ge. From the proposed studies on this system, independent work function data may be obtained as well as information concerning the nature and magnitude of the binding between the Na adsorbate and the Ge substrate. In addition, it is hoped that the relation between the binding energy and the work function will be better understood.

Very little work has been published in which Ge surfaces have been studied with field-emission microscopy. Allen (ref. 38) has studied field-emission patterns of field-desorption cleaned Ge emitter tips before and after thermal annealing. Arthur (ref. 39) has cleaned and sharpened Ge emitter tips by a combination oxygen etch-field desorption technique. Other studies (refs. 40 and 41) of field emission from Ge have been reported in which the cleanliness of the surface was not established.

Description of the Microscopes

The field-emission microscope (FEM) shown in Fig. 22 was constructed for the preliminary work. Fine willemite powder was settled out of solution to form the phosphor screen and an aquadag anode ring was applied to the inner walls of the tube. The platinum contacts to the anode ring are described below. This tube was operated with a tungsten emitter in a background pressure of 10^{-9} Torr obtained after the usual vacuum processing. At the current densities required for a bright image, pressure bursts exceeding 10^{-7} Torr occurred due to electron bombardment of the willemite screen. It is believed that the pressure bursts were due to gas desorption rather than to dissociation of the phosphor. However, extended baking of the system only slightly reduced the effect. This screen is obviously not suited for the proposed studies due to the high pressures resulting from its use.

Recent work in this laboratory in which phosphor screens have been employed has raised further objections to the use of binder-free, willemite powder screens in high vacuum structures. Small particles of phosphor have been observed in remote regions of the vacuum tube where they have migrated after many hours of operation. In one case this resulted in contamination of a surface being studied. (Also, phosphor particles were detected in the sputter pump where they were excited by the glow discharge.) Two possible solutions to this problem were apparent. The first would be to use a binder to give better adhesion between the Pyrex substrate and the phosphor powder and possibly between the phosphor particles themselves. Alternatively, one could abandon the powder systems in favor of evaporated thin-film phosphor screens which form an intimate bond with the Pyrex substrate. Because of the inherent advantages of thin-film phosphor screens the latter approach was the first to be pursued. Due to difficulties in preparing a sufficiently large screen by this method, however, the first approach has been resorted to for an immediate solution to the problem.

Among the advantages of thin-film phosphor screens over the powder phosphor screens are: (1) better image definition and resolution, (2) less surface area for adsorption of gases, (3) ability to withstand higher current densities without

danger of phosphor "burn", and (4) negligible tendency for phosphor particles to migrate and become a source of contamination. The last two are a direct consequence of the intimate binding between the phosphor and the substrate. The chief disadvantages are the somewhat reduced luminescent efficiency of most thin-film phosphor screens and the greater difficulty in preparation.

Thin-film phosphors have been formed by a variety of techniques including direct evaporation of the phosphor (ref. 42), vapor phase reactions (ref. 43) and reaction of the substrate with an evaporated condensate (ref. 44). A modification of the latter technique has been employed to prepare thin-film willemite screens in this laboratory. Zinc fluoride powder containing about 10 mole percent manganese as an activator is evaporated from a platinum crucible and condensed onto a Pyrex substrate at room temperature. The substrate is then heated in air at 650°C for one hour. The reaction is assumed to proceed as

$$2\ ZnF_2{:}Mn + 2\ SiO_2 \longrightarrow Zn_2SiO_4{:}Mn + SiF_4\uparrow \quad .$$

Small phosphor screens ranging in area up to 24 cm^2 and in thickness up to 2 microns were readily made by this method. The attempts to make larger screens suitable for use in a FEM or in an electron diffraction chamber have so far been thwarted by peeling of the film or other blemishes in the screen.

Phosphor screens which are stable in high vacuum may be prepared (ref. 45) using finely ground phosphor powder and a phosphoric acid binder. The Pyrex substrate is first coated with a transparent conducting layer (ref. 46) by reacting the substrate at $\sim$ 500°C with the fumes obtained over molten $SnCl_2$. The adherence of the screen is greatly enhanced by this conducting layer. These techniques are described in the two references cited. The phosphoric acid technique was used to deposit a phosphor screen in FEM 2 shown in Fig. 23. The phosphor is Sylvania's Type 131 silver-activated zinc sulphide. This powder is very fine and requires no additional grinding. External contact to the conductive coating in this microscope is made by two thin platinum ribbons each connecting to a one-lead press. The underside of the ribbon is embedded in the Pyrex envelope and the top side makes contact with the conducting coating which is applied after the ribbon is in place. The resistance between the Pt contacts was about 50,000 ohms until one of the contacts came open during application of the phosphor screen. (Fortunately, only one contact is required for

operation of the microscope.) No deterioration of the mechanical connection at the open contact was observed. Although the conductive coating itself is very rugged, apparently the electrical junction between the Pt ribbon and the conductive coating is subject to failure. In spite of this, it is believed that the simplicity and dependability of this contact make it superior to others used elsewhere (ref. 45).

The field emitting point is mounted on a vertical press as shown in Fig. 23. Cooling of the point may be accomplished by filling the press with liquid nitrogen. An aluminosilicate Na ion source (Sec. 2.1.3) will be mounted on the two-lead press shown at the bottom of the microscope for studies of Na overlayers on Ge field-emission cathodes.

The Field-Emission Cathodes

A tungsten emitter was employed in FEM 1 to check tube geometry, fluorescent screen brightness, operating conditions, etc. The tungsten emitter may also be a useful reference cathode for the Na adsorption studies to be performed with germanium emitters. The cathode assembly is essentially that employed by Dyke and his co-workers (ref. 47). A hairpin filament is formed from 20-mil tungsten wire to which a uranium glass bead is added for mechanical rigidity. The emitter blank, a 5-mil diameter tungsten wire, is spot-welded to the apex of the filament which has been previously reduced to 5-mils in diameter by an electrolytic etch in NaOH. The emitter point was formed by a dc electrolytic etch in 1.5 Normal NaOH with the tungsten positive with respect to a second, copper electrode. Preferential etching occurs at the electrolyte surface until the submerged portion drops off leaving a sharp point attached to the filament. An electronic circuit (after the Linfield Group)(ref. 48) was used to terminate the cell current after drop-off in order to prevent dulling of the point by continued etching.

The initial Ge emitter blanks are shown in Fig. 24a (designated type a). They consist of long, thin single crystals about 20-mils square in cross section and about 1.5 cm in length. The blanks are Ni plated in order to make electrical contact to the support filaments. A sandblasting technique (ref. 49) is then used to cut one end down to a cylinder from 5 to 8-mils in diameter. Greater control of the etching process is achieved with the smaller diameters so obtained. A 10-mil Ni support wire is next strapped to the large end of each blank by a wrapping of fine Ni wire. After the point is etched, the support wire is spot-welded to the apex of a tungsten hairpin filament identical to that used for the W emitters.

A superior design for a Ge emitter blank is shown in Fig. 24b (designated type b). In this structure, the Ge forms its own heating loop and the emitter point is formed at a

distance of only 1 mm or so from the loop. This results in better temperature control of the point than with the emitter shown in Fig. 24a. The type b emitter structure is similar to that employed by D'Asaro (ref. 50) who studied Si emitters in the FEM. However, the emitter used here has been miniaturized so that it may be accommodated in a commercial electron microscope for purposes of determining the geometry of the emitter point. As pointed out by Dyke (ref. 47), the emitter geometry must be known if accurate determinations of the work function ϕ are to be made for the various regions of the emitter surface. The current density J depends exponentially on the ratio $\phi^{3/2}/F$ where F is the electric field at the emitter surface. The variations in F can be calculated from a knowledge of the emitter geometry and the work function distribution then calculated from the observed distribution of the current density. The type b emitter is cut from 20-mil thick Ge wafers using a Raytheon Model 2-334 Ultrasonic Impact Grinder. The limitation on the size of the emitter blank imposed by the electron microscope is rather severe and fabrication problems have been experienced. These problems are now nearly solved, however.

Type a emitters are being used temporarily until greater reliability is achieved with the etching process by which the field emitting points are formed. Type a emitter blanks are relatively easy to produce, require less Ge and are considerably less fragile than type b.

Ge emitter points have been formed by a dc etch in CP-4 electrolyte in which the emitter is held positive with respect to a second electrode of Pt wire. From 10 - 20 volts is applied to the cell. The electrolyte is cooled to about -13°C with a bath of alcohol and ice. As with the W emitters, preferential etching produces a sharp point at the electrolyte surface and the etch must be terminated immediately after drop-off in order to prevent dulling of the point. The circuit used to terminate the W etch has been quite erratic and unreliable for etching Ge points, due to lack of sensitivity. A new circuit has been designed with which it is hoped to obtain points with greater reliability. Two of the Ge points etched using the original circuit were found to be suitable for use in the FEM. Both of these have been lost by dulling after only very preliminary studies in the FEM, however.

Patterns were observed from two different tungsten emitters in FEM 1. The patterns from the emitter before cleaning were similar to those reported by Becker (ref. 51) and others and are believed to be due to individual molecules weakly adsorbed on a layer of strongly adsorbed gas. Heating the emitters to about 1000°K resulted in the disappearance of these images and the appearance of a pattern which exhibits the crystal structure of the tungsten emitters. The latter patterns have been reported by a number of workers (ref. 45, p. 34).

Patterns were observed from the Ge emitters with the surfaces in the original contaminated state. Typically, about 0.3 μA emission current was obtained at 4 kV. These were similar to the patterns obtained from the W emitters before cleaning. Attempts to clean the emitters have not been successful as yet. Because of its low melting point, it is doubtful that Ge tips can be cleaned by thermal desorption alone (ref. 38). However, Ge surfaces cleaned by other techniques and later exposed to oxygen have been recleaned by heating alone.

The most promising method of cleaning Ge tips is probably by field desorption in which a high reverse field is used to strip off the contaminated surface layers. Müller (ref. 52) and others have employed this method to clean emitter tips which cannot be cleaned by heating. Arthur (ref. 39) cleaned and sharpened Ge tips by a vapor etch in oxygen at low pressure followed by field desorption of the remaining oxide. He obtained field ion images (ref. 53) of the surface during cleaning by cooling the tip to 77 °K in the presence of $\sim 10^{-3}$ Torr of hydrogen. In addition to acting as the image-forming species, the hydrogen serves to reduce the field at which field evaporation occurs.

An attempt was made to clean a Ge emitter by the oxygen etch-field desorption method used by Arthur. No provision was made for observing field ion images of the tip, however. A commercial silver-tube oxygen-leak was mounted on FEM 2 for oxygen admission and a Schulz-Phelps high-pressure ion gauge (ref. 10) was added to measure the oxygen pressure. To prevent oxidation of parts, the latter made use of a thoriated-iridium filament and platinum collector plates.

Oxygen etching of the Ge tips was effected at pressures of 0.1 to 1.0 microns of O_2 and at temperatures < 600 °C. The oxygen was then pumped from the system. Field desorption was attempted by applying a high reverse bias (emitter positive) for periods of 10 - 120 sec with the tip at room temperature and then observing the electron emission pattern. At the highest desorption fields employed (27 kV), protusions on the emitter tip were removed but it was not possible to remove the entire adsorbed film. Spurious emission occasionally limited the desorption fields to smaller values.

The pressure in the tube during the field desorption experiments was in the range from 5×10^{-9} to 1×10^{-8} Torr. Leak checks at first failed to disclose the cause of the poor vacuum conditions. The silver-tube oxygen-leak was subsequently removed from the system and checked thoroughly with Veeco's MS 9 helium-sensitive mass spectrometer leak detector. This test revealed a small leak and the silver tube was discarded. It

will be replaced with a Granville Phillips Type C high-vacuum valve for future work.

2.3 Studies of the Compound Na_3Sb

2.3.1 Studies of Na_3Sb Films

Experimental Arrangement

Experiments with Na_3Sb thin films during the previous period (ref. 6, p. 35) indicated a need for an easily controlled, uniform, and measurable evaporation rate from a pure and adequate supply of both Na and Sb. During this period, a system was completed that incorporated an evaporation method which it was hoped would meet these requirements; this system is described in a previous report (ref. 6, p. 35). Evaporation onto an intermediate Ni heater block and subsequent re-evaporation at a controlled, uniform temperature was the essential feature of this system.

The Sb source consisted of a piece of Sb of the order of .5 cc in volume, situated in a conical heater basket made of Ta wire. However, it was found upon evaporation of the Sb, that this source arrangement was not sufficiently directive, resulting in an inadequate deposit of Sb on the heater block.

The Na source was a vacuum break-in ampoule into which Na had previously been vacuum distilled by a method similar to that shown in ref. 5, Fig. 11. It was found that in order to obtain an appreciable deposit on the heater block, excessively high temperatures were necessary, resulting in a high degree of Na reaction with the Pyrex ampoule. It appeared that the heater block did not have enough Na to deposit a film of any appreciable thickness upon re-evaporation. However, before it was possible to attempt an evaporation from the heater block, a considerable leak developed in the Na ampoule at the point of vacuum seal-off. This of course caused the Na to react, ruining the experiment.

Since the experiment was never completed, the two-step evaporation method was not actually proven to be unusable. However, it had become apparent that there were rather basic difficulties with the method which could not be easily corrected, so the experiment was not repeated. Instead, attention was directed to the development of a new system based on the following recommendations resulting from the experiment. 1. In any subsequent experiment it would be desirable to evaporate Na from a container which is more resistant to Na attack than Pyrex. 2. The process of two evaporations, while providing good control, requires much too large a supply of evaporants; thus a single

evaporation would be preferable. 3. In addition to the requirement of an easily controlled evaporation source at a uniform temperature, it would be necessary to have this source provide a well directed beam. With a knowledge of the beam size and temperature one would be able to obtain an approximate evaporation rate calculation. 4. It would be desirable to incorporate an auxiliary method for instantaneous evaporation rate monitoring and film composition determination, independent of source temperatures, since it is difficult to obtain a reliable temperature measurement on a source of appreciable size. 5. Furthermore, enough information concerning Na and Sb evaporation techniques has been obtained that it would seem profitable to include in the new system provision for substrate temperature, film conductivity and photoemissive yield measurements to be performed concurrent with film formation. The system which was developed from these recommendations separates naturally into the section containing the substrates and the evaporation section.

In the development of the evaporation section, attention was first directed to the problem of providing a well directed beam of Na and Sb from containers which would not be strongly attacked by the evaporants. It was decided to have the evaporation beam originate from a small aperture in the container lid, permitting an approximate calculation of the evaporation rate, from a knowledge of the temperature of the container. It was felt that the most reliable and simple temperature measurement could be made with a thermocouple on a metal container. Evaporation from such a source could be controlled with a magnetically operated flap over the lid aperture.

Ni was chosen as the material for the Na container since it is both highly resistant to Na attack (ref. 54) and very easy to work with. Little information was available concerning the resistance of metals to attack by Sb, but since sufficient evaporation occurs at temperatures far below the melting point of Sb, the choice of container material was not as critical as for Na. Therefore, Ni was chosen for the Sb evaporator as well.

The other major consideration in designing the new evaporation unit was the choice of an independent method for evaporation rate determination. A set of criteria pertinent to these studies was established so that any method for evaporation rate determination could be properly evaluated; these criteria may be found in ref. 7. The results of a previous literature survey concerning film thickness and evaporation rate measurements were reviewed with regard to these criteria. The conclusion was reached that a piezoelectric crystal monitor would be the most suitable method for the new system.

The primary element in the piezoelectric crystal rate monitor is a quartz crystal, $\sim$ .5" square and $\sim$ .040" thick, mounted in the vacuum system in a holder which allows one face to be exposed to the evaporation. The addition of deposited material to the crystal will decrease the resonant frequency of the crystal in proportion to the mass deposited. The crystal is the frequency controlling element of an oscillator; the rate of shift in the output frequency of this oscillator provides a measure of the evaporation rate. The theory of operation as well as some experimental results may be found in refs. 55 and 56. Figure 25 contains a block diagram of the monitor and a drawing of the crystal holder.

To measure and record directly such a high frequency ($\sim$ 5 Mc) with any accuracy requires quite sophisticated instruments. However, since only the shift in frequency is of any real consequence, one normally mixes the output of the crystal oscillator with a frequency standard to produce an audio difference frequency which can be easily amplified, measured and recorded. The amplified difference frequency may also be fed to a commercial digital frequency counter with $\pm$ 1 cps accuracy. This measurement, while not easily recorded, does provide an accurate value for the total frequency shift during an evaporation. A second audio amplifier with a speaker is included to facilitate the checking of monitor operation both before and during evaporation; thus, difficulties or sudden changes may be spotted immediately without constant observation of the meter.

It was decided that the most simple, stable and reliable frequency standard would be another crystal oscillator. Since 5 Mc crystals with 10 kc tolerances are available, it is possible to pick a crystal with a resonant frequency near to that of the monitor crystal. Thus, the difference frequency will be initially small and hence, easily recorded.

Two crystal oscillator-amplifier circuits, as well as two audio amplifiers, and a frequency measuring circuit were constructed; the units are all transistorized and battery powered. With these units the ambient frequency shift, or drift, is normally no greater than 1 cps per minute. Since evaporations normally extend over a period of the order of minutes and result in a total change in frequency of the order of kilocycles, the inherent accuracy and sensitivity is well within the most stringent requirements. However, crystal frequency is also highly sensitive to changes in temperature; so precautions must be taken to ensure temperature stability. Since both Na and Sb provide sufficient evaporation rates at relatively low temperatures, it was felt that with heat shields and a suitable spacing between evaporator and crystal, temperature effects would be small (as was later verified). In any case, the net change in

frequency due to deposited material may be obtained following the evaporation when the crystal has cooled to its initial temperature.

There is a relation between the frequency shift of the crystal monitor and the mass of any material deposited (ref. 55). Therefore, a valid determination of the relative amounts of Na and Sb deposited (as well as the deposition rate) during any Na_3Sb film formation should be possible, enabling a correlation between electrical properties of the film and film stoichiometry. If one is to treat the above determination as an absolute measure of mass deposited, certain assumptions concerning elastic constants of the deposited film must be made; however, these introduce only relatively small corrections if the deposit is of the order of hundreds of Angstrom units in thickness (which is normally the case). It is sometimes desirable to calibrate the monitor for film thickness with an interference microscope (ref. 57), in order to obtain information concerning film densities as well as to provide a check on the calculated frequency-mass relation. Other workers have obtained agreement between calculation and calibration as close as the inherent accuracy of the calibrating device ($\pm$ 25 Å) (ref. 56).

A drawing of the evaporation section may be found in Fig. 26. The two Ni evaporant containers are mounted on rollers supported by two horizontal tungsten rods. These evaporators may be magnetically moved to various positions in the main section of the evaporation unit. At one position Sb may be placed into one evaporator before evacuation. A Na distilling flask (not shown in Fig. 26) is attached at another position in the main section. Na may be admitted to the flask under vacuum from an auxiliary flask into which commercial Na has been previously transferred and preprocessed. Na may then be directly vacuum distilled into one of the evaporators. (The lid of the evaporator is hinged, so that they may be magnetically opened to permit filling.) At the remaining position the evaporators are situated above a W heater filament; upon heating, evaporation proceeds from the small lid aperture, through the collimator-heat shield and onto the substrate $\sim$6" above. The evaporation source temperature is measured with a thermocouple making pressure contact to the evaporator. Halfway between evaporator and substrate are two crystal monitors which may intercept a portion of the beam. The position of a magnetically operated shield determines which of the two crystals receives the evaporation. A $1/r^2$ correction must be made in order to apply crystal monitor data to the determination of amounts of material on the substrates.

It was decided to check the operation of the evaporation section and calibrate the rate monitor previous to any major experiment. The calibration required that several individual films

be made, so it was necessary to design, for attachment onto the evaporation section, a simple trolley system with movable substrates. While designing this calibration tube, provisions for measuring photoemissive yields and approximate substrate temperatures were quite easily incorporated. Thus, it would be possible to utilize the rather lengthly Na distillation to determine preliminary photoemissive yield dependences on temperature, film composition and thickness.

The calibration substrate section is shown along with the evaporation section in Fig. 26. Twelve individual 1/4" by 1" glass slides, with pre-evaporated Au electrodes, are spring clipped onto .040" Ti backings, which in turn are supported on a magnetically operated trolley carrier. It is felt that the heavy metal backing helps to establish better temperature uniformity during heating. At the center position, a slide may receive evaporation while radiation through quartz window A strikes the sample at a 45° angle of incidence, producing photoelectrons which are collected by the Ni mask. The Ni mask provides a sharp film edge for a later interferometric thickness measurement; it also shields the other substrates from the evaporation. At this position the sample may also be heated; the substrate temperature is determined with a thermocouple fused into an identical slide in approximately the same position relative to the W ribbon heater filament. Although this method may be somewhat inaccurate, it provides a simple way of estimating the temperature of many movable samples.

After the evaporation has been completed, the film may be moved to another position where it is irradiated through a quartz window B at normal incidence, permitting a comparison with most other photoemissive yield data. Since window B is large enough to pass the entire light beam, one may obtain absolute yields (i.e., electrons per incident quantum). (Yields measured at window A should be considered only relative to each other, since the fraction of the light beam striking the sample was undetermined.) Finally, Al may be evaporated over both the bare substrate and film to provide a uniform reflective coating for the interferometric thickness measurement.

Following the preliminary experiment and calibration, the evaporation unit will be used in conjunction with a system which has provision for measuring, concurrent with film deposition, conductivity, accurate substrate temperatures, and photoemissive yield on three sapphire substrates. This system has been partially constructed and is described in ref. 7. However, the construction and measurements in the preliminary phase of the experiment consumed the remainder of the period; so this substrate section has not yet been used.

Before construction was completed on the calibration substrate section, the evaporator system was assembled and preprocessed. First, it was pumped to a pressure of 10^{-2} Torr with a Varian Vac-sorb cryopump which avoids any hydrocarbon contamination, and then further evacuated to a pressure of 5×10^{-7} Torr with a sputter pump mounted below the station. This pump was used to provide the pumping during processing. After checking the operation of the crystal monitors, heaters, and trolleys, the system was given a standard bake. The bake did not seem to affect the operation of the quartz crystals. After processing and checking, the system was opened to an atmosphere of N_2 to permit attachment of the calibration substrate section and the Na distilling flask. Sb was then placed in its evaporator, after which the system was again evacuated and processed.

At this time the auxiliary flask containing the proprocessed Na was attached to the distilling flask and the space between them was evacuated. After the break-in seals on both flasks were opened with a magnetically operated steel ball, the Na was melted and allowed to run into the distilling flask. The Na was then further outgassed and distilled into its evaporator.

An attempt was then made to outgas the Sb by heating it to its melting point. However, before the melting point was reached, a considerable amount of Sb had escaped from the edges of the hinged lid, striking hot metal parts and re-evaporating onto the walls of the tube, greatly reducing the visibility. Some of the Sb was also deposited onto the pressure contact thermocouple, causing it to stick and making it unusable. Later, when the evaporator flap was opened, a film across the small hole was observed; apparently during the outgassing, Sb had condensed on the somewhat cooler lid, forming a continuous film on the lid and flap. Thus, in order to obtain sufficient evaporation rates, it would be necessary to raise the evaporator to much higher than normal temperatures, resulting in a greater degree of contamination from the accompanying high gas pressure in the tube. The substrates were outgassed as a final step in the processing, after which a pressure of 10^{-9} Torr was obtained.

Since the crystal monitors would be the basic method of determining the evaporation rate, it was felt that the inability to measure evaporator temperatures would not appreciably hinder the experiment. Although the high temperatures necessary for evaporation were undesirable, this was not considered to be very important in view of the preliminary nature of the experiment. Thus, it was decided to proceed with the experiment in spite of the difficulties which had been encountered; however, in any future experiment it would be necessary to modify at least the Sb evaporator to eliminate these problems.

Experimental Results

An Sb film of 6.8 μ gm/cm^2 surface density (calculated from crystal monitor data) was deposited on slide number 4 (denoted by A_4). If one assumes bulk density, this film was $\sim$100 Å thick. The system was placed in a shielded box and 3.9 eV quanta were directed onto the sample through window A from a light source and monochromator arrangement described in ref. 5. Photoemissive yield measurements were made on the sample during the subsequent Na depositions and heat treatments; following each step, a spectral yield curve was obtained. Throughout the discussion of the data so obtained, Na depositions are denoted by D and heat treatments by H. S_{Na} is defined as the ratio of the amount of Na deposited to the amount of Na necessary to make the sample into stoichiometric Na_3Sb; this figure was calculated from the crystal rate monitor. The amount of Na deposited in any deposition will be referred to as a fraction of S_{Na}. The rate of change of yield with respect to time during depositions and heat treatments will be referred to as the yield rate. The rate of change of the frequency of the crystal monitor with respect to time will be referred to as the frequency rate.

During the initial part of D_1, the frequency rate was not constant even though thermal equilibrium of the evaporator had been established. A sharp jump in frequency then occurred, followed by the expected constant frequency rate. It is felt that the constant rate when extrapolated back to the commencement of deposition, gives a fairly reliable estimate of the total evaporation; however, this anomaly does raise some question as to the validity of the $S_{Na} = 0.7$ estimate for D_1. The nonlinearity and discontinuity in the frequency rate may perhaps be attributed to attack of the Al electrodes of the crystal by sodium. In subsequent depositions, the frequency rate "behaved" properly, so apparently, only the initial Na deposition on the crystal has an adverse effect.

In deposition D_1, a very high (positive and decreasing) yield rate was observed to $S_{Na} = 0.05$; this was followed by a lower constant rate to $S_{Na} = 0.1$. At some point between $S_{Na} = 0.1$ and $S_{Na} = 0.7$ the rate again increased, but it was impossible to follow this because of difficulty experienced with the light source. At the conclusion of the deposition, the yield was found to be stable at a value of 5.7×10^{-3} at 3.9 eV.

The initial high rate is attributed to emission from an increasing Na layer at the surface; the leveling off to a constant yield rate may be an indication that this photoemission process was approaching saturation. The yield measured during this constant rate interval increased from 10^{-4} to 10^{-3} in

agreement with the maximum yield obtainable from Na at 3.9 eV reported to be on the order of 10^{-3} by Maurer (ref. 26). The subsequent increase in yield rate may have occurred when Na had diffused into the Sb, forming sufficient Na_3Sb to allow emission from Na_3Sb to strongly dominate the emission from Na.

Before describing the results of the additional Na depositions, it is worthwhile to mention some results of other work on the alkali antimonides. Spicer (ref. 58) has stated that few photoelectrons will escape that originate at a distance greater than 250 Å from the surface. (Hereafter, the region within the photoelectron escape depth will be referred to as the escape region.) Imamura (ref. 59) reports that the thickness of alkali antimonide films may be expected to be a factor of 8.1 greater than the thickness of the Sb layer prior to reaction with an alkali metal. Using this figure the final thickness of the Na_3Sb sample in this experiment was estimated to be at least 800 Å. Thus, on the basis of Spicer's findings, one can expect composition changes (in the substrate region > 250 Å from the surface) for which there would be no accompanying photoemissive yield changes.

Sommer (ref. 60) in his work with K_3Sb (properties similar to Na_3Sb) found that the peak yield was reached with the ratio of K to Sb > 3:1. Upon further K deposition the yield decreased but was restored to slightly less than peak value upon baking to equilibrium at 150°C. He concluded that stable K_3Sb has a ratio of K to Sb > 3:1 and is made n type by the excess K. Spicer (ref. 58) reports that these n-type impurities give rise to an impurity emission which has a lower threshold and maximum yield than the primary intrinsic emission.

Consideration of the photoemissive yield changes which accompanied the depositions and heatings following D_1 lead one to make several conjectures concerning the film formation process. In order to simplify the discussion, Fig. 27 is presented as a history of this sample following D_1; it is a graph of the photoemissive yield at 4.4 eV vs. S_{Na}. Since only one sample has been measured so far, it is not known how reproducible these results are. Furthermore, it should be pointed out that the conclusions which follow are quite speculative in view of the difficulties experienced which made data interpretation somewhat uncertain. In addition to varying the amount of Na deposited, the maximum temperature attained in subsequent heat treatments was also varied during the first few depositions in an effort to gain a rough estimate of temperature effects. This fact, combined with the lack of knowledge of yield dependence on composition for $S_{Na} < 0.7$, make interpretation of the first few depositions more difficult than for later ones. Therefore, the final depositions, D_5 and D_4 will be considered first,

followed by a discussion of D_2 and D_3 (and the accompanying temperature effects).

The experimental results of D_4 and D_5 indicate the existence of two separate mechanisms of intrinsic yield reduction with excess Na on Na_3Sb. It is postulated that excess Na accumulates on the surface to the extent of about a monolayer, causing a yield decrease, while any further deposited Na diffuses into the sample as excess Na atoms in the Na_3Sb lattice, effecting a yield decrease similar in magnitude to that accompanying the monolayer. Furthermore, it is possible to remove the surface monolayer as well as most of the bulk excess Na at temperatures between 150°C and 170°C, resulting in a restoration of photoemissive yield. These results, will be considered in greater detail in the discussion which follows.

Na deposition D_5 resulted in three somewhat different decreases in peak yield for a total yield reduction of approximately 50% as can be seen from an inspection of the D_5 portion of the graph in Fig. 27. The first of these decreases was rather abrupt and occurred with a Na deposition of only $\sim$0.02 mg/cm^2 surface density (corresponding to about a monolayer of Na). After the abrupt decrease, the yield leveled off; this was followed by the second (similar in magnitude but more gradual) decrease to a yield value which remained constant with continued deposition, except for a very slight decrease near the end. Deposition D_4 just prior to D_5 resulted in a yield reduction similar in magnitude to that observed initially in D_5. Again as in D_5, this decrease resulted from only a monolayer of Na. With no further Na deposition beyond this amount, the yield remained constant with time.

It seems plausible to attribute the yield decrease in D_4 to a quasi-stable surface effect since there appeared to be no gradual yield changes with time such as might be expected to accompany any bulk diffusion of Na. Due to the striking similarity between D_4 and the first monolayer or so of D_5, it is assumed that the initial yield decrease in D_5 was also due to a quasi-stable surface monolayer of Na. A continued build up of Na on the surface would be evidenced by a yield decrease persisting as long as Na was deposited, since the yield would be reduced both by Na atom scattering of internal photoelectrons and greater light absorption in the increasing metallic Na layer. However, such a continued yield decrease was not observed, but instead, a leveling off occurred. Thus, the surface excess Na was apparently limited to about one monolayer. Since the Na deposited beyond the monolayer in D_5 effected a further yield decrease, rather than an increase, it is assumed that the escape region was already stoichiometric, so that Na diffused into the bulk as a stoichiometric excess. The mechanism of this yield

decrease could very well be inelastic scattering of a sizeable fraction of the internal photoelectrons by excess Na atoms in the Na_3Sb lattice. The second leveling off in the yield vs. deposition curve in D_5 no doubt occurred when the escape region could accommodate no further excess Na, causing the remainder of the deposited Na to diffuse into the substrate region where it could have no effect on photoemission. Further evidence for bulk diffusion of the deposited Na may be found in a comparison of yield curves A (after H_4), and B (after D_5) in Fig. 28. These curves reveal that the D_5 deposition resulted in an increase in low photon energy emission along with a decrease in high energy emission. The low photon energy yield has been attributed to emission from donor impurity levels, resulting from the presence of excess Na in the lattice (Spicer, ref. 58). Thus, enhancement of this yield must have been due to an increase in the number of impurity levels by introduction of additional excess Na into the bulk of the film.

The effects of heating the sample (H_3, H_4 and H_5) will now be considered. During H_4, following D_4, the yield (4.4 eV) was restored to the value which had been obtained prior to D_4; the increase occurred between 150°C and 170°C substrate temperature. Since there was no net yield change from D_4 and H_4, it is assumed that heating completely removed the proposed surface monolayer of Na. This removal is essential to the assumption that the same surface monolayer was responsible for the initial yield drop in D_5. During H_5 the yield increased (at about the same temperature as in H_4) and upon cooling increased somewhat more to a value slightly lower than that obtained prior to D_5. The near restoration of yield in H_5 is attributed to the removal of nearly all the bulk Na excess as well as the surface monolayer (as in H_4). The removal of excess Na is evidenced also by the decrease in impurity yield (curve C) in Fig. 28. The removal was most probably by evaporation rather than by diffusion into the substrate region, since the substrate region should also have been in equilibrium composition by this time ($S_{Na} > 1.0$). A similar yield increase was observed during H_3 (again between 150°C and 170°C) indicating a removal of excess Na. Since the amount of Na deposited prior to this was insufficient to make the entire sample stoichiometric, much less provide an excess of Na, this effect is taken as further evidence that stoichiometry was attained preferentially in the region near the surface.

Referring again to Fig. 28, it is not clear why both intrinsic and impurity threshold yield regions are considerably higher for curve A (after H_4) than for C (after H_5), since presumably the sample had been restored to its former condition by heat treatment H_5. It will be noticed, however, that the peak yields for both types of emission appear to be greater for

curve C than for curve A. While it has been postulated that approximately a monolayer of Na on the surface effects a yield decrease, it is conceivable that a small fraction of that amount might actually enhance emission, as is found, for example, in studies of Na overlayers on Ge. If this is indeed the case, then the lateral shift of curve C toward higher energies might be explained by the removal of this fraction of a monolayer during the rather high (230°C) heat treatment H_5.

At the conclusion of the experiment summarized in Fig. 27, the spectral yield was measured at window A (45° light incidence) and at window B (normal light incidence). A plot of the ratio of these two spectral yield measurements (Fig. 29) indicates that the sample was somewhat inhomogeneous along the thickness of the sample. One would normally expect this ratio to be greater than unity in at least the threshold yield regions of both intrinsic and impurity emission, since the photoelectron escape probability is increased when a greater percentage of the light is absorbed near the surface. However, the ratio calculated from measured values was less than unity for intrinsic emission; in the region where impurity emission breaks away from intrinsic emission (3.2 - 3.5 eV), the ratio increased rapidly to a rather constant value of 1.8. The measured yield at window A was no doubt lower than absolute yield since the light was not completely confined to the sample; this might account for the fact that the ratio was less than unity in the intrinsic region. However, any such shifts should affect the whole spectrum by a constant factor and thus do not account for the salient features of this graph, namely, the rather abrupt change in the "break-off region" and the constant values on either side. A possible explanation would be the existence of an impurity concentration gradient normal to the surface, the impurity concentration being greater near the surface. The percentage of the 45° incident light absorbed in the region of high impurity concentration would have been greater than for normal incidence, thus, increasing the yield ratio for impurity emission. Although it is plausible, this explanation is by no means conclusive since other effects (such as a possible difference in spectral reflectivity dependence for the two incidence angles) have not been taken into consideration.

With the previous interpretations as a background, the results of the first two additional depositions and heatings will now be considered. After D_1, upon allowing the sample to remain at room temperature for 18 hours, the intrinsic yield had increased, while the impurity yield had decreased (same effect as resulted from heating following deposition). Since S_{Na} was considerably less than unity, it is possible that the excess Na present in the escape region diffused into the Na-deficient substrate region during the 18 hour period. The escape region

was thus "free" to accommodate additional excess Na in deposition D_2, as is evidenced by the accompanying yield decrease. It is not clear why the yield decreased so rapidly in D_2, since the "bulk excess effects" in the other depositions were much more gradual. A surface monolayer effect is practically ruled out since presumably the surface had not been previously "cleared" of Na, (the sample had not yet been heated). In any case, the intrinsic yield was slightly more than restored upon heating to 75°C (H_2) while the impurity yield remained essentially unchanged. It is thought that the slight net increase in intrinsic yield may have been due to the formation of Na_3Sb near the escape region--substrate region boundary. While an elevated temperature no doubt speeded up the Na diffusion to this region, this formation might well have occurred at room temperature with sufficient time. It is felt that the 75° heating did not effect any removal of Na, either surface or bulk excess, since such a removal should have been evidenced in the subsequent deposition D_3 by a yield reduction similar to that observed in D_5. However, the D_3 yield reduction was very slight and quite gradual, indicating a near saturation of excess Na in the escape region. The 50% yield increase observed during H_3 (mentioned earlier) between 150°C and 170°C seems to represent the first removal of both bulk excess Na and the surface monolayer. Apparently, a temperature of about 150°C is indeed necessary to remove excess Na from Na_3Sb, in agreement with Sommer (ref. 60). If one adds the Na excess removal effects to the peak yields obtained after H_1 and H_2 in Fig. 27, it becomes apparent that this "corrected" yield did not vary appreciably. This indicates that the basic composition of the escape region was not altered significantly beyond $S_{Na} = 0.7$, supporting the conjecture that near stoichiometry was obtained preferentially in the region nearer the surface of the film. Furthermore, it appears that the reaction of Na with Sb to form Na_3Sb went very nearly to completion at room temperature; this is in agreement with Sommer and Vine (ref. 61) who recently observed a similar phenomena in experiments with Cs_3Sb.

2.3.2 Studies of Bulk Na_3Sb

A summary of a literature survey on the photoemitting and semiconducting properties of the alkali antimonides appears in ref. 1. It was concluded from this survey that an experimental program designed to synthesize and study these materials in the bulk form would be of considerable value to the overall program.

Samples of polycrystalline Na_3Sb have been prepared by several methods described in refs. 5 and 6. The results of these experiments and of an attempt to measure the conductivity of a sample of Na_3Sb, ref. 6, indicated the necessity of protecting the Na_3Sb from any appreciable concentration of most gases and of providing a working space in which a sample of

Na_3Sb could be prepared and shaped. As a result of the above considerations it was decided to obtain a high quality glovebox and purification train.

A glovebox was built to the design and specifications of Argonne National Laboratories.* The glovebox is made up of an aluminum frame onto which glass panels and thick aluminum panels are clamped. The seals between the frames and panels consist of O rings seated in polished grooves in the frame. The thick aluminum end panels allow the use of O ring gaskets and bolts to seal an accessory panel and a vacuum airlock to the glovebox. The gloves are attached to molded phenolic gloveports which in turn are sealed to the glass panels with neoprene gaskets. The glovebox is shown in Fig. 30. The frame, panels, gaskets and other necessary items were purchased from various manufacturers. These items were machined and polished to meet specifications and to improve the leak-tightness of the finished glovebox.

A vacuum-airlock to be used in conjunction with the glovebox was purchased from S. Blickman, Inc. The airlock is necessary to allow the operator to introduce items into the glovebox without opening it to the air and to remove residual gases from constricted areas in the items which are introduced into the glovebox. This airlock permits the continuous operation of the glovebox without exposing its contents to the atmosphere.

A study was made of the feasibility of making an argon purifier to be used in conjunction with the glovebox. Specifications for an argon purification system were drawn up and submitted to several commercial suppliers. It was found that an argon purification system made by United States Dynamics was suitable for our use. Their system recirculates argon at a maximum rate of 400 SCFH reducing the hydrogen, oxygen, water, and hydrocarbon concentration to less than 1 ppm, at the output. Since this system compared favorably with any system we could make and was more economical, it was decided to purchase the gas purification system from United States Dynamics. This system consisted of three independent subassemblies. One such subassembly contains two alternate tanks for removing water vapor and hydrocarbons. One tank is always being regenerated while the other is removing these impurities in the argon from the glovebox. This subassembly also contains the pump and motor necessary to recirculate the argon atmosphere in the glovebox. The second subassembly contains one tank to remove oxygen noncatalytically from the argon. This subassembly is bypassed during the relatively short time it takes to regenerate itself

*William D. McNeil conferred with L. R. Kelman and W. H. Livernash of Argonne National Laboratories regarding the construction of the glovebox.

with hydrogen. The third subassembly consists of a tank which removes hydrogen from the argon by catalytic combination with oxygen.

Upon receiving the subassemblies of the argon purification train, considerable time was spent in assembling the piping necessary to connect the various subassemblies and the glovebox system. Also, the tubing necessary to provide the various gases, water, and drains to the subassemblies was assembled. Figures 31 and 30 show a flow diagram and a photograph of the completed system. The glovebox, airlock, subassemblies, and piping were tested with a Veeco MS9A leak detector, a helium sensitive mass spectrometer. The glovebox and airlock were found to be free of leaks. Some leaks were discovered in the piping and the subassemblies; these leaks were repaired.

Upon putting the glovebox and argon purification system into operation, it was found, by observing a slow decrease in pressure in the glovebox, that a small leak in the system was still present. At this time a small quantity of NaK, a highly reactive alloy of sodium and potassium which is liquid at room temperature, was exposed to the atmosphere in the glovebox. After approximately five minutes a change in color of the surface of the alloy was observable, indicating a thin reacted film had formed on the surface of the alloy. This indicates a significant improvement in purity of the glovebox atmosphere over the atmosphere maintained in the original glovebox mentioned in ref. 6 in which NaK would only remain unreacted for approximately 5 seconds.

Some work was done to get a quantitative measurement of the reactive impurities in the glovebox atmosphere. It consisted of burning out filaments of light bulbs in an atmosphere of a known pressure of oxygen. It appears as though the time necessary to burn out these filaments is too long in the degree of oxygen impurity we hope to maintain in the glovebox to be used as a continuous check on the purity of the glovebox atmosphere. Work will continue in this area to gain a quantitative idea of the impurity level in the glovebox at some future date.

The design and construction of various items necessary to the production and testing of Na_3Sb is in progress. Among these items is a larger and more stable model of a furnace which was already successfully tested, made with a slotted stainless steel heating element and three stainless steel heat shields. Also designed was a device to hold a rectangular parallelepiped of the reaction product while conductivity versus temperature and Hall effect versus temperature measurements are being made.

2.4 Anomalous Photovoltaic Effects in Semiconductor Films

2.4.1 Evaporated Ge Films

The bell-jar vacuum system to be used in the study of anomalous photovoltaic effects in evaporated semiconducting films was described briefly in ref. 7, p. 30. The apparatus for the inside of the bell-jar has been completed so that evaporation of films can be started shortly.

Anomalous photovoltages were first reported in cadmium telluride by Goldstein and Pensak (ref. 62), and later in silicon and germanium by Kallmann, et al., (ref. 63). In all three materials, photovoltages up to several hundred volts per centimeter of film length were obtained, but these high photovoltages could not be uniformly reproduced in successive films. In the present investigation, germanium films will be studied. Germanium was chosen because of the obvious simplifications due to the use of an elemental semiconductor and because, of the well-known elemental semiconductors, it is evaporated most easily. The germanium will be evaporated from a sapphire crucible onto a quartz substrate which is nine inches above the crucible. The separation between the crucible and the substrate was made as large as possible to minimize thermal gradients caused by the hot crucible and to make the definition of an angle of deposition more meaningful.

The substrate is attached to an O.F.H.C. copper block containing a heating element and the copper block is clamped in a stainless steel holder which can be rotated through 90° from outside the bell-jar by means of a rotary motion feedthru. The stainless steel holder contains a coolant reservoir and provision has been made for supplying the reservoir by a bellows arrangement so that in future experiments it will be possible to cool the films to liquid nitrogen temperature without removing them from the bell-jar. There is a two inch viewing port on the bell-jar opposite the substrate so that after deposition the substrate may be rotated into position for exposing the film to light. This arrangement will also allow the angle of incidence of the radiation to be varied in addition to the angle of deposition.

The vacuum system itself has been designed to yield a clean, ultra-high vacuum by using low vapor pressure materials throughout and by using a sputter pump and cryogenic forepump. For adsorption studies, there is a gas admission system which will control the pressure inside the bell-jar by the admission of the desired gas through a servo-controlled variable leak valve.

The bell-jar and the internal apparatus necessary for conducting the experiment have been assembled. After processing of the system is complete, deposition and measurements can be started.

2.4.2 Sputtered Ge Films

Larger than band gap photovoltages in evaporated CdTe films were observed by Goldstein and Pensak (ref. 62); Kallmann and others also observed anomalous photovoltages in evaporated Ge films (ref. 63). Both of the above papers concluded that an oblique angle of deposition of evaporated materials was essential to the production of photovoltages. But both experiments failed to get reliable reproducibility.

Since the crystal structure and characteristics of Ge are better known than CdTe or other materials, Ge presents a better choice for further photovoltaic study. And by sputtering instead of evaporating Ge onto substrates, temperature gradients associated with oblique deposition by evaporation can be avoided. The tube is currently under construction. Two argon discharge tubes will be used for depositing Ge films and gold electrodes respectively. In this way the quartz substrates can be first cleaned by rf sputtering (ref. 64). The argon discharge tubes will have cathodes at both ends of the plasma column to increase the plasma density so that the deposition rate may be increased. The substrates can be rotated through an angle of about 0 to 70 degrees.

3. CONCLUSIONS

3.1 Overlayer Studies

Further studies of the system Na on Ge show that the dependence of the work function on the degree of coverage displays anomalies similar to those previously observed in measurements of the photoelectric threshold vs. coverage. The work function curves seem, however, to be more complex, particularly when the overlayer is deposited in atomic form. The electron diffraction studies and the secondary yield measurements indicate the source of some of this complexity, apart from the obvious influence of the adsorbed sodium on the surface dipole moment, it also has two auxiliary effects made evident by these measurements. In the first place surface strains seem to be relaxed by the adsorption of a small fraction of a monolayer, so that the surface can achieve the 2-dimensional periodicity characteristic of the bulk. Secondly, this same small coverage may cause a drastic change in the nature of the surface space-charge layer, i.e., convert the surface from p-type to n-type.

The experimental results seem to indicate that the dependence of work function on coverage differs according to whether the coverage is achieved by deposition of atoms or of ions. It is possible that this effect is only apparent and is due, for example, to a change with coverage of the atomic sticking factor. On the other hand, a real energy-dependent adsorption phenomena may be making itself evident--further experimentation is obviously required.

The electron diffraction apparatus developed in this laboratory has proven to be suitable for the intended purpose and furthermore, provides a convenient structure in which secondary electron yields may be measured and the energy distribution of the secondary electrons determined. The advantages of the use of "as grown" germanium web for electron diffraction studies have been demonstrated.

Germanium which has been cleaned by argon bombardment exhibits 1/2 integer order beams in addition to stronger integer order beams on the (111) face. Also very weak 1/8 order beams are observed in certain azimuths indicating a weak but long range surface interaction.

The results obtained on germanium with sodium overlayers are not yet conclusive but merit the following general remarks. The overlayer of sodium is not seen because of its small atomic number in comparison with germanium. The overlayer exhibits an indirect effect on the diffraction pattern through changes it produces on the germanium substrate. The double-spaced surface structure observed for clean germanium is relaxed by low coverages of sodium giving a strong Ge (111) 1-Na structure. No other structures are observed unless the crystal is heated with sodium on the surface, in which case two more structures are produced. A Ge (111) 4-Na structure was observed after heating the crystal at low coverages. A Ge (111) 1-Na structure distinct from the above mentioned Ge (111) 1-Na structure was produced by heating at a lower temperature with full coverage. These low-temperature heating studies indicate that the sodium diffuses into the crystal making interpretation of the resulting structures difficult.

The secondary emission yield increased by a factor greater than 4 due to deposition of sodium. Maximum yield occurs at a coverage just sufficient to achieve minimum work function. Further deposition results in decreased yields. Electron yield enhancement by work function reduction increases with increasing primary energy. A proposed explanation for the break in the yield vs. work function curves (Figs. 16, 17) suggests a rapid change in internal field upon initial deposition of sodium such that the work function and electron affinity are coincident

over the range of straight line fit on the semi-logarithmic plots (Figs. 16, 17). The secondary yield appears to be an exponential function of electron affinity. Energy distribution measurements demonstrate a characteristic plasma loss of 17 eV and another suggested loss of about 10 eV. The increasing width of the slow energy peak with increasing primary energy is compatible with the greater enhancement of yield with work function reduction at high primary energies.

It appears that higher desorption fields will be required to clean Ge field-emitter tips than are obtainable with the present dc voltage source. It will be necessary to improve this technique so that higher fields may be employed while maintaining control of the desorption process.

3.2 Studies of the Compound Na_3Sb

It was concluded that the double evaporation method for evaporation control is not feasible for these studies. Though some difficulty has been experienced with the crystal rate monitor during Na evaporation, with appropriate precautions, it should provide a reliable measure of evaporation rate and film composition. It has been demonstrated that with slight modifications, the present system of metal evaporators will provide a suitable evaporation source for Na and Sb. The technique of monitoring film deposition and heating with photoemissive yield measurements has proved very useful in providing information concerning film formation processes.

The photoemissive yield measurements on one Na_3Sb film during and subsequent to its formation, showed that the photosensitive region of the film (escape region) was made nearly stoichiometric with much less Na present than that necessary for complete film stoichiometry. It was suggested that Na deposition on the Sb layer resulted in a gradient in the Na concentration (normal to the plane of the film), as opposed to a uniform distribution of Na. There was evidence that a gradient of excess Na also existed. Moderate heating may have been necessary for complete activation of the film. Nevertheless, the reaction appeared to go very nearly to completion at room temperature. It was observed that excess Na effected two distinctly different peak yield decreases. The one which resulted from about a monolayer of Na is attributed to a surface effect, while the second is thought to be a result of photoelectron scattering by excess Na which diffused into the bulk. It was concluded from the results of heat treatments of the sample, that nearly all excess Na was removed by evaporation at temperatures between 150°C and 170°C.

The inert-atmosphere facility recently installed has been shown to provide a much purer argon atmosphere than did the system previously employed. Synthesis of bulk Na_3Sb should be possible in the new system.

4. RECOMMENDATIONS

4.1 Overlayer Studies

The work function studies should continue with particular emphasis on the differences between atomic and ionic deposition and on the influence of the annealing following the sputter-cleaning process. The germanium web used in the diffraction experiments should be used in the work function studies as well because of the more nearly perfect surface available. Once the factors which control the work function-coverage curve have been clarified, concurrent photoemission and work function studies should be carried out. Such studies were initiated previously and were shown to be very informative; they were however temporarily suspended until more reproducible surfaces could be achieved using the work function by itself as a monitor. The photoelectric investigation should include measurements of the energy distribution of the photoelectrons since such information would be of assistance in determining the source of the photoelectrons (i.e., surface or bulk).

Since there is some evidence that Na atoms can diffuse into the Ge crystal even at relatively low temperatures, a study of the diffusion of Na in Ge should be carried out and the influence of dissolved Na on the electrical properties should be determined.

The diffraction patterns observed on Na-covered Ge are believed to be characteristic of the Ge surface as modified by the presence of Na. If the atomic number of the absorbate were considerably higher it might be possible to observe the latter directly. It is therefore recommended that the diffraction study be repeated using Cs as the absorbate. Further development of the aluminosilicate emitters should make possible a suitable Cs source for this purpose.

The secondary emission measurements should be completed, with emphasis of the effect of coverage on the electron energy distribution and on attempts to deduce the internal energy distribution from this data.

The field emission study should be a valuable complement to those already in existence and its continuation is recommended. The field desorption technique should be modified so that continuous observation of the desorption process is possible

and the electrolytic etching techniques should be refined in order to increase the reliability of the process. An aluminosilicate Na ion source should be incorporated into the PEM.

4.2 Studies of the Compound Na_3Sb

The experiment currently in progress to determine photoemissive yield dependence on deposition parameters (in addition to crystal monitor calibration) should be completed. Some films should be formed with a thickness on the order of the photoelectron escape depth to obtain a more accurate dependence of yield on film stoichiometry. It will be advantageous to subject subsequently deposited films to a sequence of heat treatments, controlled in a manner which will provide more conclusive information on film formation processes. Following the completion of this experiment, the evaporators should be modified in order to prevent evaporation onto the side wall of the tube. The evaporation control flap should be positioned elsewhere than on the evaporators in order to prevent plugging of the aperture; the evaporator temperature measurement should also be improved. The possible adverse effects of Na on the quartz crystals should be further investigated. The proposed conductivity-photoemission measurements section of the tube should be completed and used in conjunction with the modified evaporation unit to contribute further to the correlation of photoemissive yield of Na_3Sb with its semiconducting properties and film deposition parameters.

Since the new inert-atmosphere facility now seems ready for use, the synthesis of bulk Na_3Sb should be attempted immediately. The first trial should involve maintaining a sodium vapor pressure of one atmosphere over Na_3Sb at its melting point. When the conductivity type of the resulting product is determined the conditions to be used on subsequent trials can be determined. The resistivity and Hall effect of the resulting samples should be measured as a function of temperature, with the objectives of locating and identifying the impurity levels and of determining the carrier scattering mechanisms.

4.3 Anomalous Photovoltaic Effects in Semiconductor Films

The bell-jar system and the sputtering system should be put into operation, Ge films prepared and the photovoltaic effects determined as a function of the deposition parameters. The latter should include substrate temperature, deposition rate, and the angle of incidence of the evaporated or sputtered atoms onto the substrate.

REFERENCES

1. W. T. Peria, "PHOTOEMISSION STUDIES" Scientific Report No. 1, Contract AF 33(616)-6455, University of Minnesota, Minneapolis, Minnesota. June 15, 1959 to September 15, 1959.

2. W. T. Peria, "PHOTOEMISSION STUDIES" Scientific Report No. 2, Contract AF 33(616)-6455, University of Minnesota, Minneapolis, Minnesota. September 16, 1959 to December 15, 1959.

3. W. T. Peria, "PHOTOEMISSION STUDIES" Scientific Report No. 3, Contract AF 33(616)-6455, University of Minnesota, Minneapolis, Minnesota. December 16, 1959 to March 15, 1960.

4. W. T. Peria, "PHOTOEMISSION STUDIES" Scientific Report No. 4, Contract AF 33(616)-6455, University of Minnesota, Minneapolis, Minnesota, March 16, 1960 to June 15, 1960.

5. W. T. Peria, "PHOTOEMISSION STUDIES" Interim Report, Contract AF 33(616)-6455, University of Minnesota, Minneapolis, Minnesota. December 16, 1960 to June 15, 1961.

6. W. T. Peria, "PHOTOEMISSION STUDIES" ASD-TDR-62-231, Final Report, Contract AF 33(616)-6455, University of Minnesota, Minneapolis, Minnesota. June 16, 1959 to December 15, 1961.

7. W. T. Peria, "PHOTOEMISSION STUDIES" Interim Engineering Report No. 1, Contract AF 33(657)-8041, University of Minnesota, Minneapolis, Minnesota. December 16, 1961 to June 15, 1962.

8. L. D. Hall, "Electronic Ultra-High Vacuum Pump," Rev. Sci. Instr. 29, 367 (1958).

9. J. M. Lafferty and T. A. Vanderslice, "The Interplay of Electronics and Vacuum Technology," Proc. IRE 49, 1136 (1961).

10. G. J. Schulz and A. V. Phelps, "Ionization Gauge for Measuring Pressures up to the Millimeter Range," Rev. Sci. Instr. 28, 1051 (1957).

11. H. H. Madden and H. E. Farnsworth, "High Vacuum Studies of Recombination Velocity for Germanium," Phys. Rev. 112, 793 (1958).

12. Farnsworth, Schlier, George, and Burger, "Application of the Ion Bombardment Cleaning Method to Titanium, Germanium, Silicon, and Nickel as Determined by Low-Energy Electron Diffraction," J. Appl. Phys. 29, 1150 (1958).

13. R. Riesz and G. H. Dicke, "The Analysis and Purification of Rare Gases by Means of Electric Discharges," J. Appl. Phys. 25, 196 (1954).

14. G. P. Blewett, "Filament Sources of Positive Ions," Phys. Rev. 50, 464 (1936).

15. Barton, Harnwell, and Kunsman, "Analysis of Positive Ions Emitted by a New Source," Phys. Rev. 27, 739 (1926).

16. R. M. Barrer and W. M. Meier, "Exchange Equilibria in a Synthetic Crystalline Exchanger," Trans. Faraday Soc. 55, 1 (1959).

17. D. W. Breck, W. G. Eversole, R. M. Milton, T. B. Reed and T. L. Thomas, "Crystal Zeolites. I. The Properties of a New Synthetic Zeolite, Type A," J. Am. Chem. Soc. 78, 5963 (1956).

18. H. E. Farnsworth, "A Simple Contamination-Free Electron Gun," Rev. Sci. Instr. 21, 102 (1950).

19. H. E. Farnsworth, "A Method of Obtaining an Intense Beam of Low-Velocity Electrons," J. Opt. Soc. Am. 15, 290 (1927).

20. See, for example, P. A. Anderson, "A Direct Comparison of the Kelvin and Electron Beam Methods of Contact Potential Measurement," Phys. Rev. 88, 655 (1952).

21. R. H. Fowler, "The Analysis of Photoelectric Sensitivity Curves of Clean Metals at Various Temperatures," Phys. Rev. 38, 45 (1931).

22. A. E. Carlson in Metal Finishings, N. Hall, ed., p. 287, 30th ed., Metals and Plastics Publications Inc. (1962).

23. A. Logozzo in Metal Finishings, N. Hall, ed., p. 274, 30th ed., Metals and Plastics Publications Inc. (1962).

24. F. G. Allen, T. M. Buck, and G. T. Law, "P-Layers in Vacuum Heated Silicon," J. Appl. Phys. 31, 979 (1960).

25. G. A. Dillon, Jr., and H. E. Farnsworth, "Work Function Studies of Germanium Crystals Cleaned by Ion Bombardment," J. Appl. Phys. 28, 174 (1957); A. B. Fowler, "Contact Potential Measurements on Cleaned Germanium Surfaces," J. Appl. Phys. 30, 556 (1959).

26. R. G. Maurer, "The Photoelectric and Optical Properties of Sodium and Barium," Phys. Rev. 57, 653 (1940).

27. J. J. Lander and J. Morrison (unpublished). We are grateful to Dr. Lander for providing us with a preprint describing this work.

28. J. J. Lander, J. Morrison, and F. Unterwalt, "Improved Design and Method of Operation of Low Energy Diffraction Equipment," Rev. Sci. Instr. 33, No. 7, 782-3 (1962).

29. R. W. Soshea and A. J. Dekker, "Fine Structure of Secondary Emission vs. Angle of Incidence of the Primary Beam on Titanium Single Crystals," Phys. Rev. 121, 1362 (1961).

30. J. B. Johnson and McKay, "Secondary Electron Emission from Germanium," Phys. Rev. 93, 668 (1954).

31. P. C. Borziak and O. C. Sarbei, "Photoelectric and Secondary Electron Emission from Germanium," Soviet Physics-Technical Physics 3, 1752 (1958).

32. P. Handler and W. M. Portnoy, "Electronic Surface States and the Cleaned Germanium Surface," Phys. Rev. 116, 516 (1959).

33. A. R. Shul'man and D. A. Ganichev, "Secondary Electron Emission and Elastic Reflection of Electrons from Germanium Single Crystals at Small Electron Energies," Soviet Physics-Solid State 2, 495 (1960).

34. J. Scheer, "Some Preliminary Experiments Concerning the Influence of Band-Bending on Photo-Electric Emission," Philips Res. Reports 15, 584 (1960).

35. C. C. Dousmanis and R. C. Duncan, Jr., "Calculations on the Shape and Extent of Space Charge Regions in Semiconductor Surfaces," J. Appl. Phys. 29, 1627 (1958).

36. L. Marton and L. B. Leder, "Energy Loss of Electrons in Passage through Thin Films," Phys. Rev. 94, 203 (1954).

37. R. H. Good, Jr., and E. W. Müller, "Field Emission," Handbuch der Physik 21, 176 (1956).

38. F. G. Allen, "Field Emission from Silicon and Germanium; Field Desorption and Surface Migration," J. Phys. Chem. Solids 19, 87 (1961).

39. J. R. Arthur, Jr., "Field Emission from Germanium," The Ninth Field Emission Symposium, University of Notre Dame, Indiana (1962).

40. M. I. Elinson and G. F. Vasiliev, "Certain Features of the Field Emission of Germanium," Rad. Engr. and Electron. 4, 246 (1959).

41. Yu. V. Zubenko, et al., "Current Voltage Characteristics of the Autoelectron Current from Semiconductors," Phys. Solid State 1, 1691 (1960).

42. C. Feldman and M. O'Hara, "Formation of Luminescent Films by Evaporation," J. Opt. Soc. Am. 47, 300 (1957).

43. F. J. Studer and D. A. Cusano, "Transparent Phosphor Coatings," J. Opt. Soc. Am. 45, 493 (1955).

44. L. R. Koller, "A New Method for Forming Thin Films of Phosphors," Report on Eighteenth Annual Conference Physical Electronics, M.I.T. (1958) p. 132.

45. R. Gomer, Field Emission and Field Ionization, Harvard University Press, Cambridge (1961) pp. 168-9.

46. R. Gomer, "Preparation and Some Properties of Conducting Transparent Glass," Rev. Sci. Instr. 24, 493 (1953).

47. W. P. Dyke, et al., "The Field Emitter: Fabrication, Electron Microscopy, and Electric Field Calculations," J. Appl. Phys. 24, 570 (1953).

48. E. E. Martin, et al., "Research on Field Emission Cathodes," WADD Technical Report 59-20 (1960).

49. F. Barbieri and J. Durand, "Method for Cutting Cylindrical Crystals," Rev. Sci. Instr. 27, 871 (1956).

50. L. A. D'Asaro, "Field Emission from Silicon," J. Appl. Phys. 29, 33 (1958).

51. J. A. Becker, "Adsorption on Metal Surfaces and Its Bearing on Catalysis," Advances in Catalysis VII, Academic Press (1955) p. 185.

52. E. C. Cooper and E. W. Müller, "Field Desorption by Alternating Fields. An Improved Technique for Field Emission Microscopy," Rev. Sci. Instr. 29, 309 (1958).

53. E. W. Müller, "Field Ionization and Field Ion Microscopy," Advances in Electronics and Electron Physics XIII, Academic Press (1960) p. 83.

54. L. R. Kelman, et al., Resistance of Materials to Attack by Liquid Metals, Argonne National Laboratory Publication No. 4417 (1950).

55. K. H. Behrndt and R. W. Love, "Control of Deposition Rate and Film Thickness with the Crystal Oscillator," Vacuum Symposium Transactions, 1960, pp. 87-91.

56. S. J. Lins and H. S. Kukuk, "Resonance Frequency Shift Thin Film Thickness Monitor," Vacuum Synposium Transactions, 1960, pp. 333-338.

57. S. Tolansky, Multiple Beam Interferometry, Oxford University Press, London (1948).

58. W. E. Spicer, "Photoemissive, Photoconductive and Optical Absorption Studies of Alkali-Antimony Compounds," Phys. Rev. 112, 114 (1958).

59. S. Imamura, "Electrical Properties of Alkali Antimonides," J. Phys. Soc. Japan 14, 1491 (1959).

60. A. H. Sommer, "n-Type and p-Type Conduction in Alkali-Antimonide Photoemitters," J. Appl. Phys. 29, 1568 (1958).

61. A. H. Sommer and B. H. Vine, Improved Uniformity of Photocathode Sensitivity, Interim Engineering Report No. 3, Contract No. AF 33(616)-8303. November 1, 1961 to January 31, 1962.

62. B. Goldstein and L. Pensak, "High-Voltage Photovoltaic Effect," J. Appl. Phys. 30, 155 (1959).

63. H. Kallmann, et al., "Photovoltages in Silicon and Germanium Layers," J. Electrochem. Soc. 108, 247 (1961).

64. G. S. Anderson, et al., "Sputtering of Dielectrics by High-Frequency Fields," J. Appl. Phys. 33, No. 10 (1962).

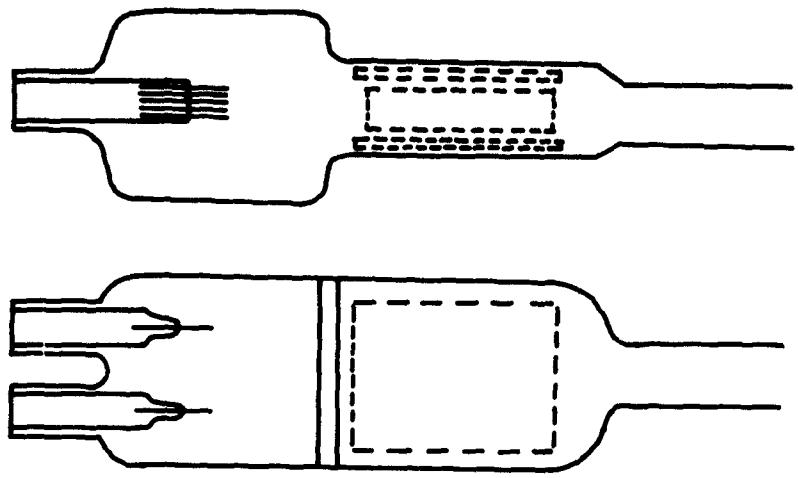

PYREX ENVELOPE

(POSITION OF PUMP SHOWN DOTTED)

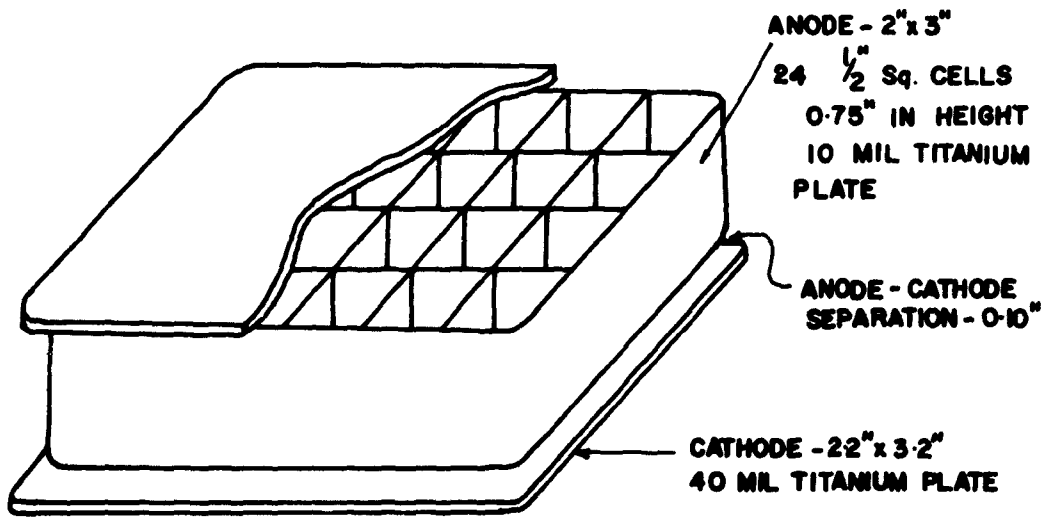

PUMP ELECTRODES

Fig. 1 Titanium Sputter Pump

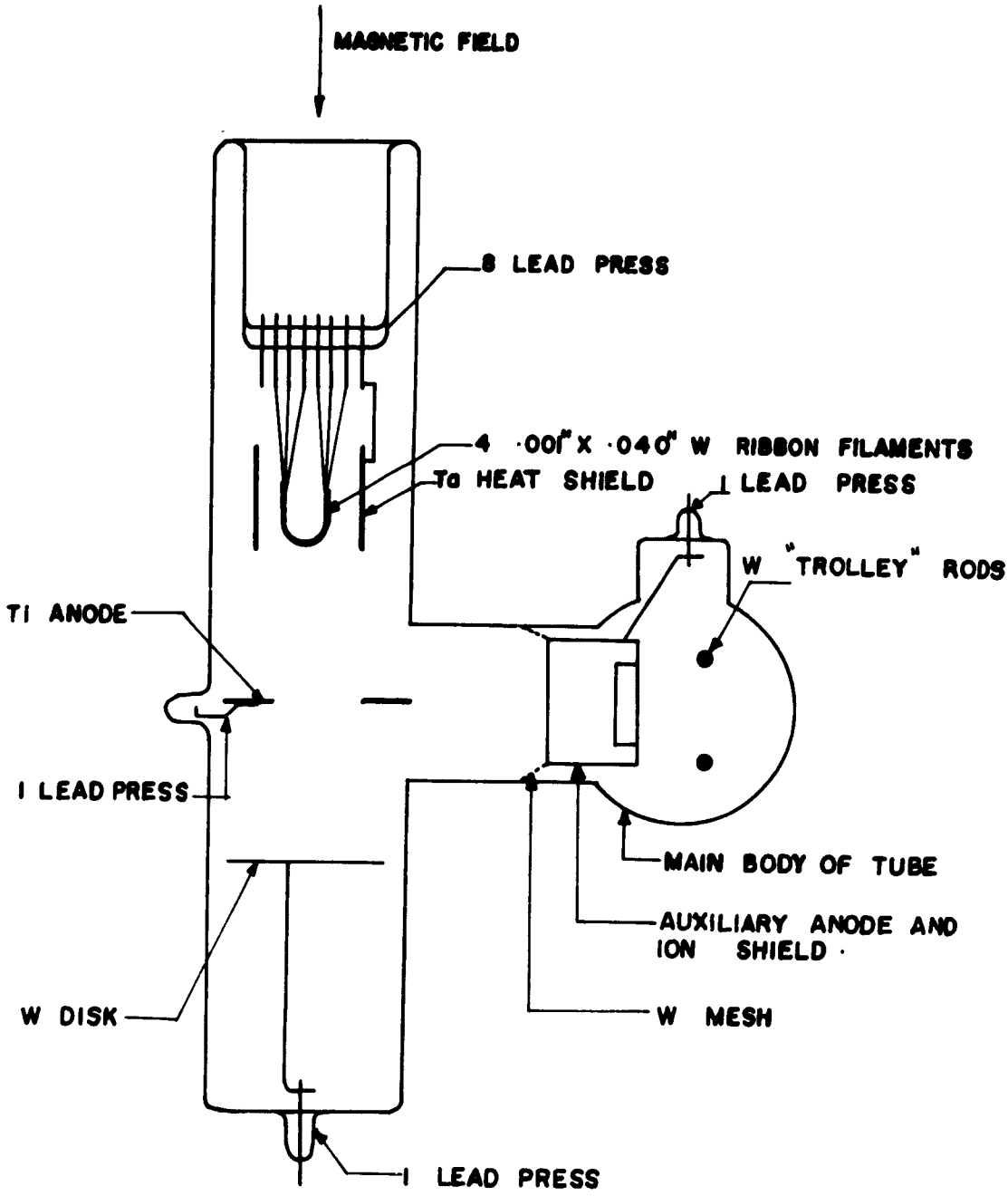

Fig. 2 Discharge Tube for Argon Sputtering

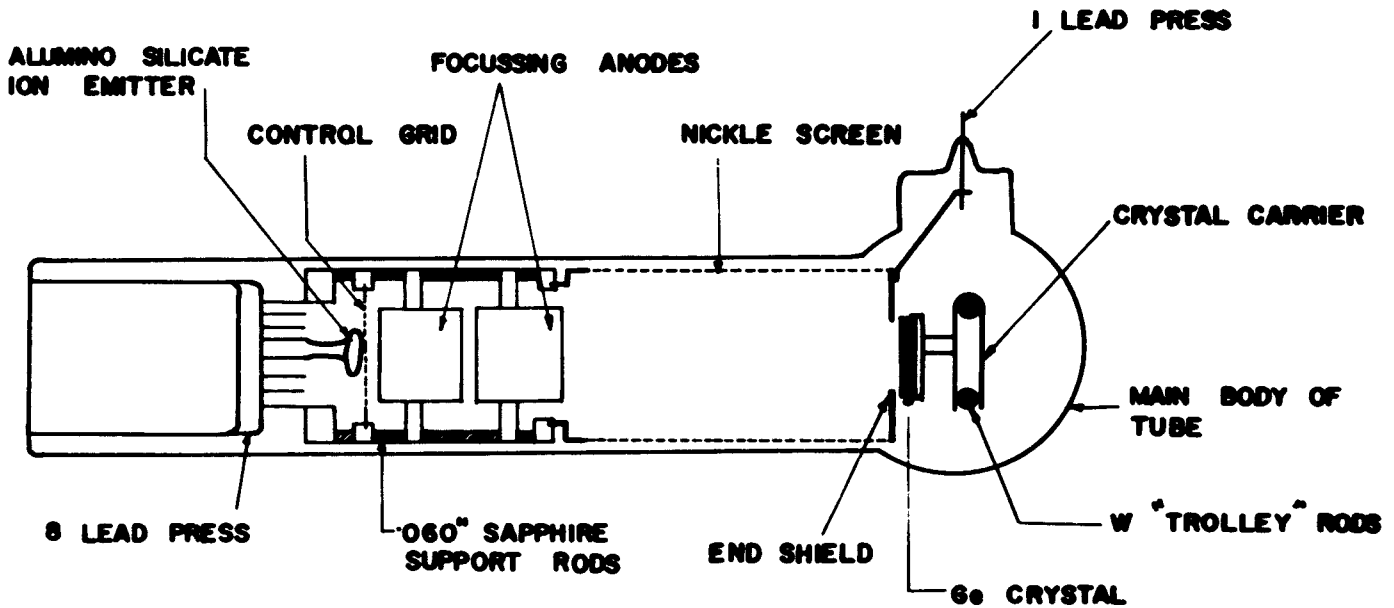

Fig. 3 Modified Version of Ion Gun

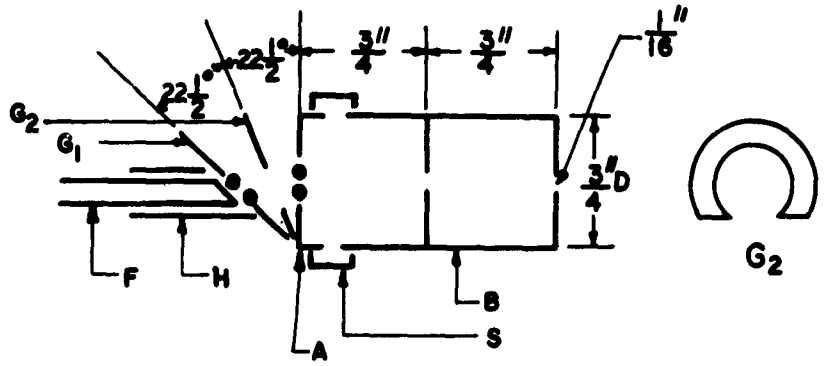

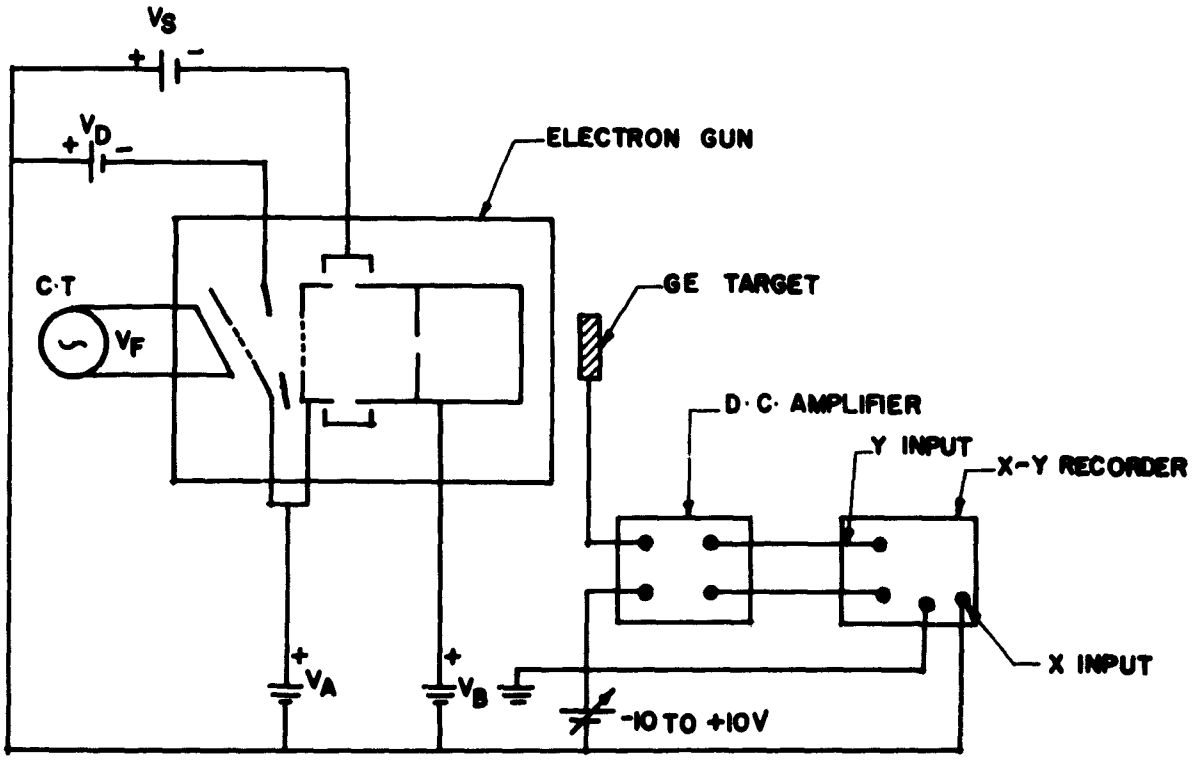

Fig. 4a Low Energy Electron Gun

4b Circuit Used in Conjunction with Low Energy Electron Gun

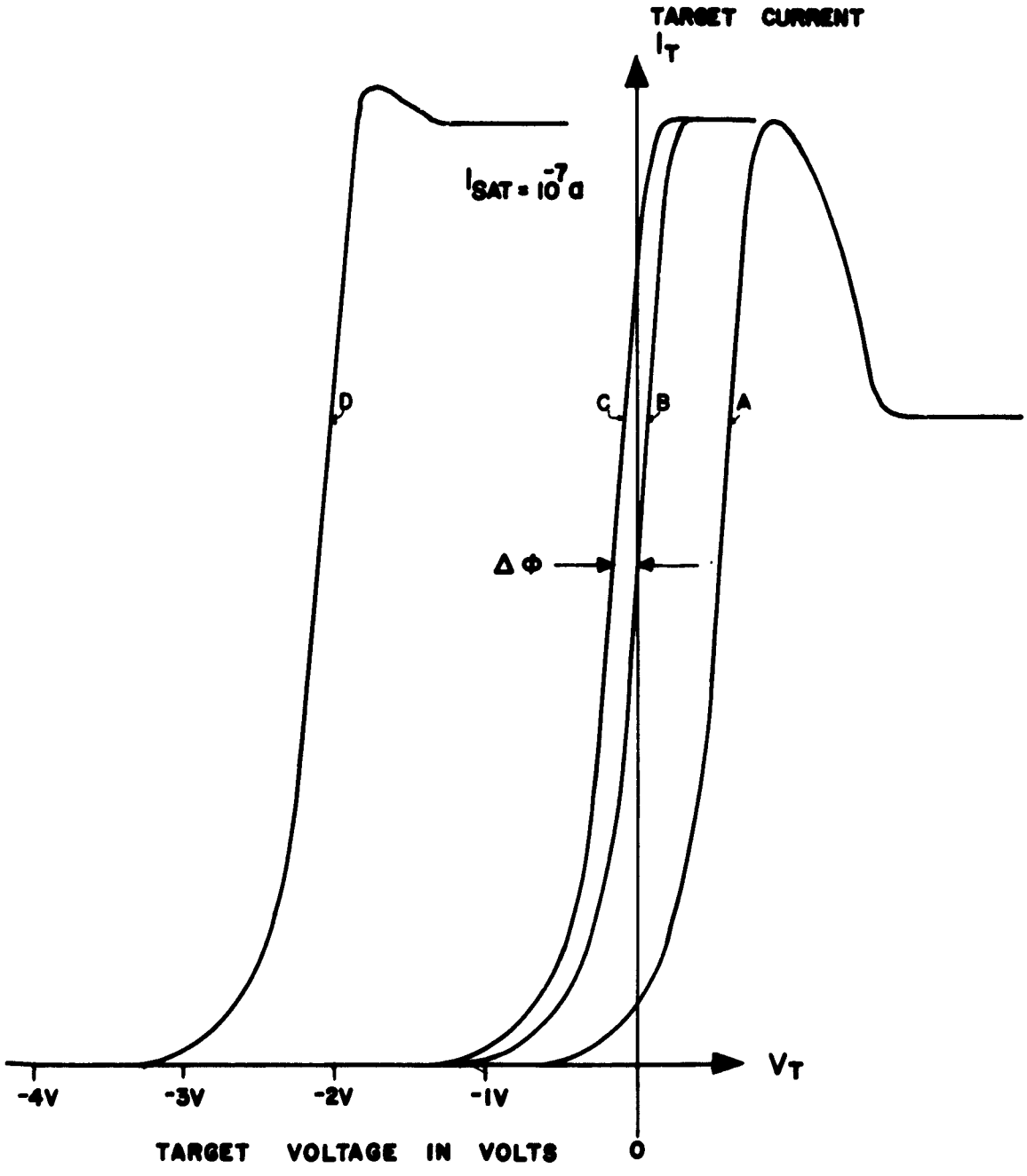

Fig. 5 Typical V-I Traces Obtained with Low Energy Electron Gun with the Ge Crystal as the Target

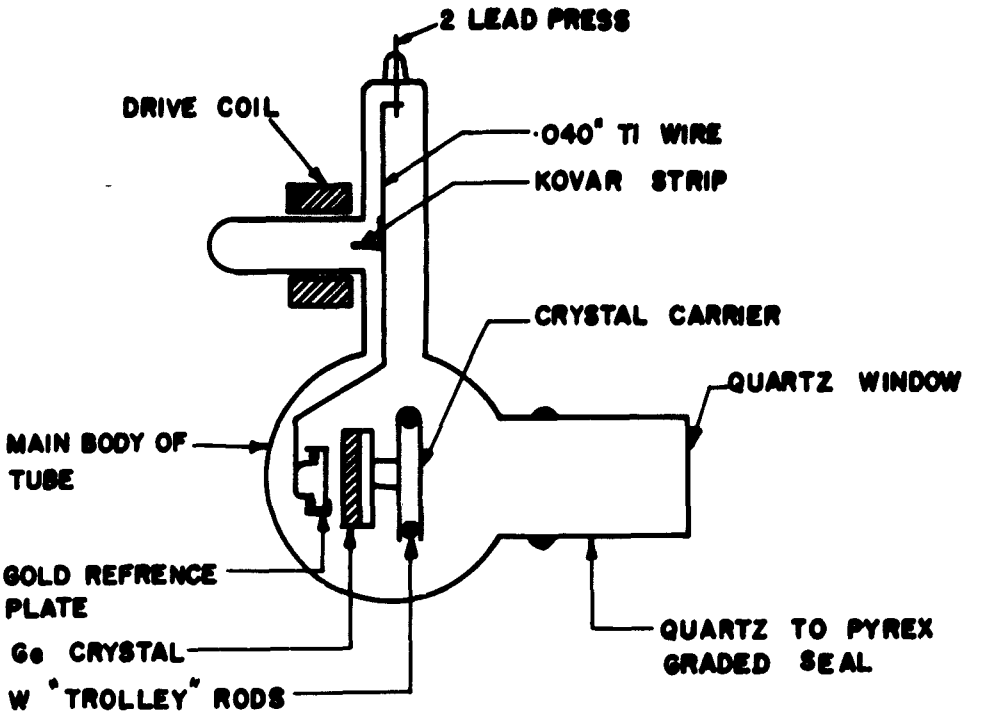

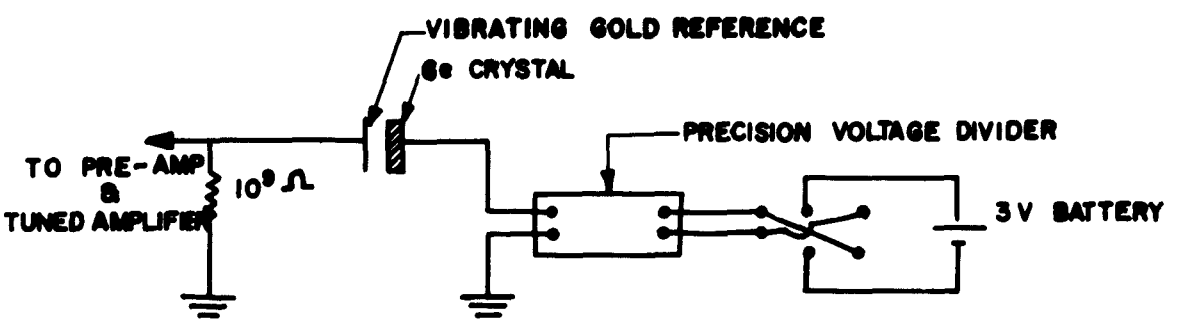

Fig. 6a Vibrating Capacitor Used for CPD Measurements

6b Circuit Used for CPD Measurements

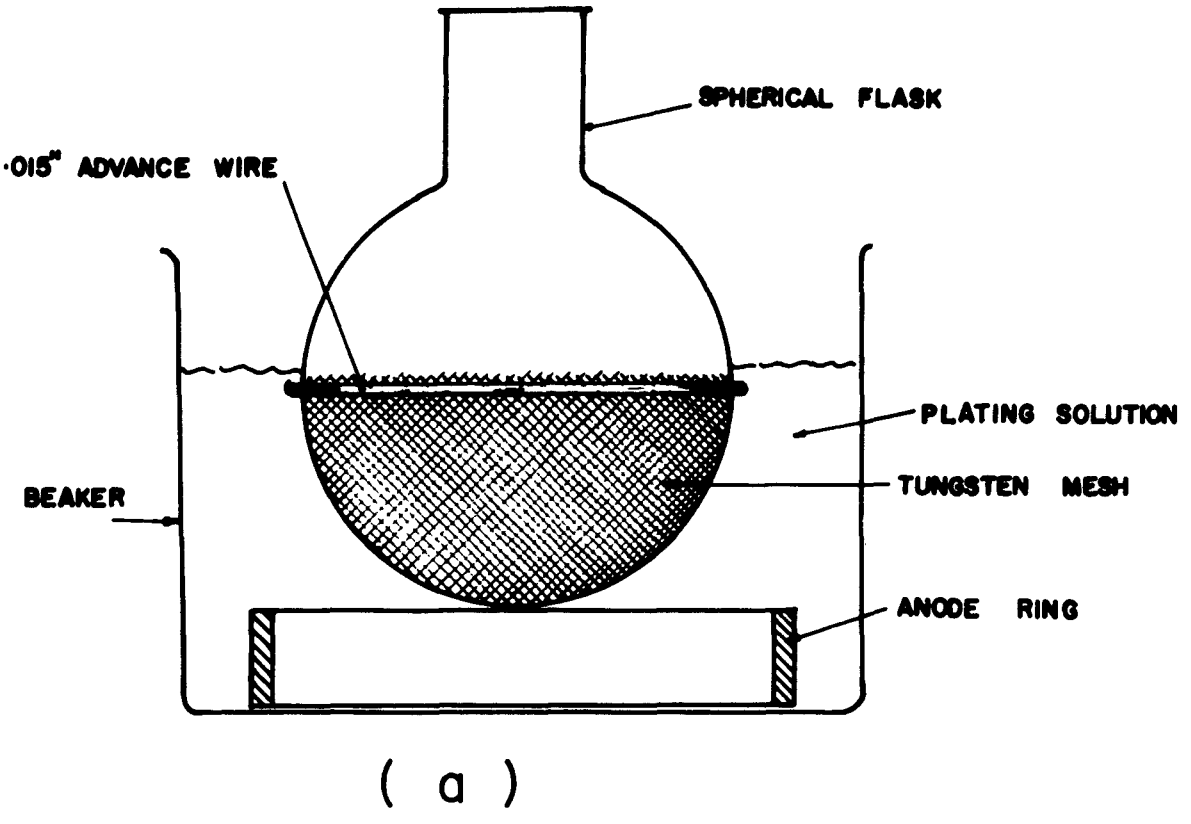

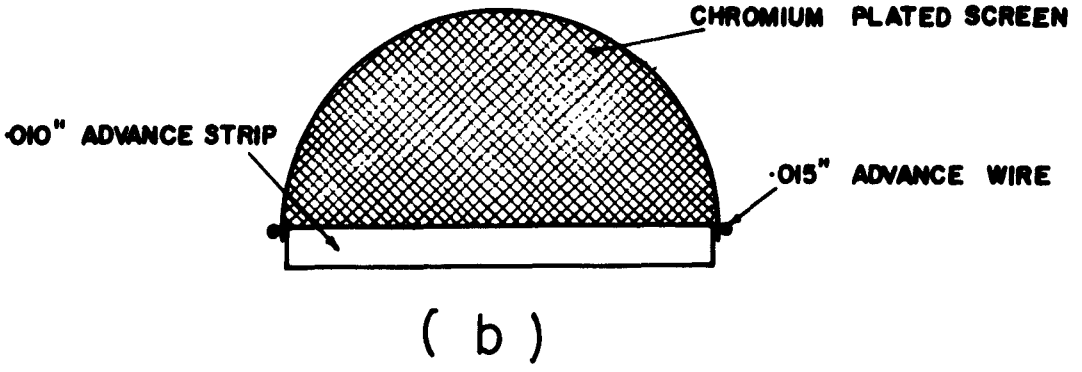

Fig. 7 Technique for Constructing Chromium Plated Spherical Grids

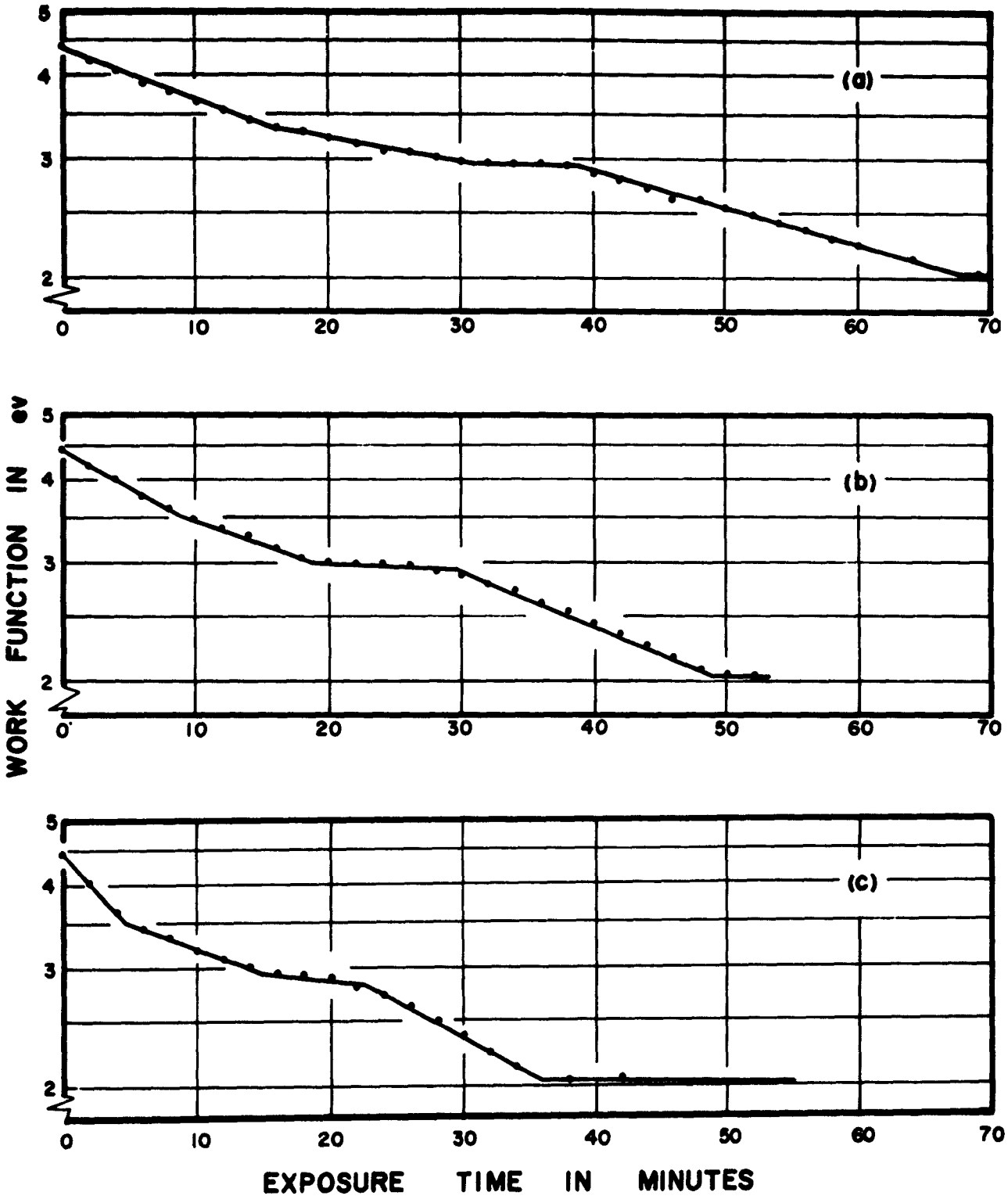

Fig. 8 Work Function vs. Exposure Time for Na:Ge

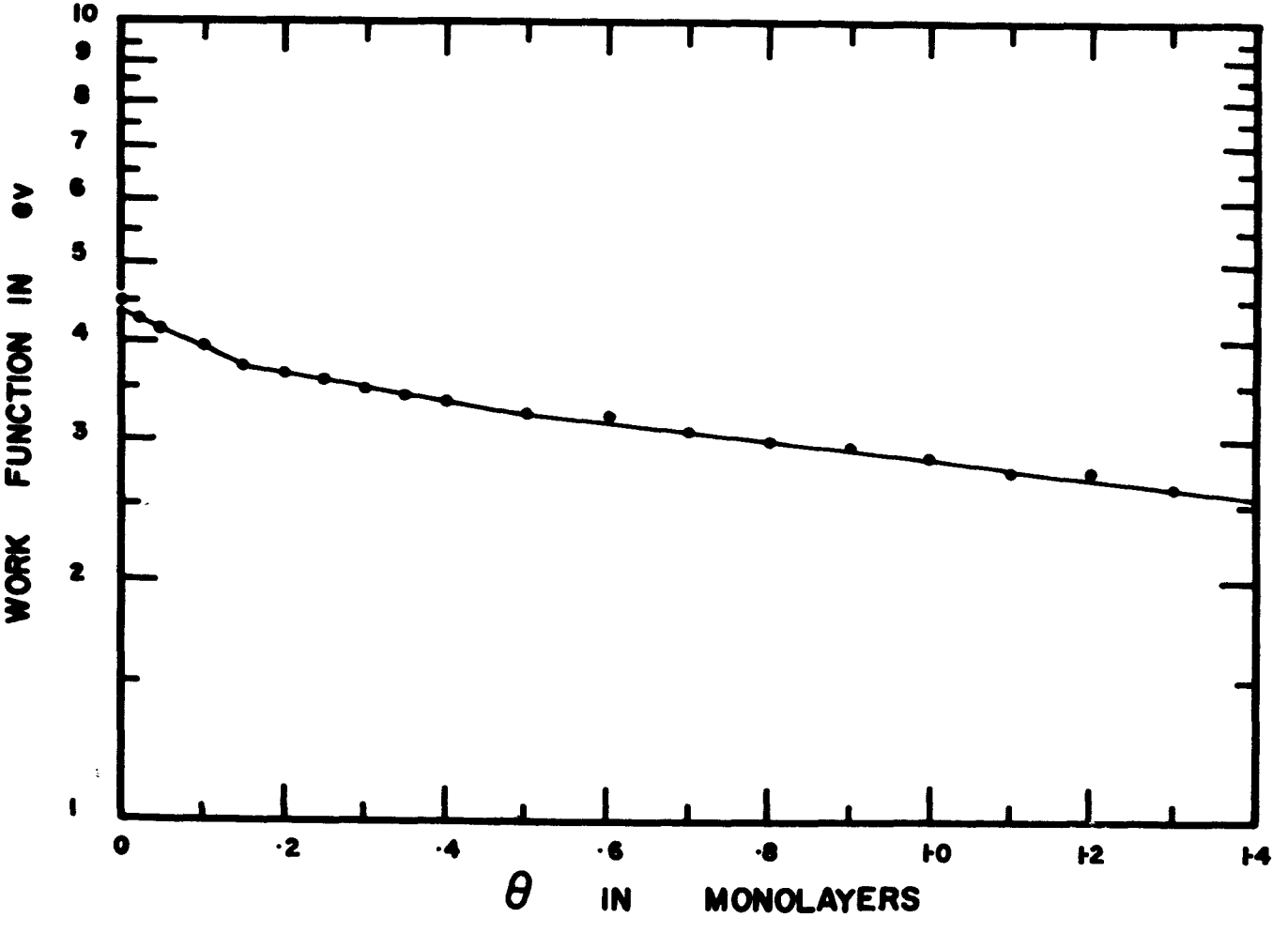

Fig. 9 Work Function vs. Overlayer Coverage for Na:Ge Using Ionic Deposition

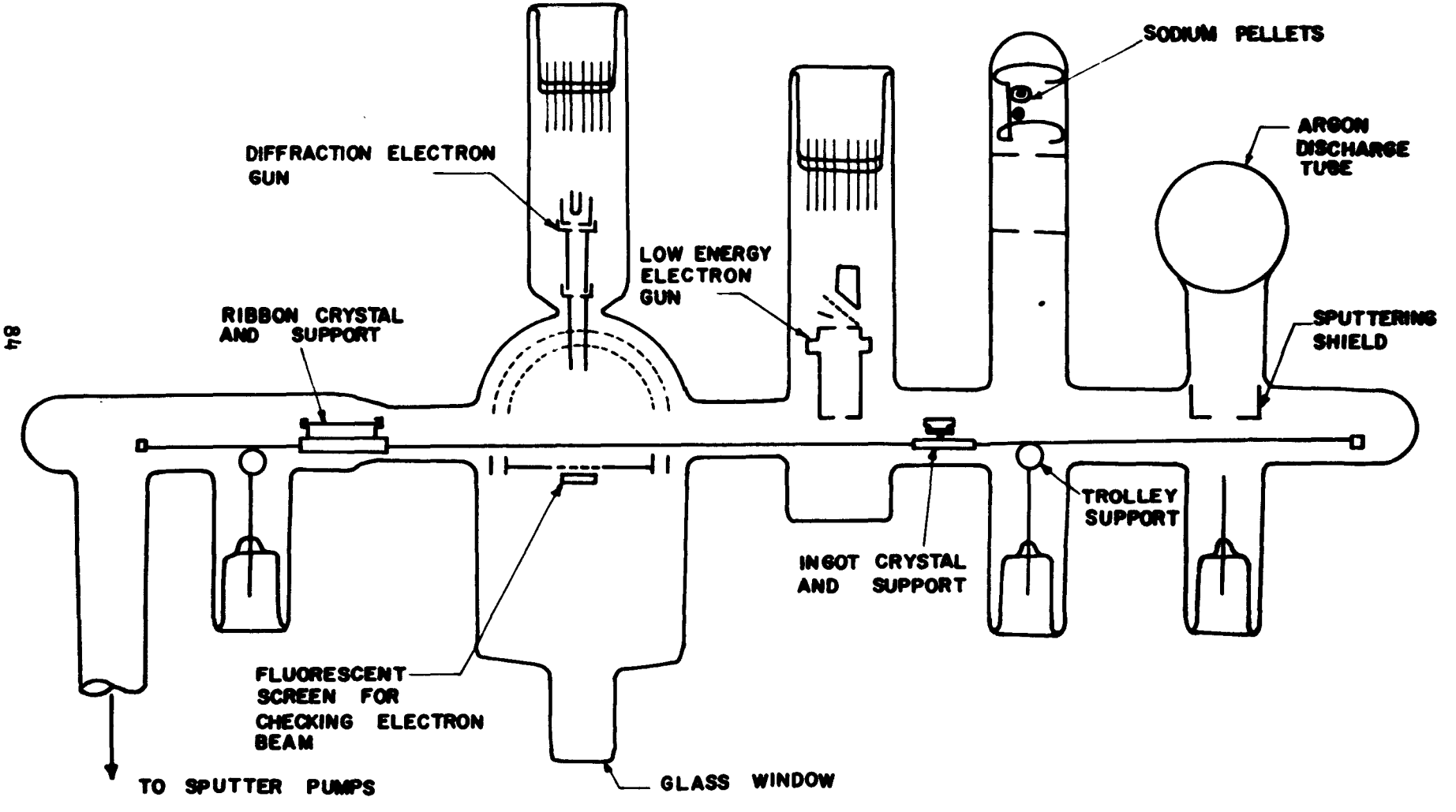

Fig. 10 Electron Diffraction Tube for Sodium Overlayer Studies

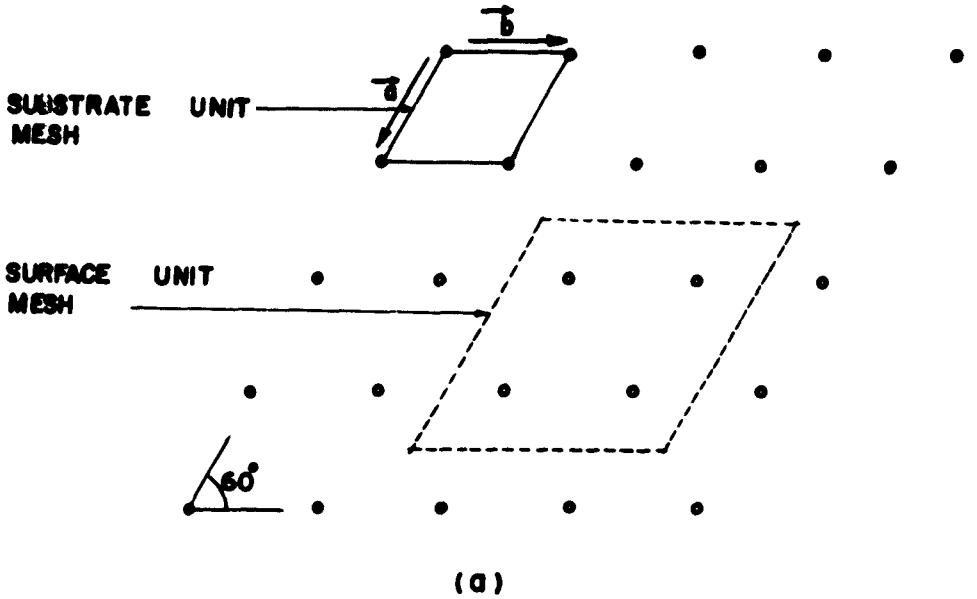

(a)

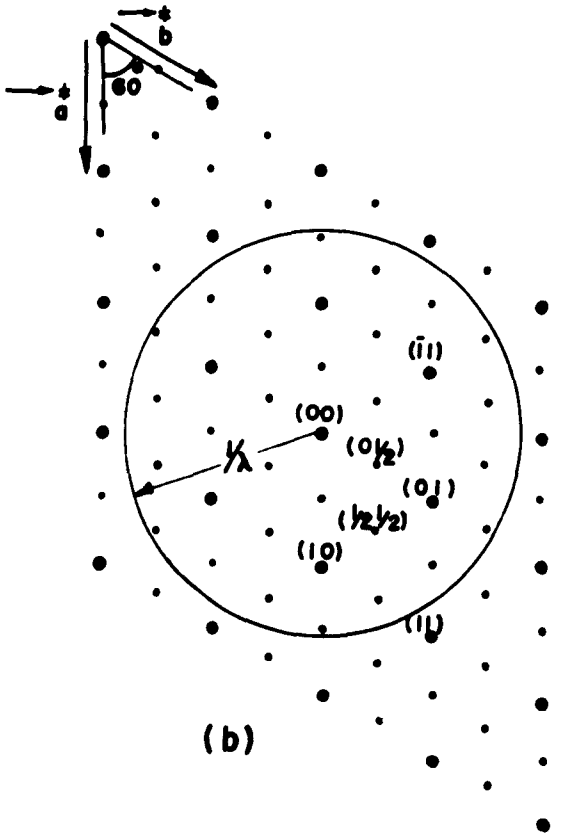

(b)

Fig. 11 Real and Reciprocal Lattice for Ge(111) 2 Structure

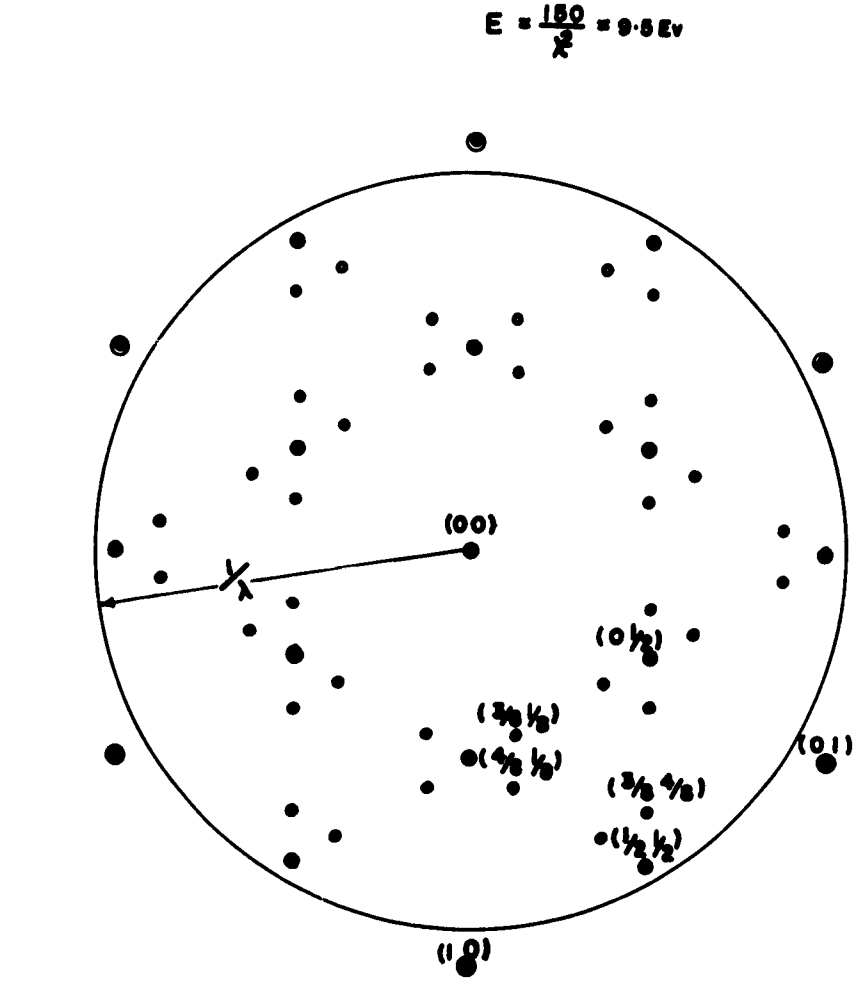

Fig. 12 Diffraction Pattern Observed from Clean Germanium

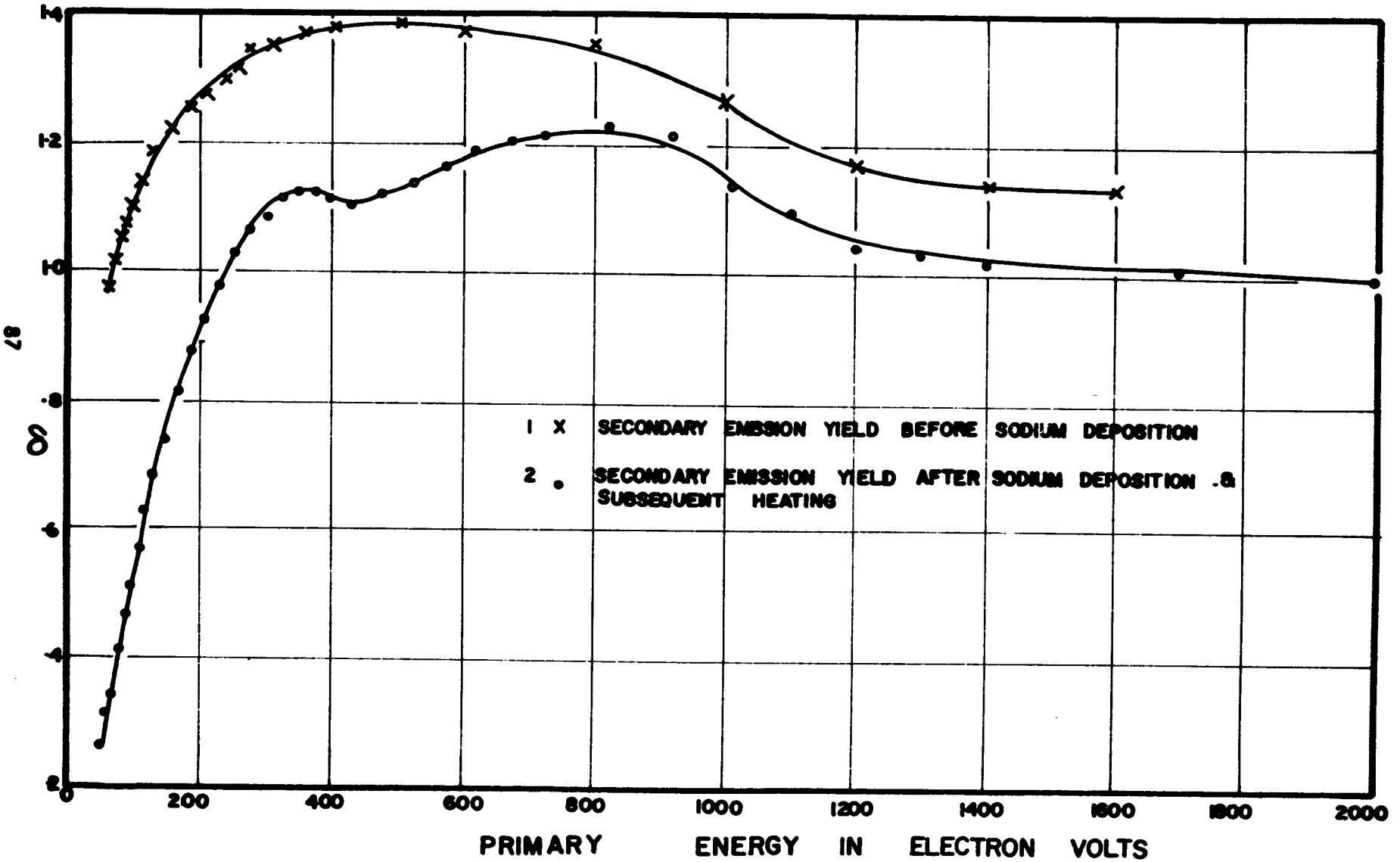

Fig. 13 Yield Curve Illustrating the Effect of Sodium Contamination

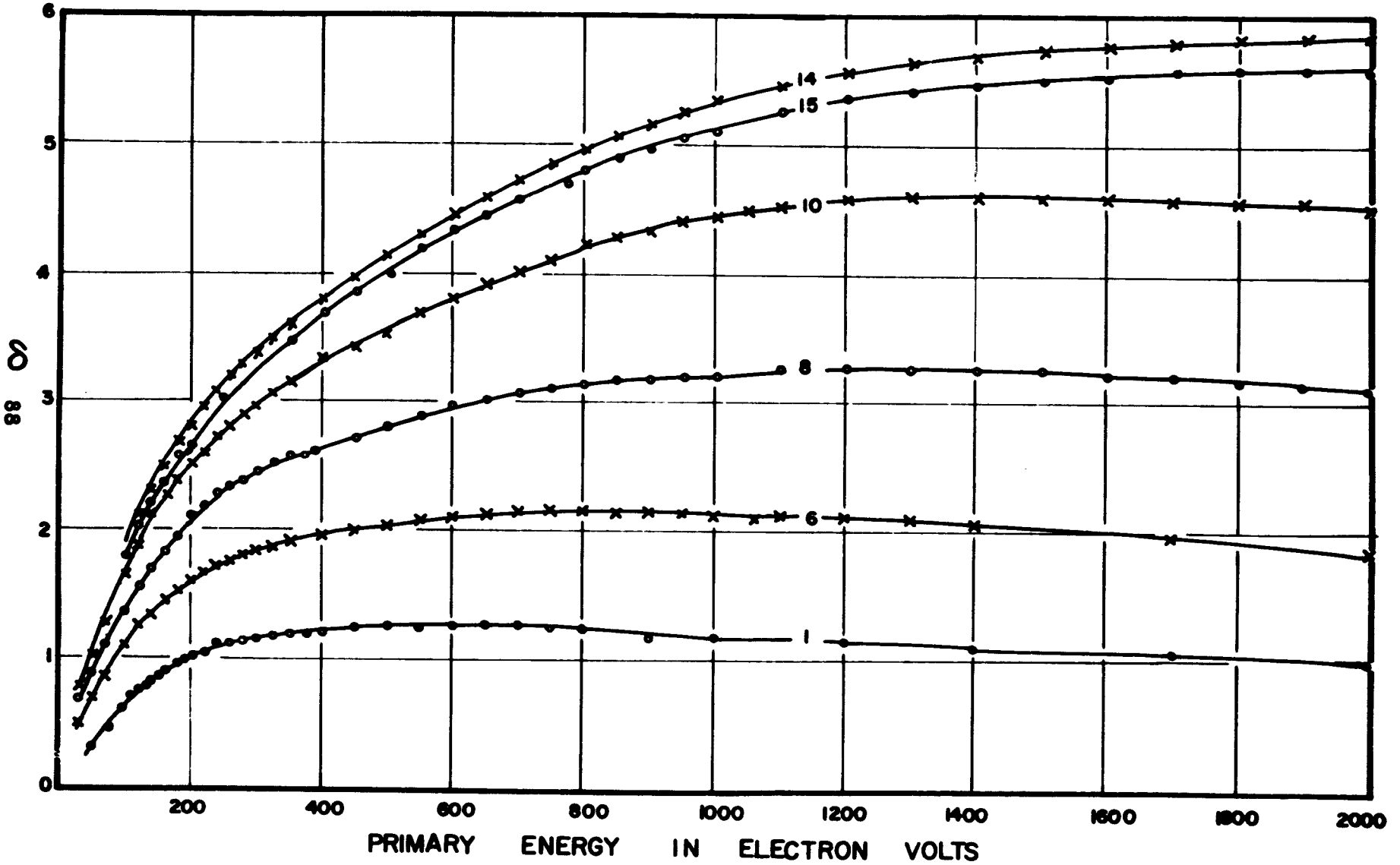

Fig. 14 Yield Curves from Germanium at Various Overlayer Coverages

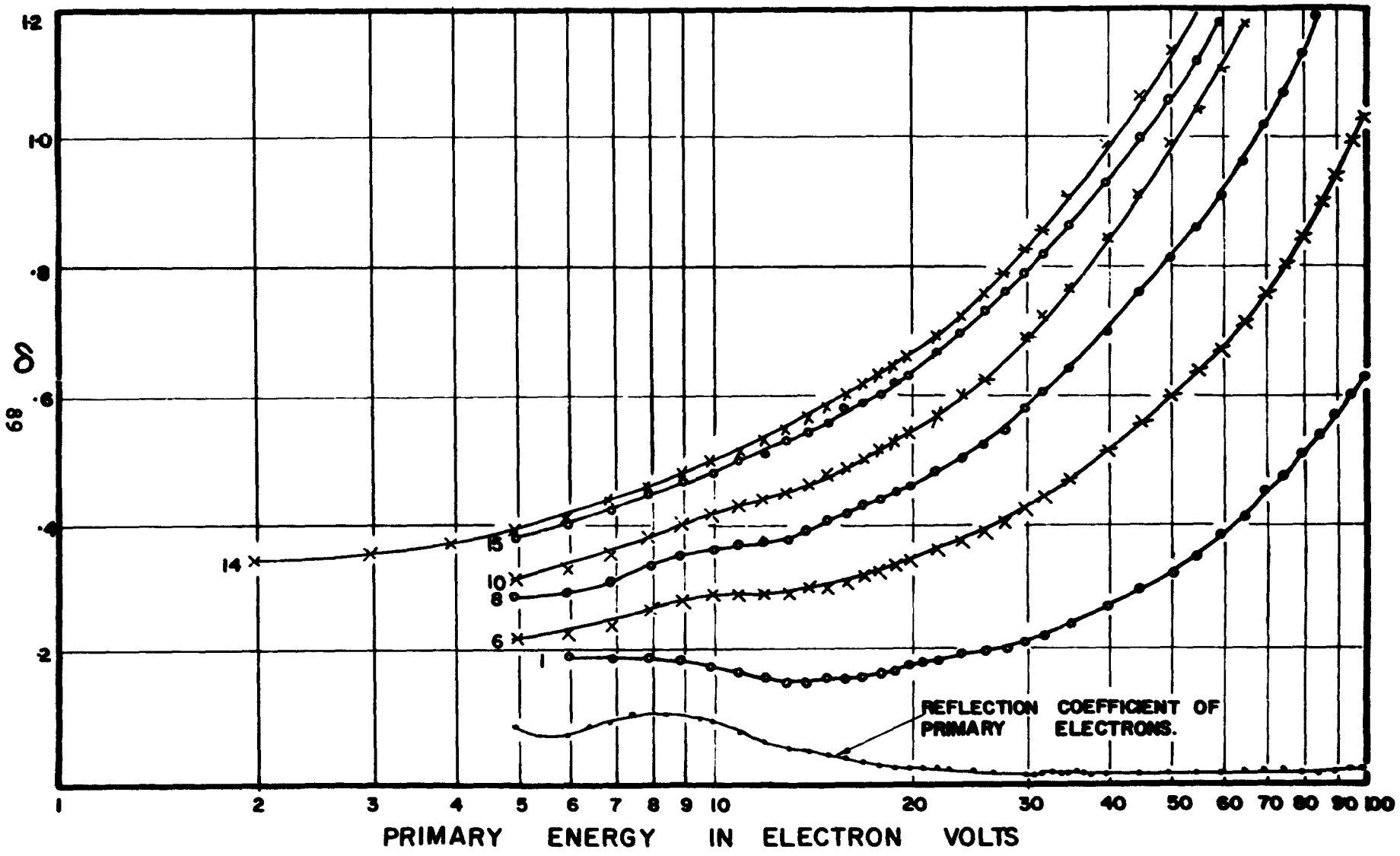

Fig. 15 Low Energy Yield Curves at Various Overlayer Coverages and Reflection Coefficient from Germanium

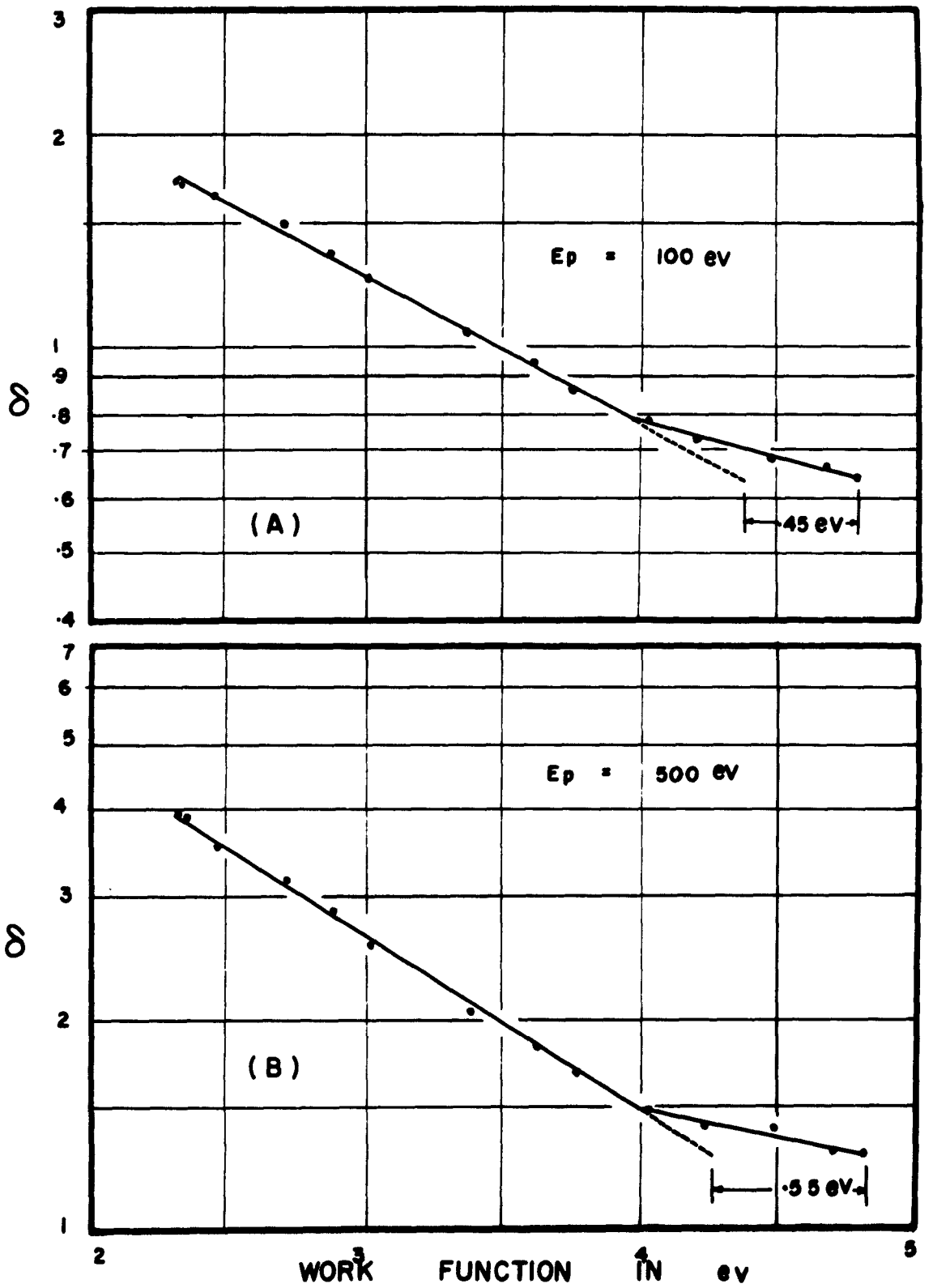

Fig. 16 Yield vs. Work Function

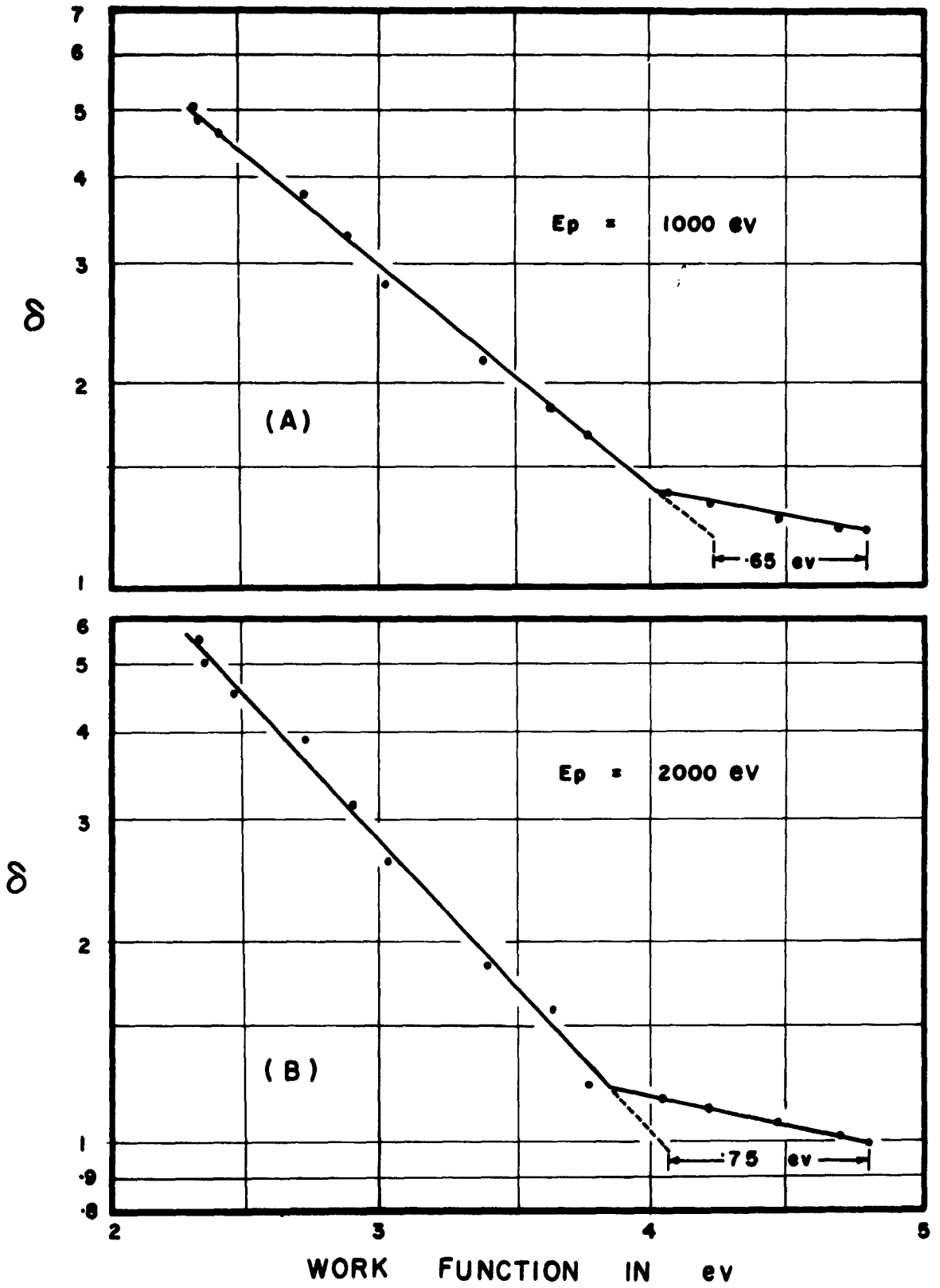

Fig. 17 Yield vs. Work Function

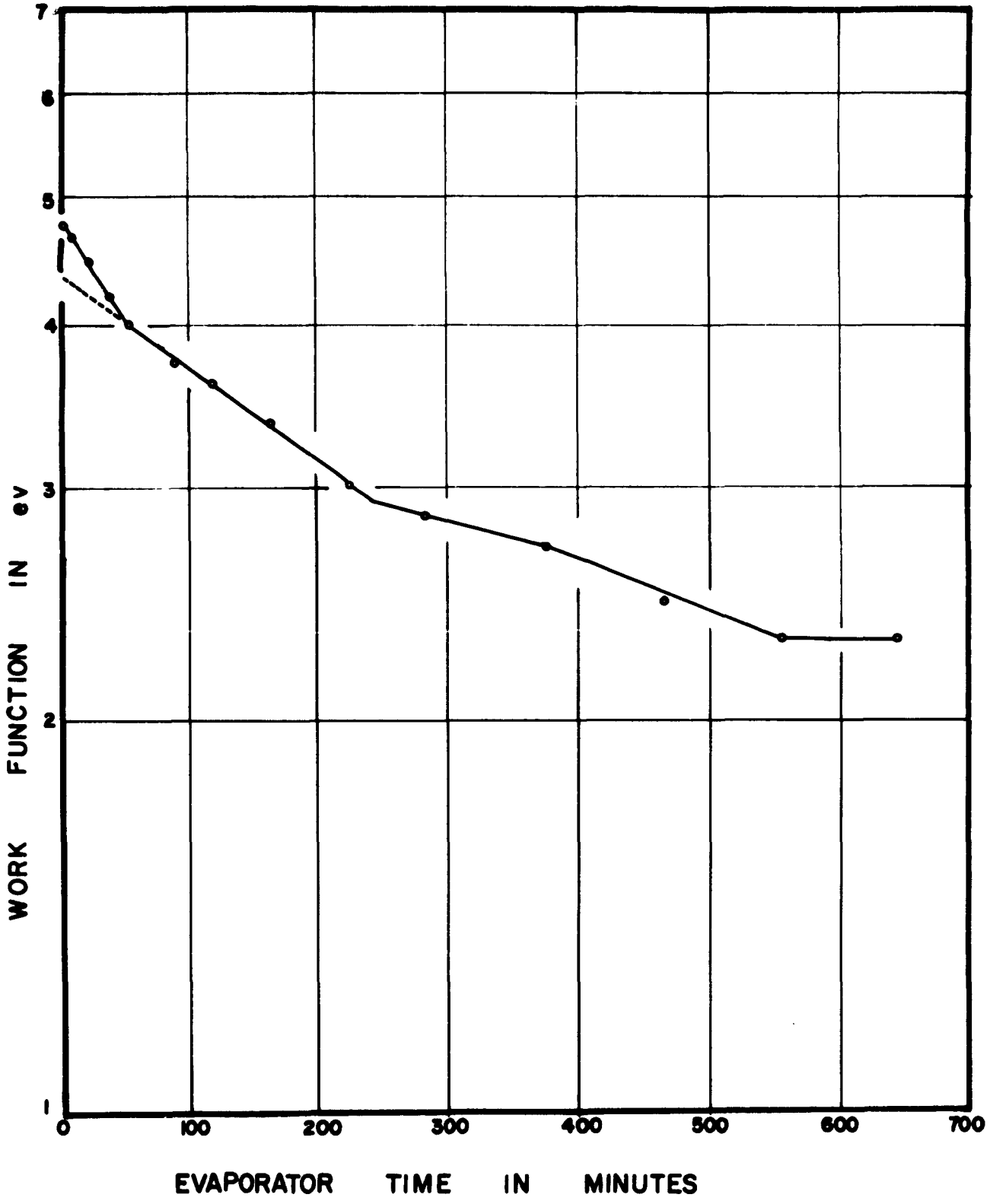

Fig. 18 Work Function vs. Evaporator Exposure Time

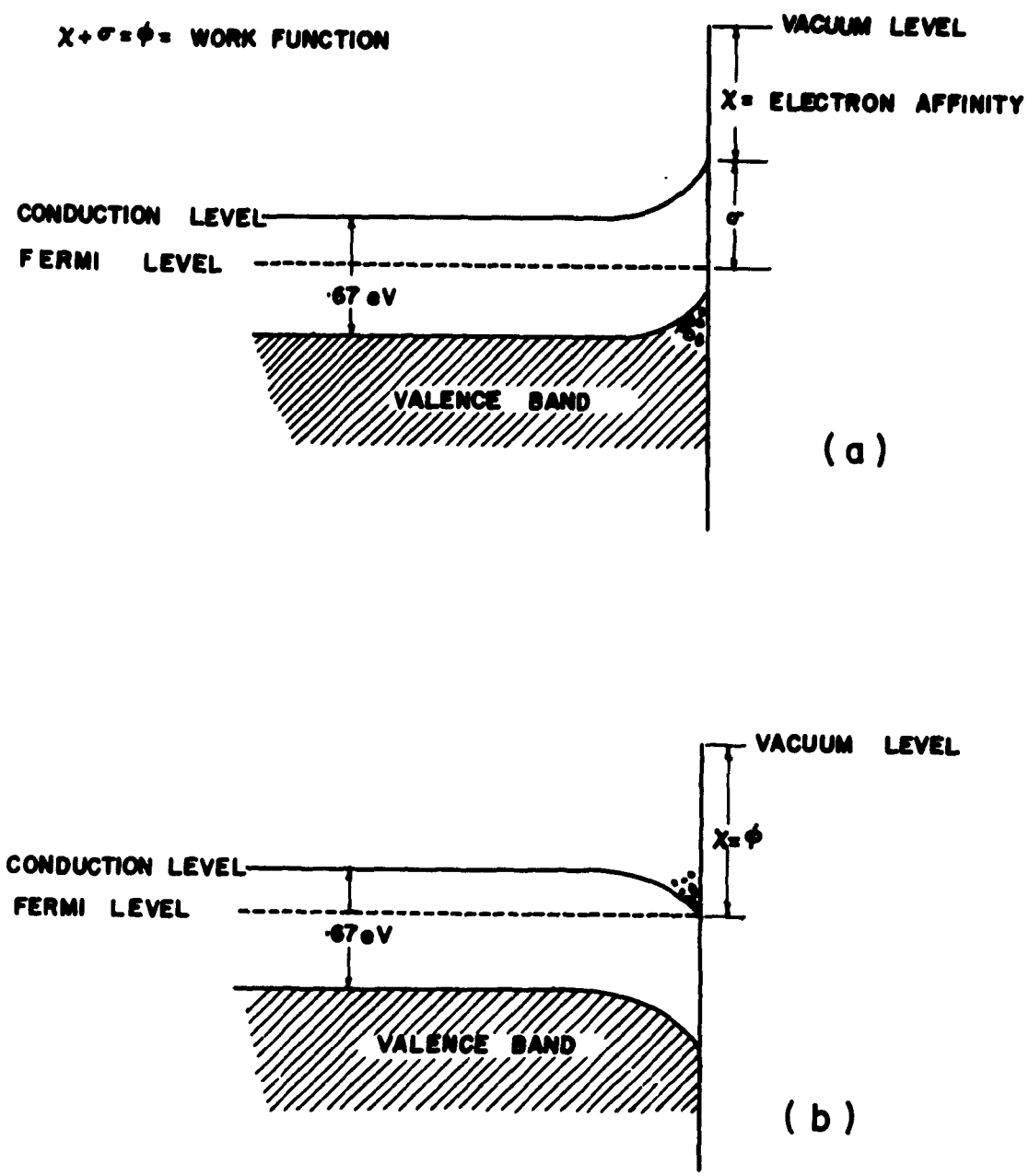

Fig. 19 Energy Band Models

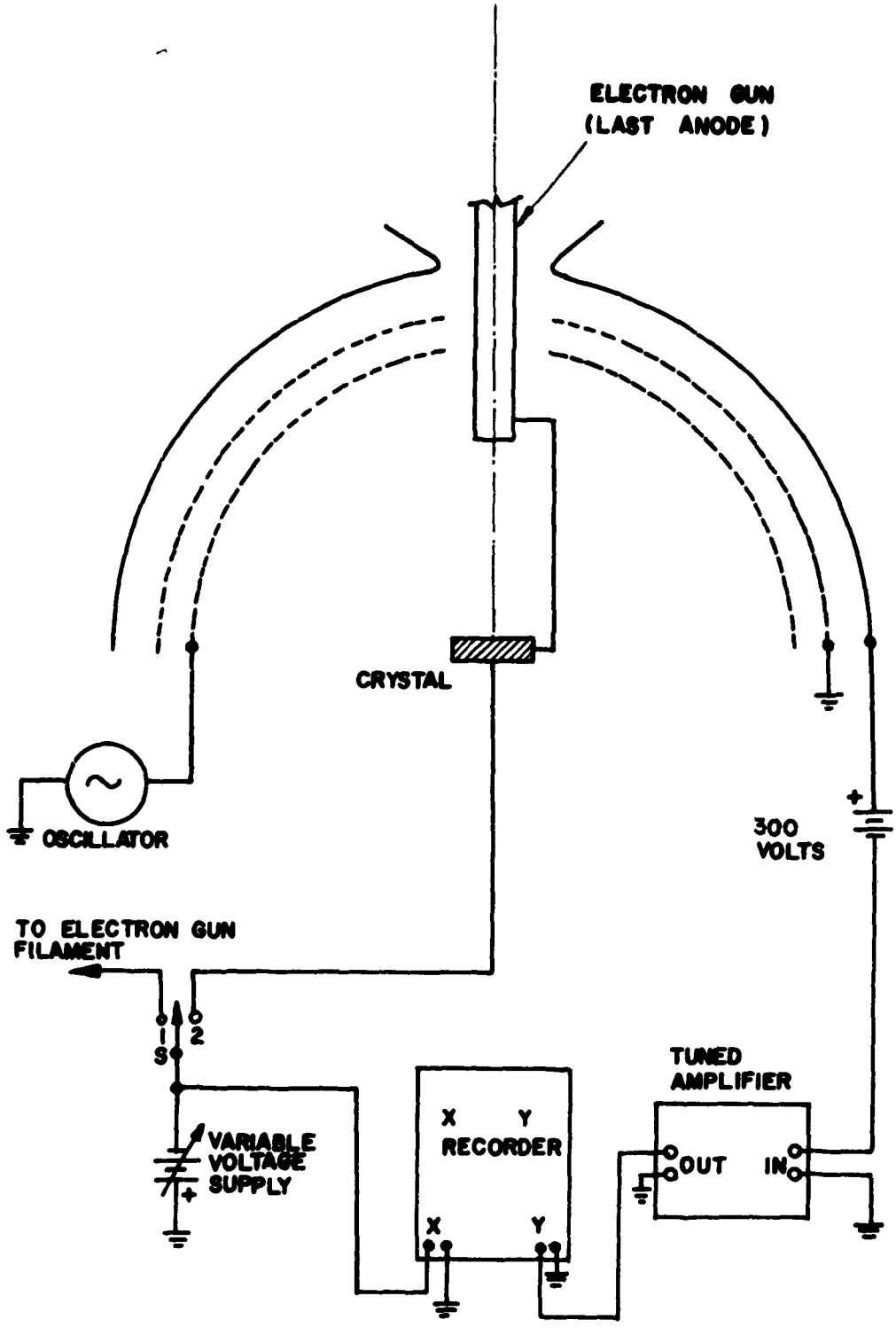

Fig. 20 Schematic Diagram of Circuit Employed for Energy Distribution Measurements

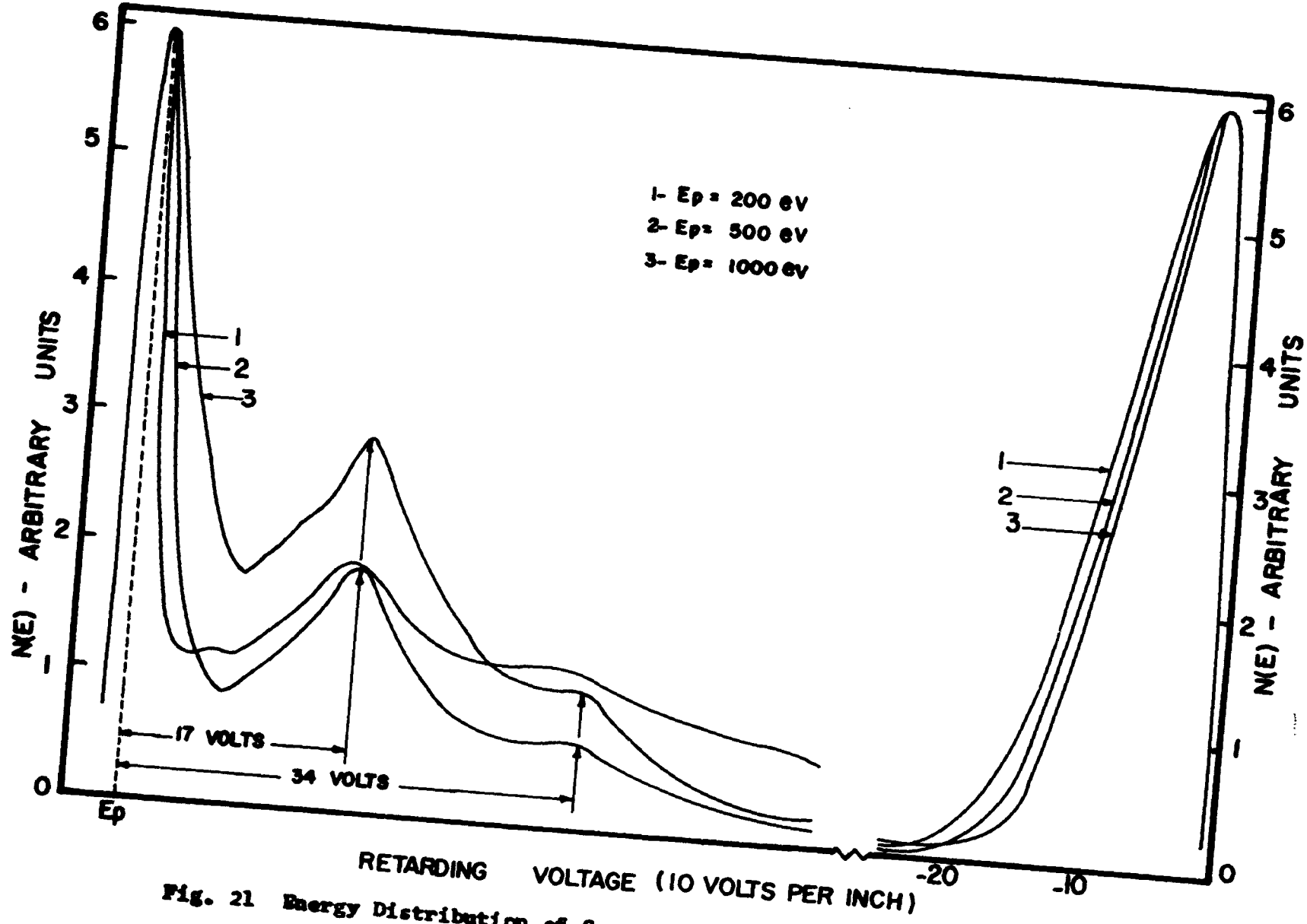

Fig. 21 Energy Distribution of Secondary Electrons from Germanium

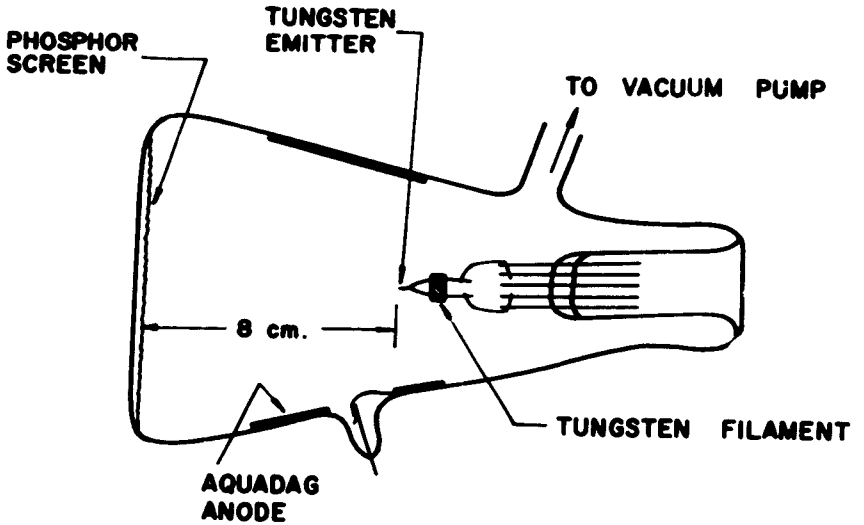

Fig. 22 Field Emission Microscope for Preliminary Studies

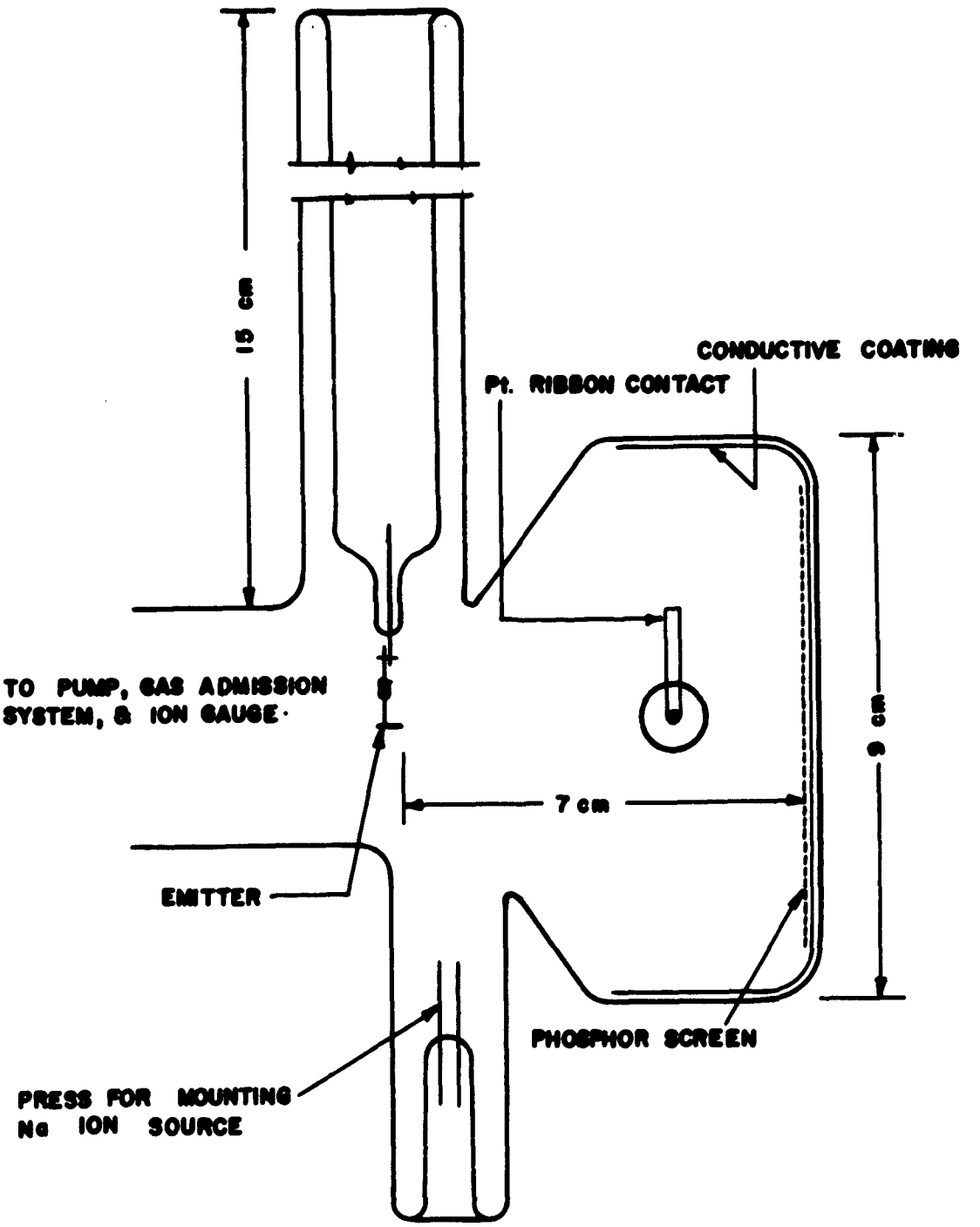

Fig. 23 Field Emission Microscope No. 2

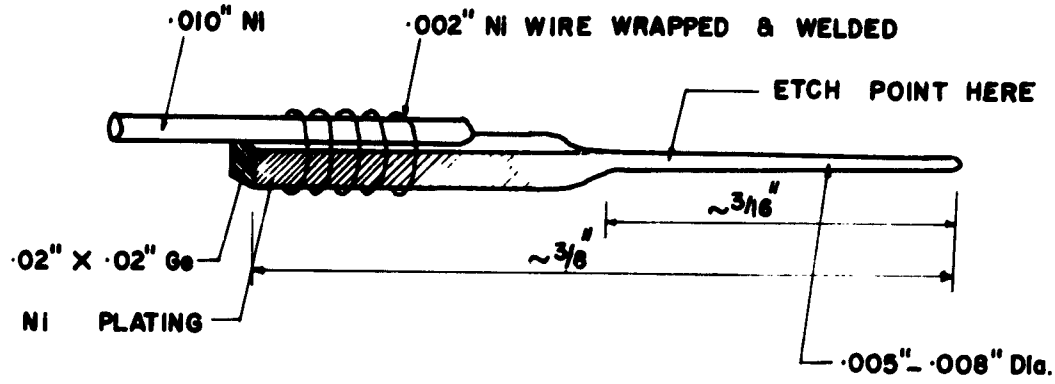

a. Ge EMITTER BLANK (AFTER SANDBLASTING)

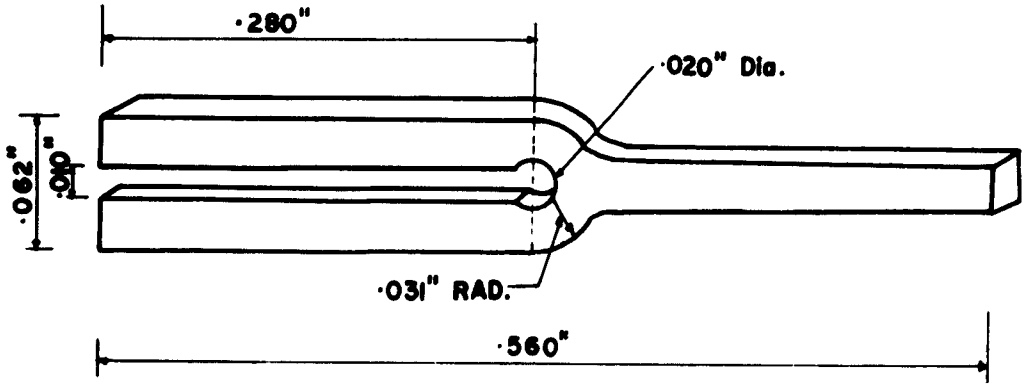

b. IMPROVED Ge EMITTER BLANK (BEFORE SANDBLASTING)

Fig. 24 Germanium Emitter Structures

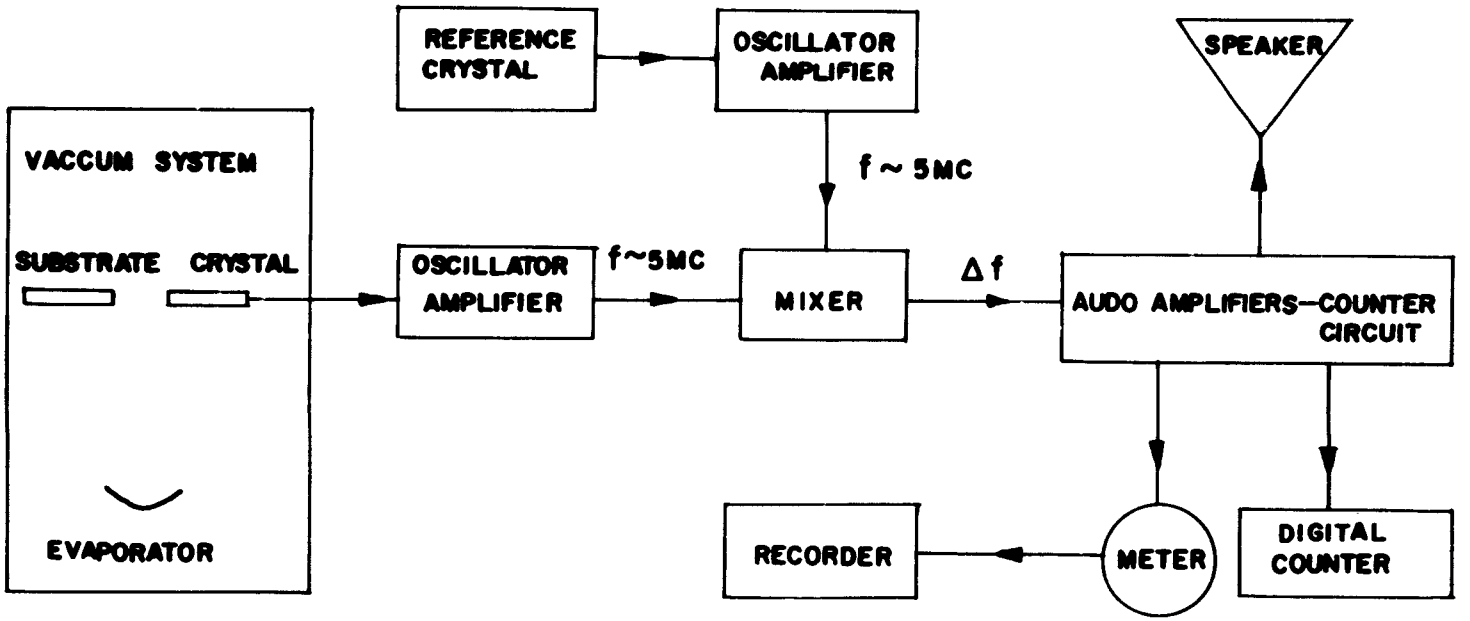

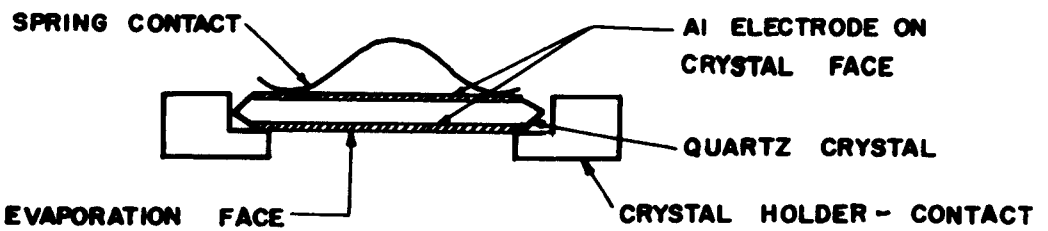

Fig. 25 Quartz Crystal Holder and Piezoelectric Rate Monitor Block Diagram

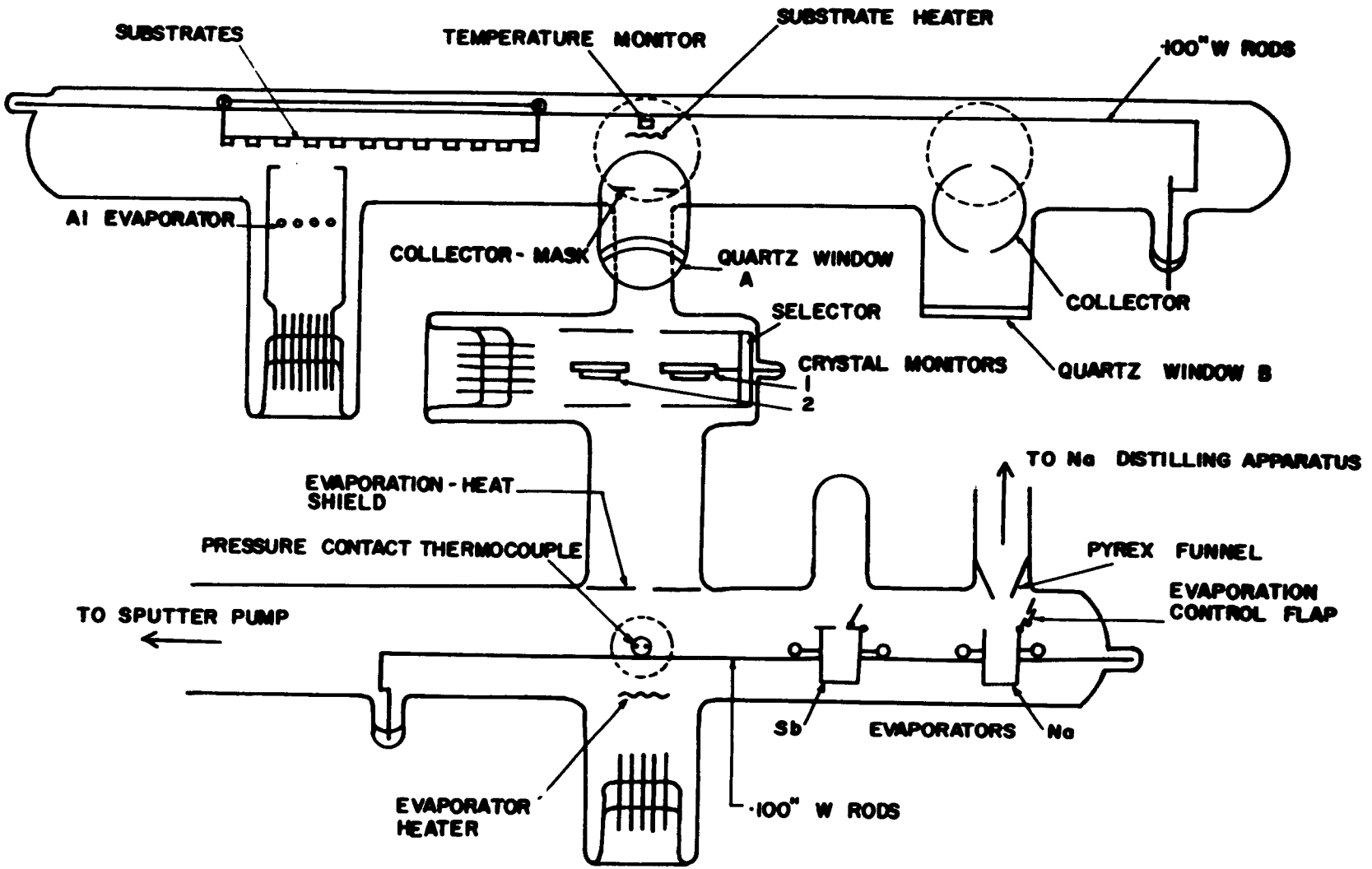

Fig. 26 Experimental Vacuum System for Na_3Sb Thin Film Studies

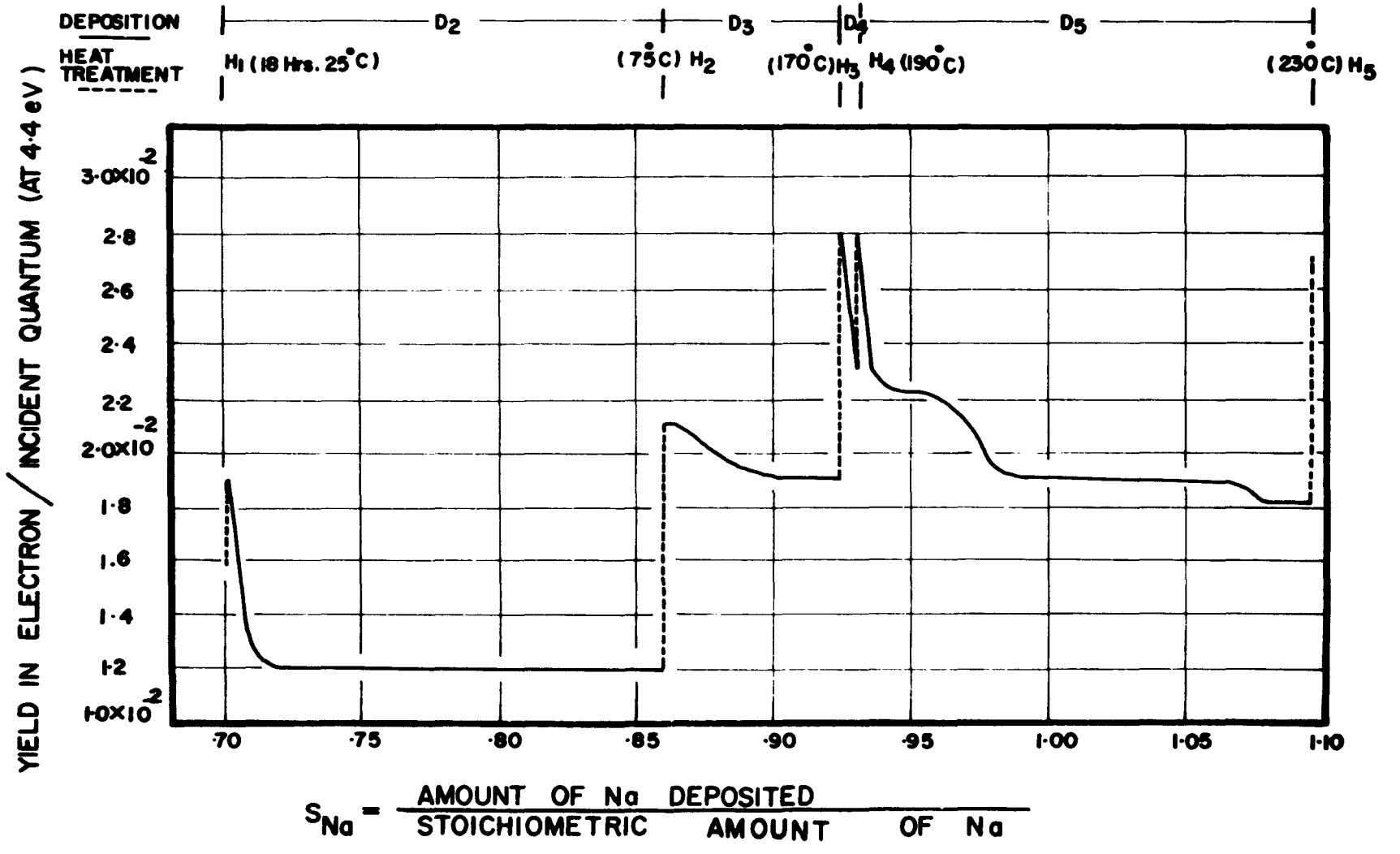

Fig. 27 Yield vs. Stoichiometry for Na_3Sb Film

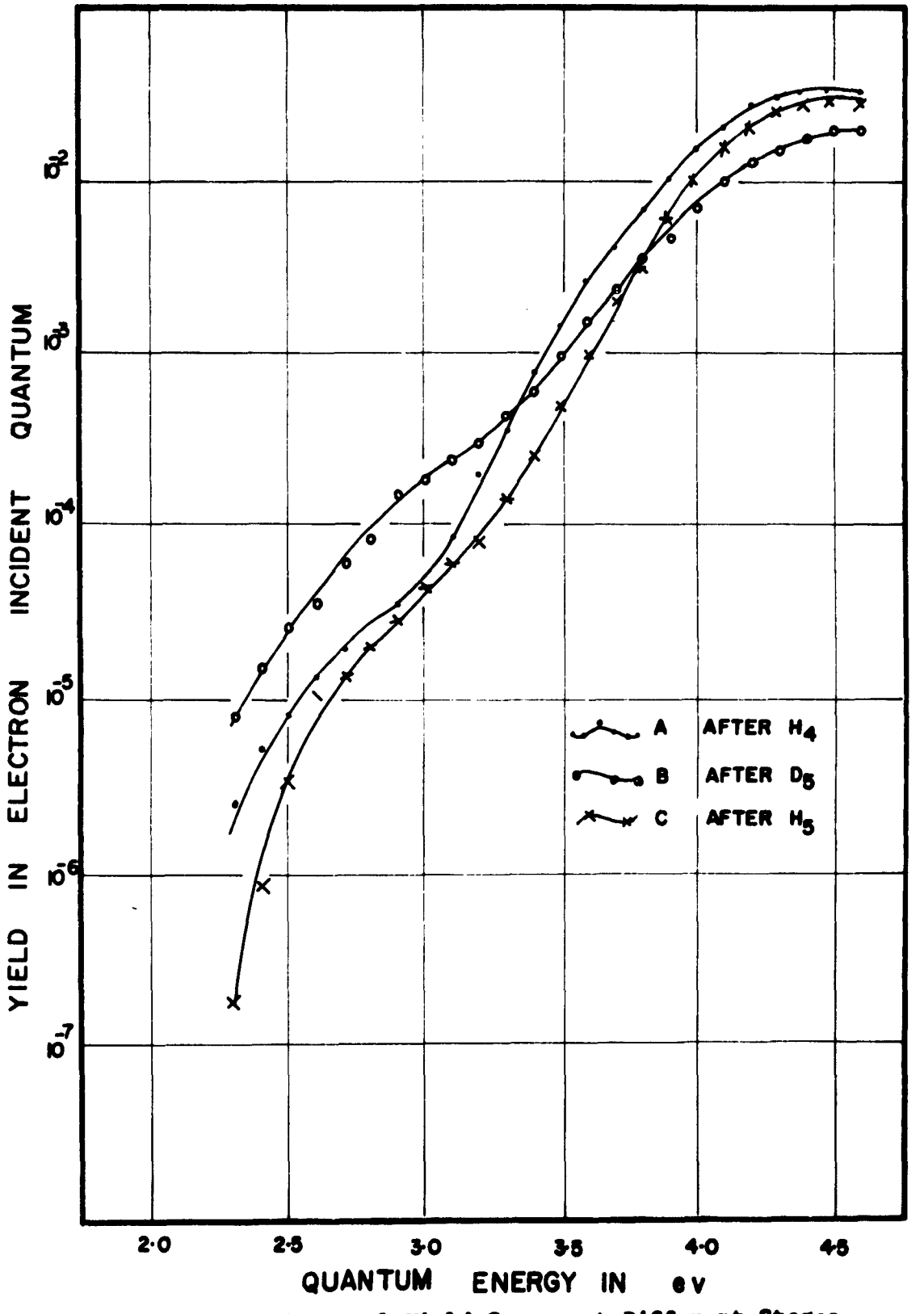

Fig. 28 Spectral Yield Curves at Different Stages of Na_3Sb Film Formation

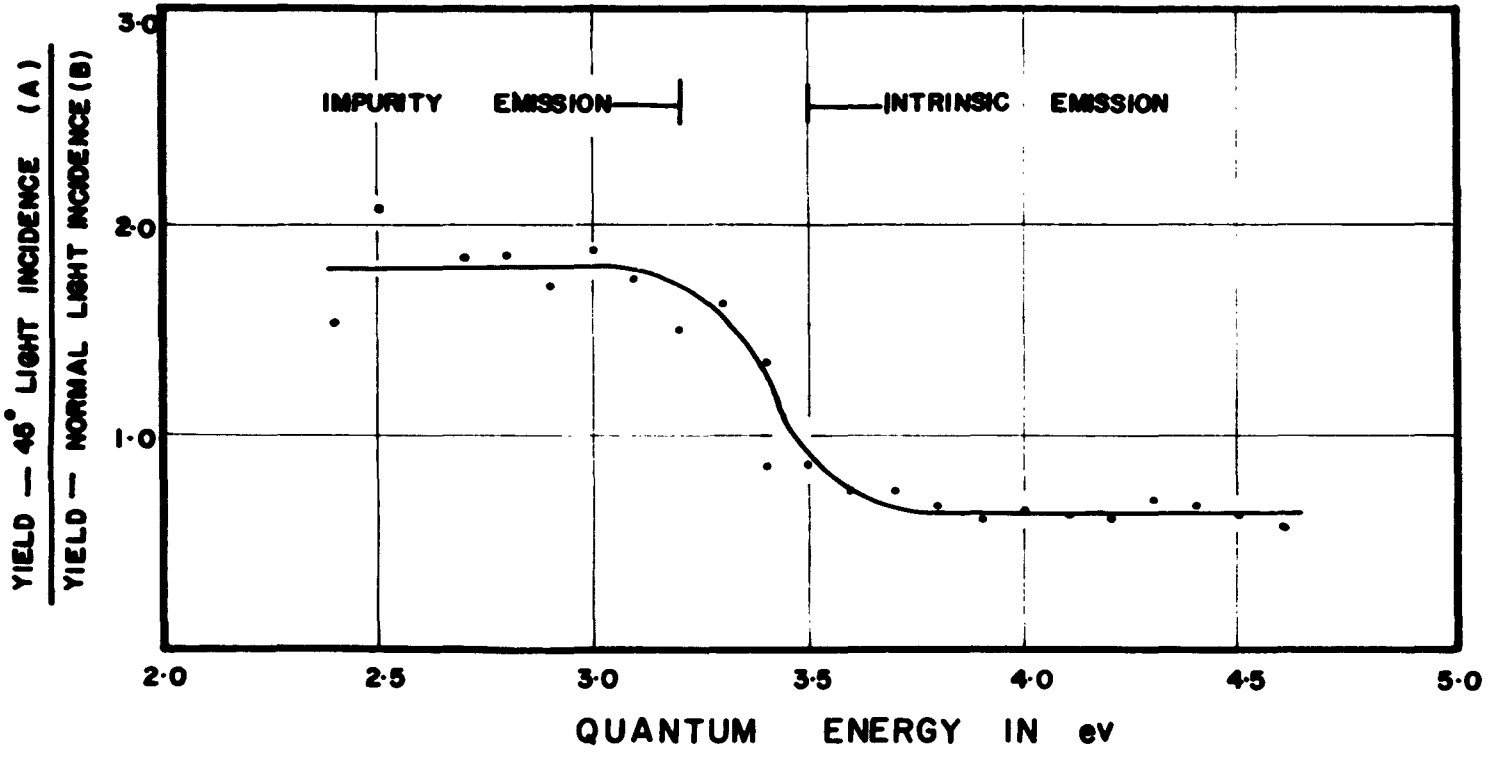

Fig. 29 Ratio of Na_3Sb Spectral Yields for Two Light Incidence Angles

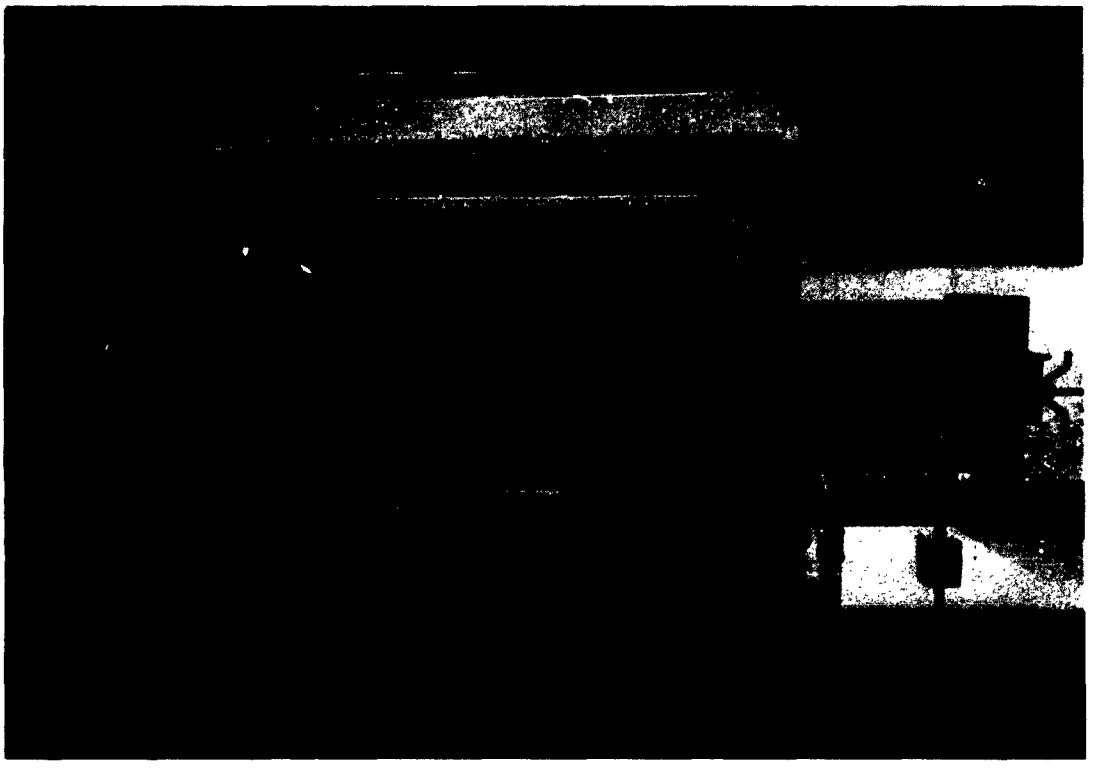

Fig. 30 Inert Atmosphere Enclosure and Oxygen Removal Unit

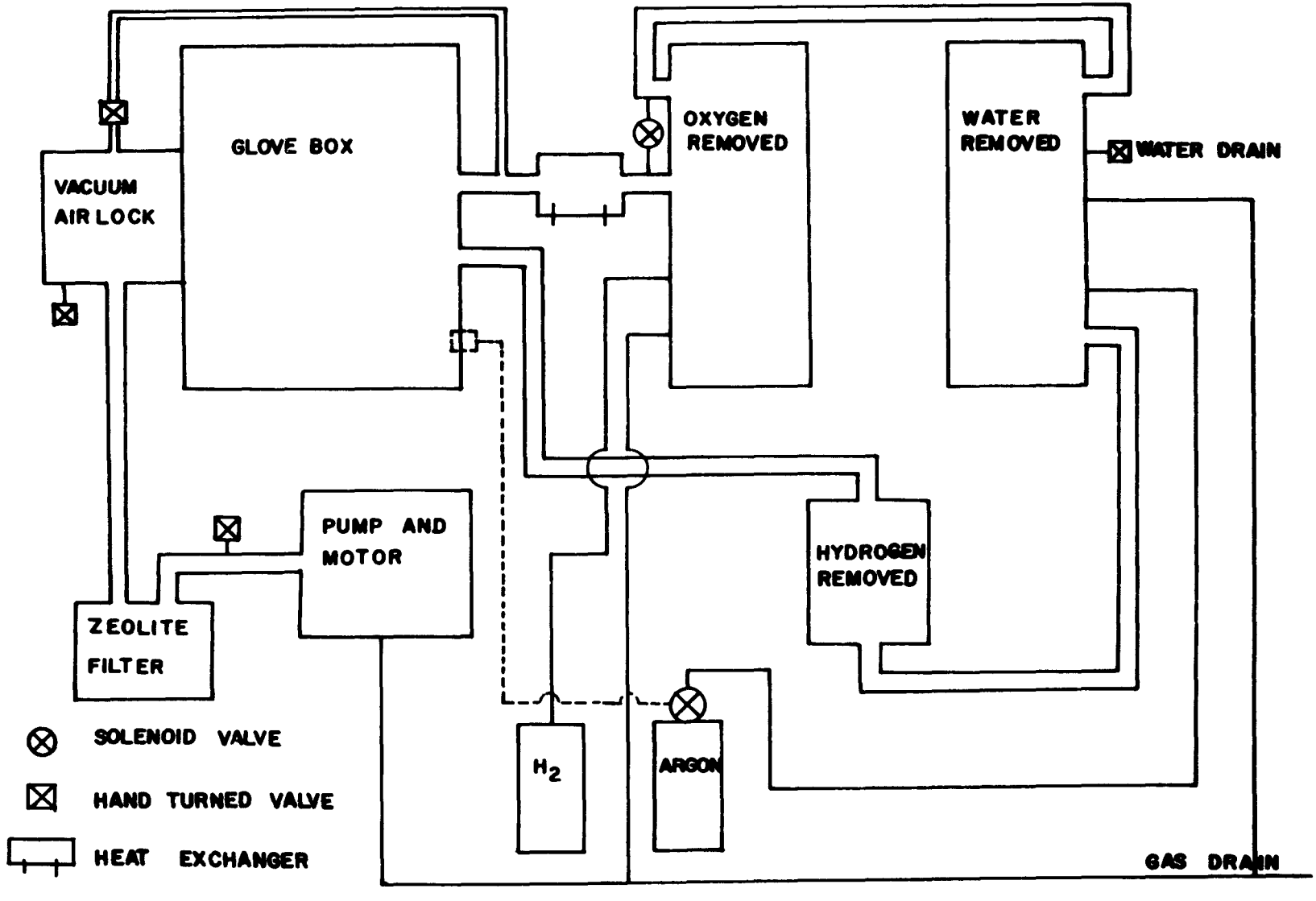

Fig. 31 Flow Diagram for the Argon Purification System and Inert Atmosphere Enclosure

Aeronautical Systems Division, Dir/Avionics, Electronic Technology Lab., Wright-Patterson AFB, Ohio.
Rpt Nr ASD-TDR-63-340, RESEARCH ON PHOTOEMISSION. Final Report, March, 1963, 112 pp. incl. illus., tables, 64 refs.

Unclassified

Techniques used to obtain high vacua, to provide clean surfaces, to deposit Na on these surfaces and to measure their work functions are described. A method used to fabricate hemispherical grids is also included. Work function, electron diffraction and secondary emission studies of

(over)

UNCLASSIFIED
1. Photoemission
2. Crystal structure
3. Photoelectrons
4. Work function
5. Photoemitters
I. AFSC Project 4156, Tasj 415605
II. Contract AF 33(657)-8041
III. Department of Electrical Engineering, University of Minnesota, Minneapolis 14, Minnesota
IV. Edited by: W. T. Peria
V. Aval for OTS
UNCLASSIFIED

sodium-covered germanium are presented. Preparations for a field-emission study of the same system are described. In the study of the compound Na_3Sb, preliminary data on the details of film formation have been obtained and the inert atmosphere facility for the preparation of the bulk material has been completed. A brief description of the apparatus to be used in the study of anomalous photovoltaic effects in Ge films is given.

UNCLASSIFIED
VI. In ASTIA collection

UNCLASSIFIED